BEST AVAILABLE IMAGES

Defective images within this document are accurate representations of the original documents submitted by the applicant.

Defects in the images may include (but are not limited to):

- BLACK BORDERS
- TEXT CUT OFF AT TOP, BOTTOM OR SIDES
- FADED TEXT
- ILLEGIBLE TEXT
- SKEWED/SLANTED IMAGES
- COLORED PHOTOS
- BLACK OR VERY BLACK AND WHITE DARK PHOTOS
- GRAY SCALE DOCUMENTS

IMAGES ARE BEST AVAILABLE COPY.

As rescanning documents *will not* correct images, please do not report the images to the Image Problem Mailbox.

REMARKS

As an initial matter, Applicants wish to thank the Examiner for discussing the application and proposed claim amendments in a telephonic interview on June 11, 2004.

Claims 1-15 and 17-19 are presently under examination. Claims 1-13, 15, and 17-18 have been amended at the request of the Examiner for purposes of improved clarity. In order to expedite prosecution, claim 1 has also been amended to specify that the claimed conotoxin peptides comprise either 4 cysteine residues which are bonded in pairs to form two disulfide bonds or 6 cysteine residues which are bonded in pairs to form three disulfide bonds. Claim 14 has been canceled. Applicants reserve the right to prosecute the subject matter of claim 1, as filed, and claim 14 in future applications. Claims 20-26 have been added. Support for claim 20 can be found, for example, in the specification on page 3, lines 4-6 and in Table 1. Support for claims 21-23, can be found, for example, in the specification on page 15, lines 23-30. Support for claims 24 and 25 can be found, for example, in the specification on page 1, lines 8-25 and page 15, lines 23-30. Support for claim 26 can be found, for example, in the specification on page 14, lines 26-30. After entry of the present amendments, claims 1-13, 15, and 17-26 will be pending.

Claim objections

Claims 1-15 and 17-18 have been amended as suggested by the Examiner.

Rejection under 35 U.S.C. § 112, first paragraph

Claim 1-9, 11-15, and 17-19 remain rejected under 35 U.S.C. § 112, first paragraph, for alleged lack of enablement because practice of the claimed inventions allegedly would entail undue experimentation. Applicants respectfully traverse because there is no evidence of record so much as suggesting that those skilled in the art would be unable to practice the claimed inventions. Although the Office Action provides a lengthy analysis of certain factors to be considered in assessing whether undue experimentation would be required, close inspection not only reveals that these factors do not support rejection of the present claims but, in fact, indicate that any experimentation associated with the practice of the claimed inventions would be routine in nature and well within the level of skill in the art.

1. BREADTH OF THE CLAIMS

Although the Office Action makes bare assertions that the claims are broad in scope, it fails to provide evidence that their breadth is beyond the level of skill in the art. As noted below, those skilled in the art were quite familiar with the various types of conotoxin peptides and techniques for cyclizing them. Given this familiarity, there is no reason to believe that the breadth of the claims would present an impediment to practice of Applicants' claimed inventions.

2. THE PRESENCE OR ABSENCE OF WORKING EXAMPLES

The Office Action also fails to provide any evidence that the number of working examples provided in the specification would be insufficient for those skilled in the art to practice the claimed inventions. Although the Office Action notes that the specification does not include examples documenting synthesis and use of each claimed compound, such examples are not required as a condition for patentability. In fact, it is well-established that an applicant need not include *any* working examples demonstrating a claimed invention. *In re Fouche*, 169 U.S.P.Q. 429, 434 (C.C.P.A. 1971). Thus, Applicants' provision of representative examples falls far short of demonstrating any lack of enablement.

3. THE STATE OF THE PRIOR ART

The Office Action acknowledges that the use of conotoxin peptides is well documented, indicating that those skilled in the art *would* be able to practice the claimed inventions without undue experimentation. The Office Action makes a bare assertion that the knowledge and level of skill in the art would be insufficient (and identifies certain types of information that the specification allegedly "needs to provide"), but fails to cite any references (or otherwise identify evidence) supporting the assertion. *In re Wright*, 27 U.S.P.Q.2d 1510, 1513 (Fed. Cir. 1993) (examiner must provide evidence or technical reasoning substantiating doubts expressed regarding enablement).

4. PREDICTABILITY OF THE ART

The Office Action fails to provide any evidence demonstrating any unpredictability as to whether the claimed compounds will demonstrate some measurable level of activity.

Although the Office Action notes that certain cyclization procedures have decreased the activity of conotoxin peptides, the patent laws do not require any threshold level of activity. In fact, it is improper for the PTO to require any showing regarding the degree of effectiveness of therapeutic inventions, such as those now claimed M.P.E.P. § 2107.02; *In re Sichert*, 566 F.2d 1154 (C.C.P.A. 1977). Although it might be difficult to predict which among the claimed compounds will exhibit the highest activity, in the absence of any reason to believe that any of the claimed compounds will be entirely inactive, the mere fact that some of them might be more active than others fails to demonstrate any lack of enablement.

In relying upon Armishaw *et al.* (*American Peptide Society,* 2001, 113-114) for the proposition that the art of cyclizing conotoxin peptides is unpredictable, the Office Action fails to note that the authors give little consideration to the selection of an appropriate linker sequence to span the N- and C-termini. The present application, however, clearly describes the importance of considering the structural characteristics of the conotoxin peptide that is to undergo cyclization when designing the linker sequence. In the Armishaw reference, the authors hypothesize that it will only take one or two residues in the linker to join the N and C-termini of α-conotoxin ImI. If, however, the authors had followed the directions in the present specification, they would have looked more closely at the structure and easily seen that the N- and C-termini were 11Å apart, clearly requiring more than two residues to join them. Once it is known that the spacing of the linker peptide can affect the connectivity of the peptide and the structure, a skilled practitioner would know to select a linker that has a sufficient number of residues for that particular conotoxin peptide. Such a selection is routine and easily performed by one of skill in the art.

5. AMOUNT OF GUIDANCE PRESENTED/ QUANTITY OF EXPERIMENTATION

Here, too, the Office Action presents a bare allegation without any supporting evidence. Although the Office Action asserts that Applicants should have presented more working examples, the question that remains unanswered is "why?". The Office Action, for example, asserts that "it is necessary to have additional guidance on amino acid sequences of the various cyclized conotoxin peptides" (Office Action at 7), but there is no evidence of record demonstrating that those skilled in the art would, in fact, have considered such

information to have been "necessary" to practice the claimed inventions. Absent some evidence indicating that those skilled in the art having read Applicants' specification would not be able to practice the claimed inventions, there is no reason to believe that the guidance provided in the specification is insufficient within the meaning of §112.

6. THE NATURE OF THE INVENTION

The Office Action fails to provide any evidence that the nature of Applicants' inventions is such that they could not be practiced by those skilled in the art. In fact, the arguments that the Office Action presents regarding this factor (*e.g.*, the claims are broad, the number of examples is insufficient) are entirely derivative of those presented with respect to the other factors.

Thus, as is evident from the foregoing analysis, the Office Action's unsupported contentions as to alleged difficulties that those skilled in the art would encounter in practicing the claimed inventions simply do not constitute evidence or technical reasoning of the sort required to substantiate allegations that there is a lack of enablement.

The Office Action also appears to express unwarranted concern that structural differences among conotoxin peptides embraced by the claims would prevent those skilled in the art from practicing Applicants' inventions. The claimed conotoxin peptides all belong to structural classes that are characterized by common disulfide bond frameworks. Claim 1 recites that the claimed peptides comprise either 4 cysteine residues which are bonded in pairs to form two disulfide bonds or 6 cysteine residues which are bonded in pairs to form three disulfide bonds. The specification, in turn, provides detailed instructions on how to cyclize conotoxin peptides generally, and ω- and α-conotoxin peptides specifically. In particular, examples 1, 2, 5, and 6 provide detailed synthesis steps for the cyclization of exemplary ω- or α-conotoxin peptides. As evidence of the structural similarity between the ω-conotoxins, Applicants herewith submit an article by Nielsen *et al.* (*J. Mol. Biol.* 1996, 263, 297-310, Exhibit A). The Nielsen article provides a comparison of the structures of a number of ω-conotoxins, concluding that they share a common framework, the only known structural difference being minor and confirmed to local elements. Figure 1 of the article demonstrates the near identity of the backbone structure conferred by the disulphide bridge arrangement. In particular the article states the following at page 307, column 2, paragraph 3:

"Using MVIIA as a model, we confirm that the ω-conotoxins are rigid

peptides with a structure that is likely to be little altered on changing the environment. Rigidity is conferred by three disulphide bonds which direct the folding of the ω-conotoxins into a class of four-loop peptides that possess almost identical secondary structure, despite considerable differences in primary structure. Structural similarities among the ω-conotoxins suggest that this class of peptide binds to a common VSCC macrosite that varies slightly amongst the different VSCC subtypes. Several other classes of four-loop peptides from Conus spp. have activity at less related sites, including the δ-conotoxins, which delay inactivation of voltage sensitive sodium channels, and the μO-conotoxins and κ-conotoxins, which block the sodium and potassium channels, respectively. From this work, it is evident that these too will adopt similar structures to the ω-conotoxins."

It is clear from this quotation that this research foreshadowed later findings that not only do all ω-conotoxins share the same structural framework, but there is considerable structural identify with other classes of 4-loop conotoxins, including κ-conotoxins, δ-conotoxins and μO-conotoxins, and these have subsequently been classified into the same superfamily (O-superfamily) of conotoxins based on similarity of structure. There are a number of publications confirming the striking similarity of structures amongst members of this superfamily (See, for example, Scanlon *et al.*, (1997), Exhibit B). The α-conotoxins belong to the 2-loop structural class of conotoxin peptides characterized by a common disulfide bridge network and similar structural features. Because of this structural similarity among the various conotoxin peptides, known methods of cyclizing one peptide can be routinely used to cyclize another. Accordingly, after reading the specification and the numerous, representative examples provided therein, a person skilled in the art would be readily able to cyclize the claimed conotoxin peptides.

The Office Action also expresses unwarranted concern as to use of cyclized conotoxin peptides in the treatment of specific diseases. It is well known that conotoxin peptides interfere with neurotransmission by targeting a variety of receptors and ion-channels. Moreover, it is widely believed that blocking those receptors or ion-channels is useful in the treatment of diseases, including neurological disorders. For example, as stated in the specification on page 2, the MVIIA conotoxin had entered clinical trials for the treatment of stroke and pain at the time of filing (See, for example, Perez-Pinzon, 1997, *J. Neur. Sci*, 153, 25-31, Exhibit C; Brose et al. *Clin J. Pain* 1997, 13(3), 256-259, Exhibit D). Further, as demonstrated by an abstract by Verweij *et al.* (*Neurol Res.* 1997, 19(3):334-339, Exhibit E),

the ω-conotoxin SNX-111 can be used to treat traumatic brain injury. As previously discussed, as long as the guidance in the specification is followed, the cyclization of the peptides will not render them inactive.

In summary, Applicants submit that the Action has mischaracterized the state of the prior art and the relative skill of those in the art of conotoxin peptide chemistry and has improperly rejected the claims as non-enabled. Accordingly, Applicants respectfully request that the rejection of the claims under 35 U.S.C. § 112, first paragraph, be withdrawn.

Rejection under 35 U.S.C. § 112, second paragraph

Claim 14 and 15 are rejected under 35 U.S.C. § 112, second paragraph, as allegedly indefinite. In order to expedite prosecution, claim 14 has been canceled. Claim 15 has been amended to recite a method of treating a condition or disease associated with abnormal ion channel or nicotinic acetylcholine receptor activity.

The foregoing represents a *bona fide* attempt to advance the present case to allowance. Applicants submit that this application is now in condition for allowance. Accordingly, an indication of allowability and an early Notice of Allowance are respectfully requested.

Date: June 23, 2004

Leslie E. Aberman
Registration No. 54,836

Woodcock Washburn LLP
One Liberty Place - 46th Floor
Philadelphia PA 19103
Telephone: (215) 568-3100
Facsimile: (215) 568-3439

J. Mol. Biol. (1996) 263, 297–310

JMB

A Consensus Structure for ω-Conotoxins with Different Selectivities for Voltage-sensitive Calcium Channel Subtypes: Comparison of MVIIA, SVIB and SNX-202

Katherine J. Nielsen, Linda Thomas, Richard J. Lewis Paul F. Alewood and David J. Craik*

Centre for Drug Design and Development, University of Queensland, Brisbane, 4072 QLD, Australia

**Corresponding author*

The ω-conotoxins are a set of structurally related peptides that have a wide range of specificities for different subtypes of the voltage-sensitive calcium channel (VSCC). To understand their VSCC subtype differentiation we studied the structure of two naturally occurring ω-conotoxins, MVIIA (specific to N-type) and SVIB (specific to P/Q-type) and a synthetic hybrid, SNX-202, which has altered specificities to both VSCC subtypes. The secondary structures of the three peptides are almost identical, consisting of a triple-stranded β-sheet and several turns. A comparison of NMR data emphasizes the structural similarities between the peptides and highlights some minor structural differences. In the three-dimensional structures of SVIB and MVIIA these are manifested as orientational differences between two key loops. The structural rigidity of MVIIA was also examined. H^{α} shifts are similar in a range of solvents, indicating that there are no solvent-induced changes in structure. The ω-conotoxins form a consensus structure despite differences in sequence and VSCC subtype specificity. This indicates that the ω-conotoxin macrosites for the N/P/Q-subfamily of VSCCs are related, with specificity for receptor targets being conferred by the positions of functional side-chains on the surface of the peptides.

Keywords: ω-conotoxin; nuclear magnetic resonance; peptide solution structure; voltage-sensitive calcium channel antagonist

Introduction

Voltage-sensitive calcium channels (VSCC) are implicated in the control of a multitude of cellular processes. Several subtypes of the VSCC, characterised by their distinct electrophysiological properties, have been detected in neuronal tissue (for a review, see Miljanich & Ramachandran, 1995). A major function of the VSCC is to mediate the calcium-dependent secretion of neurotransmitters from presynaptic nerve terminals in the initiation of synaptic transmission. The N/P/Q subfamily of VSCCs is directly involved in this process, and therefore it is not coincidental that most naturally occurring VSCC blockers are specific for these subtypes (Miljanich & Ramachandran, 1995). In particular, selective N-type and P/Q-type VSCC blockers have been identified in the venoms of piscivorous snails belonging to the family *Conidae* (Olivera *et al.*, 1984, 1985; Hillyard *et al.*, 1992; Ramilo *et al.*, 1992) and in the venoms of funnel web spiders (Bindokas & Adams, 1989; Adams *et al.*, 1990; Bindokas *et al.*, 1991; Venema *et al.*, 1992). These peptides are referred to as ω-conotoxins and ω-agatoxins, respectively. The ω-conotoxins are of fundamental interest as they represent a group of structurally related peptides that display a wide

Abbreviations used: VSCC, voltage-sensitive calcium channel; NMR, nuclear magnetic resonance; 2D, two-dimensional; 3D, three-dimensional; DQF-COSY, double quantum filtered correlated spectroscopy; TOCSY, total correlated spectroscopy; NOESY, nuclear Overhauser enhancement spectroscopy; E-COSY, exclusive correlated spectroscopy; RMSD, root-mean-square deviation(s); TFE, trifluoroethanol; ppm, parts per million.

0022-2836/96/420297-14 $25.00/0

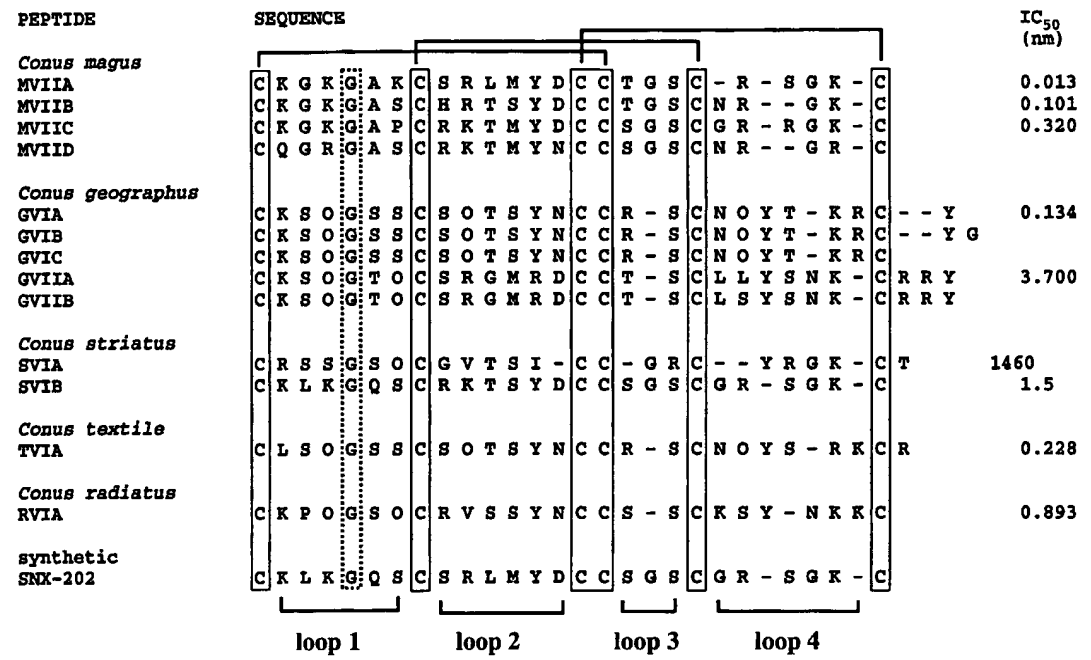

Figure 1. The primary structure of ω-conotoxins. The amino acid sequences of several ω-conotoxins (for a review, see Miljanich & Ramachandran, 1995) together with their IC_{50} values (Miljanich *et al.*, 1993) for displacing [^{125}I]MVIIA from the MVIIA binding site on N-type VSCCs. The amino acid denoted O represents hydroxyproline. Conserved residues are boxed and the four loops are indicated at the bottom of the Figure.

range of specificities for different VSCCs (Figure 1). They possess a four-loop cysteine scaffold, with each loop showing sequence variability amongst the set, particularly with respect to interchanges between positively charged and hydroxyl-bearing side-chains.

The N-type VSCC is widely distributed throughout the central nervous system and the potential therapeutic uses of antagonists specific to this subtype are manifold. In particular, the highly selective N-type VSCC blockers ω-conotoxins GVIA and MVIIA possess anti-hypertensive, neuroprotective and analgesic properties (Miljanich & Ramachandran, 1995; Miljanich *et al.*, 1993) and are consequently prototypes for the design of peptidomimetic drugs. VSCC blockers (i.e. MVIIC and SVIB) that are specific to the P/Q-subtypes, which exist primarily at the neuromuscular junction, are not targets as they are likely to be lethal (Bowersox *et al.*, 1994). Consequently, it is important to identify those elements, structural and functional, that contribute to N-type specificity as opposed to the P/Q-type so that adverse toxicity can be avoided. Despite their potential toxicity, P/Q-type VSCC antagonists are of interest as diagnostic indicators of specific autoimmune neurological disorders such as Lambert-Eaton syndrome (Miljanich & Ramachandran, 1995).

As the VSCC subtype specificities of the ω-conotoxins vary within the group (Figure 1), it is important to carefully compare their structural features to understand which factors influence VSCC specificity. Clearly, the identical disulphide arrangement and a conserved glycine are not involved in this but instead provide a structural framework, since the δ-conotoxins, which are specific for voltage-gated sodium channels, also have these features (Miljanich & Ramachandran, 1995). Cone snails have used this framework to evolve ligands having different specificities for structurally related targets, as seen by the fact that the non-cysteine intraloop residues are critical to ω-conotoxin binding and activity (Miljanich & Ramachandran, 1995). Knowledge of 3D structure of the ω-conotoxins is an essential step towards understanding the relationship between their structure and activity, and in the design of peptidomimetic drugs.

Here we describe the structures of two naturally occurring ω-conotoxins with differing VSCC subtype specificities (MVIIA and SVIB) and one hybrid peptide, SNX-202, which has residues 9 to 12 in SVIB replaced by the corresponding residues in MVIIA. These residues were found to be important for VSCC selectivity in recent radioligand displacement studies (Nadasdi *et al.*, 1995). SNX-202 has a 38-fold increase in affinity for the N-type VSCC compared to SVIB, while another hybrid peptide, SNX-201, with residues 9 to 12 in MVIIA replaced by the corresponding residues in SVIB, displays a fourfold reduction in affinity compared to MVIIA (Nadasdi *et al.*, 1995). Of this sequence, residues 9 to 10 are of particular significance and are consistently Arg and Lys in blockers of the P/Q-type VSCC but Ser and hydroxy-Pro or Arg in blockers of the N-type VSCC.

The aim of this study was to detect structural trends which are common to all ω-conotoxins, thus reflecting the features important for these peptides in binding to VSCCs, and to detect differences which may underlie subtype specificity. The three peptides, MVIIA, SVIB and SNX-202 were synthesised and studied by ^{1}H NMR spectroscopy. A comparison of the peptides was made at two levels. First, an indication of local structural differences was obtained from NOEs, $^3J_{NH\text{-}H^\alpha}$ coupling constants and secondary H^α chemical shifts. Second, the 3D structures of MVIIA and SVIB were calculated from NOE-based distance restraints and torsion angle restraints. These structures aid in the interpretation of activity data (Nadasdi *et al.*, 1995; Haack *et al.*, 1993; Lampe *et al.*, 1993; Sato *et al.*, 1993; Kim *et al.*, 1994, 1995), which indicate that subtle differences in side-chain nature and positioning are likely to affect VSCC specificity.

All ω-conotoxins studied by ^{1}H NMR to date have been in aqueous solution (Basus *et al.*, 1995; Kohno *et al.*, 1995; Pallaghy *et al.*, 1993; Davis *et al.*, 1993; Skalicky *et al.*, 1993; Sevilla *et al.*, 1993; Nemoto *et al.*, 1995; Farr-Jones *et al.*, 1995). To assess the structural integrity of these peptides, the effect of solution environment on the structure of MVIIA was studied using H^α chemical shifts as a sensitive marker for changes in local conformation. MVIIA was studied in H_2O, 20% CD_3CN and 50% TFE solutions, and in the presence of 2 mM $CaCl_2$.

Results

Secondary structure

The ^{1}H NMR spectra of MVIIA, SVIB and SNX-202 were assigned using the protocol developed by Wüthrich (1986).

From the variation in sequential H^α-NH_{i+1} and NH-NH_{i+1} NOE strengths over the length of the peptides, the number of large ($\geq$8.5 Hz) and small ($\leq$6 Hz) $^3J_{NH\text{-}H^\alpha}$ coupling constants and the presence of several medium range NOE connectivities and slow exchange NH protons (Figure 2), it is clear that MVIIA and SVIB adopt well-defined structures in solution. A similar situation exists for SNX-202 (data not shown). Secondary structural features identified for these peptides are summarised below.

In each of the peptides, the dominant form of secondary structure is a triple-stranded β-sheet. The long range NOEs used to identify this motif are summarised in Figure 3, where residues 19 to 21 form a peripheral β-strand, linked to the central β-strand (residues 24–25 in MVIIA and 25–26 in SVIB and SNX-202) by a β-turn (residues 21 to 24) in MVIIA, and a five residue turn in SVIB and SNX-202 (residues 21 to 25), forming a β-hairpin structure. The other peripheral β-strand comprises residues 6 to 8 in each peptide. Additional support for the presence of the triple stranded β-sheet is provided by the sequential NOE data given in Figure 2. Here, the strong H^α-NH_{i+1} and weak NH-NH_{i+1} NOEs for residues 6 to 8, 19 to 21 and

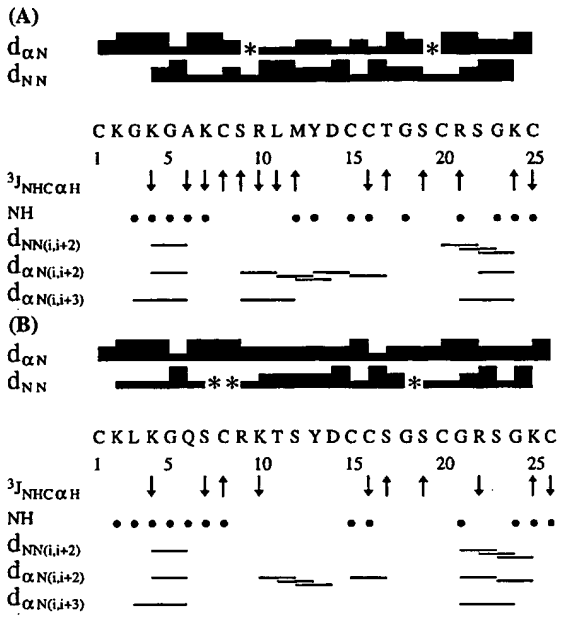

Figure 2. NMR data summary. Local and medium range NOE information (bars), $^3J_{NH\text{-}H^\alpha}$ coupling constants ($\uparrow$ $^3J_{NH\text{-}H^\alpha} \geq 8.5$ Hz; $\downarrow$$^3J_{NH\text{-}H^\alpha} \leq 6$ Hz) and slow exchange NH protons (filled circles) for (A) MVIIA and (B) SVIB.

24–25 (residues 25–26 for SVIB) are characteristic of extended conformations. This is supported by the $^3J_{NH\text{-}H^\alpha}$ coupling constants which are large for residues 8, 19, 21 and 24 (residue 25 for SVIB and SNX-202). The NH protons of residues 6, 8, 21 and 23–25 (residues 24–26 for SVIB and SNX-202) are slowly exchanging, supporting the proposed H-bond network shown in Figure 3. There is some evidence that regions of the β-sheet are distorted from ideal since Ala6, Lys7 and Cys25 (Cys26 for SVIB and SNX-202) have small $^3J_{NH\text{-}H^\alpha}$ coupling constants.

The medium-range NOE data (i.e. H^α-NH_{i+2}, NH-NH_{i+2} and NH-NH_{i+3} connectivities) indicate that several turns are present in MVIIA, SVIB and SNX-202. In addition to the aforementioned β-turn comprising residues 21 to 24 in MVIIA, a β-turn at residues 3 to 6 and a series of overlapping turns along the region incorporating residues 9 to 18, which links the β-strand 6 to 8 to the central β-strand, are identifiable. Similarly, these connectivities are observed in SVIB and SNX-202. Having determined the major elements of secondary structure, the NMR data described in the following sections were used to identify structural similarities and differences amongst the ω-conotoxins, particularly in the hypervariable loop regions.

Secondary H^α chemical shifts and $^3J_{NH\text{-}H^\alpha}$ coupling constants

Figure 4 shows a comparison of the secondary H^α shifts (i.e. chemical shifts relative to random coil values based on values obtained from Wishart *et al.*, 1991, 1995) for MVIIA, SVIB and SNX-202

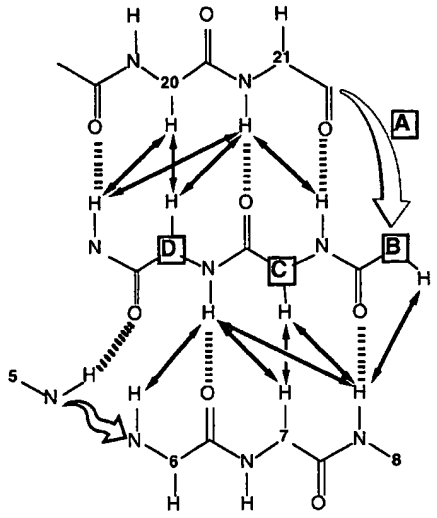

Figure 3. The ω-conotoxin β-sheet. Schematic of the triple-stranded β-sheet observed for MVIIA, SVIB and SNX-202. Because of sequence differences, the generic residue labels A to D are used where, in MVIIA, A = Ser22, B = Gly23, C = Lys24 and D = Cys25; for SVIB and SNX-202, A = residues 22 to 23, B = Gly24, C = Lys25 and D = Cys26. Double-headed arrows indicate observed NOEs, the turn forming part of the β-hairpin is represented by an open single headed arrow and broken lines indicate proposed H-bonds. Note that an H-bond from the amidated C terminus to residue 19 has not been detected experimentally, but is indicated here to show that its presence may stabilise the β-sheet.

from this study and for MVIIC (Farr-Jones *et al.*, 1995). As anticipated, the secondary shifts are almost identical, reflecting similar backbone conformations. The alignments used are those depicted in Figure 1, apart from in the β-hairpin region, where residues Arg21-Ser22 in MVIIA correspond to residues Gly21-Arg22 in MVIIC, SVIB and SNX-202. This is based on similarity of backbone conformation rather than residue type so that the position of the positive charge on Arg21 in MVIIA is shifted by one residue with respect to the corresponding positive charge on Arg22 in SVIB, MVIIC and SNX-202. Apart from effects due to these changes in loop 4, the only region that exhibits secondary shift differences is within loop 2. Although relatively minor, all residues in this loop have differences in secondary H^{α} shifts amongst the set of peptides. Most notable are those of residues 9–10, which are similar in SVIB and MVIIC but different to those of MVIIA and SNX-202. In addition, Tyr13 and Asp14 in SVIB have different shifts to the corresponding residues in the other peptides, and this may reflect a conformational change in loop 2 (see later).

Changes in local conformation across a set of peptides are detectable by analysis of their $^{3}J_{NH\text{-}H^{\alpha}}$ values. These are shown in Figure 5 for MVIIA, SVIB and SNX-202. Overall, the likeness is remarkable, indicating that despite the low sequence identity the ω-conotoxins maintain similar elements of local structure. Differences are evident at residues 6, 12 and 22 in MVIIA. The local conformational difference at residue 6 is not likely to be significant in VSCC subtype discrimination, as the corresponding residue in MVIIC has, in common with MVIIA, a low $^{3}J_{NH\text{-}H^{\alpha}}$ value (Farr-Jones *et al.*, 1995). An analogous situation applies to residue 10, which has a small $^{3}J_{NH\text{-}H^{\alpha}}$ value

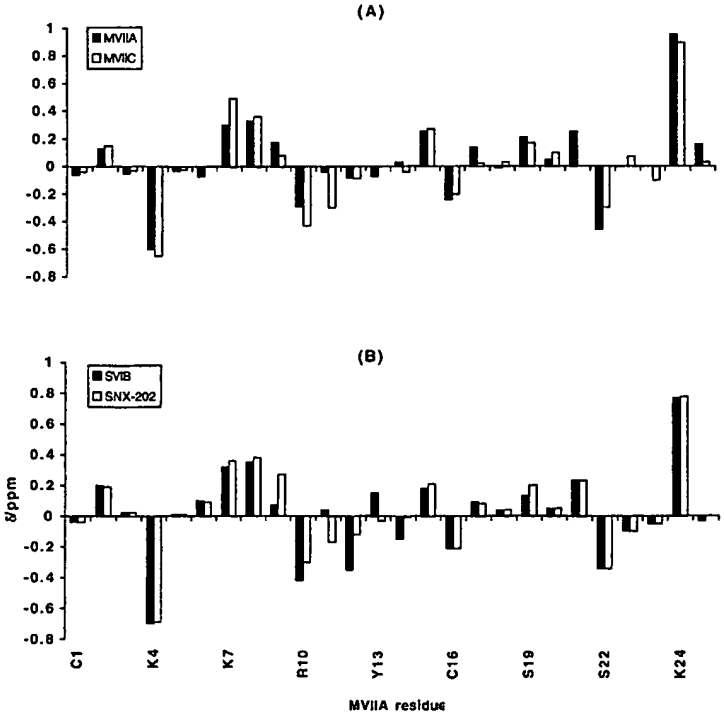

Figure 4. Secondary H^{α} shifts. (A) MVIIA (shaded) and MVIIC (outlined) and (B) SVIB (shaded) and SNX-202 (outlined). The comparison is made on two graphs for clarity and the shifts are plotted using the MVIIA numbering scheme. For Ala6 in MVIIC, the appropriate shift correction for a residue preceding Pro has been made (Wishart *et al.*, 1995).

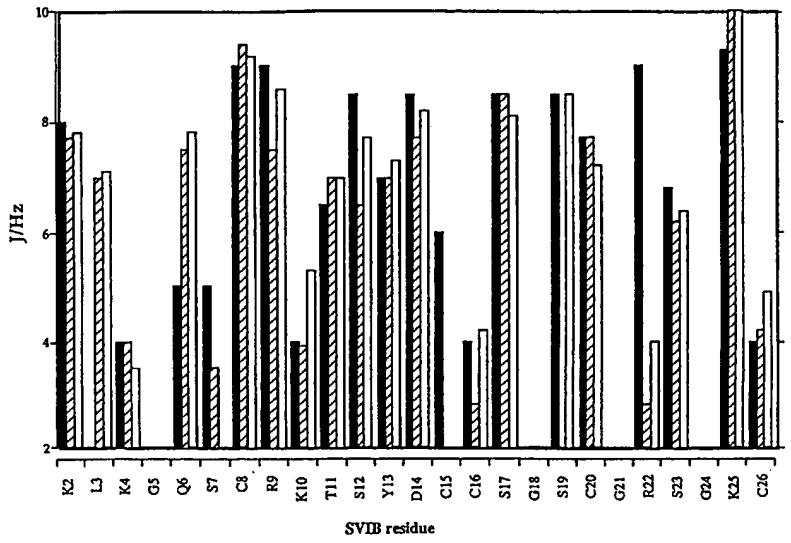

Figure 5. $^3J_{NH\text{-}H^\alpha}$ coupling constants. $^3J_{NH\text{-}H^\alpha}$ coupling constants plotted against SVIB numbering scheme for MVIIA (filled), SVIB (hatched) and SNX-202 (open).

for all peptides except MVIIC (Farr-Jones *et al.*, 1995; data not shown). The variation seen for residue 12 may reflect conformational differences; however, it may also arise from errors associated with the broad NH linewidths of this residue. The large $^3J_{NH\text{-}H^\alpha}$ for Arg21 in MVIIA is consistent with an extended conformation, consistent with its involvement in the β-sheet, while the small coupling constants for the corresponding residues in SVIB and SNX-202 suggest that Arg22 resides on the β-hairpin turn. Interestingly, this is similar to what is observed for MVIIC (Farr-Jones *et al.*, 1995).

In summary, the qualitative analysis of the raw NMR data described above confirms that the structures of MVIIA, SVIB and SNX-202 are remarkably similar. Conformational differences appear to be localised mainly in loops 2 and 4. Changes in loop 2 are significant because it incorporates residues that are reputedly involved in VSCC subtype discrimination in ω-conotoxins (Nadasdi *et al.*, 1995). Loop 4 has sequence substitutions and deletions over the set of peptides and, in MVIIA, contains a residue (Arg21) that contributes significantly to binding with the N-type VSCC (Nadasdi *et al.*, 1995). Changes in loop size may have an effect on the placement of functionally important side-chains but to verify this it was necessary to determine 3D structures, as described below.

3D structure of MVIIA and SVIB

A set of 50 structures was calculated using a total of 323 (369) distance restraints derived from 139 (135) intraresidual, 86 (94) sequential and 98 (140) long/medium range NOEs, 24 (22) distance restraints defining 12 (11) H-bonds and torsional restraints defining 19 (15) φ and 9 (11) χ1 dihedral angles (values for SVIB are shown in parentheses). The 20 lowest energy structures were chosen to represent MVIIA and SVIB in solution. Side-by-side views in Figure 6 show that the peptides have almost identical compact structures with loops 1, 2 and 4 protruding from the core. The only discernible difference is the relative orientation of loops 2 and 4, where loop 4 adopts an upward tilt towards loop 1 in the SVIB structures.

Quality of structures

As the backbone pairwise RMSD values show (Table 1), the MVIIA structures are better defined than the SVIB structures, despite the larger number of NOEs observed in the latter case, but reflecting more $^3J_{NH\text{-}H^\alpha}$ derived torsion angle restraints for MVIIA. Both structures satisfy experimental and empirical criteria; the average deviations from ideal covalent geometry and experimental restraints are low and the potential-energy and restraint energy contributions are favourable (Table 1).

The atomic RMSD by residue for the backbone atoms of MVIIA and SVIB shows that the best agreement amongst the structures is in the β-sheet regions and for residues involved in disulphide bridges. Both sets of structures exhibit higher RMSD values in loops 2 and 3, reflecting either motion or a lack of NOEs at these sites. The backbone angular order parameters, $S(\phi)$ and $S(\psi)$ are well defined (≥ 0.8) for all residues in MVIIA; however, as foreshadowed by elevated RMSD values, some residues in loops 2 and 3 have marginally lowered S values. For SVIB, these are further reduced due to fewer φ angle restraints in loop 2. For residues 10 to 12, the low S values are misleading since the ϕ/ψ angles are not dispersed, but are clustered into two distinct regions of the Ramachandran plot. This suggests that both conformations are consistent with the experimental data or alternately, that a concerted flip between the two conformations occurs. The latter hypothesis is more consistent with the observed $^3J_{NH\text{-}H^\alpha}$

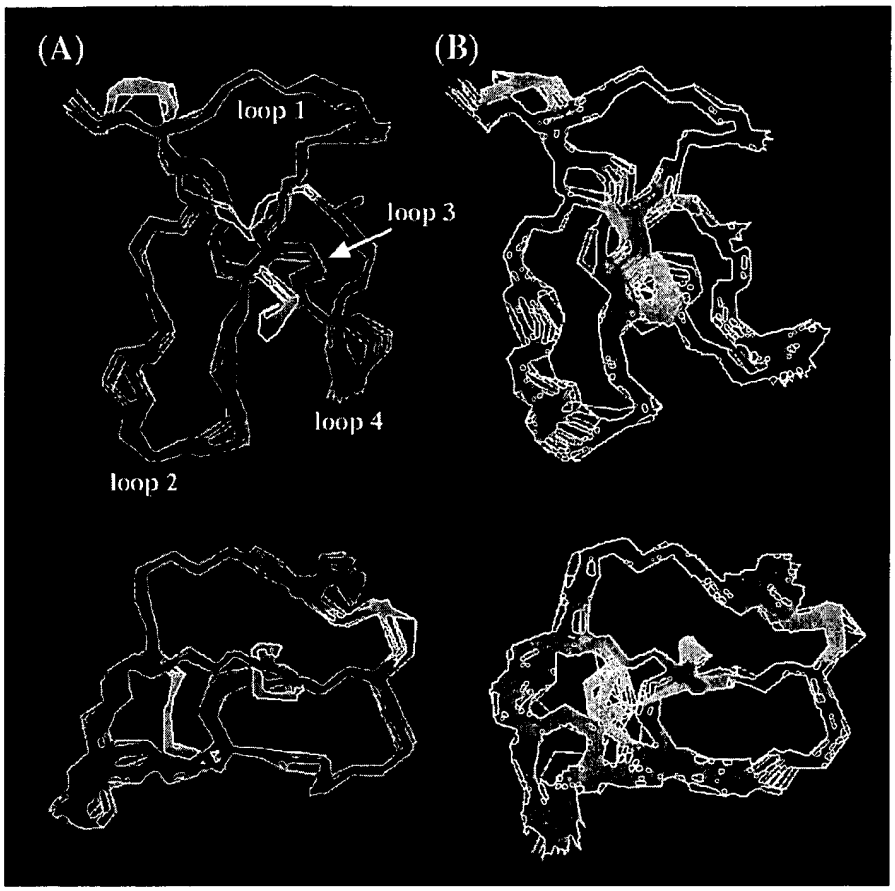

Figure 6. Global backbone superimpositions of the 20 lowest energy structures. (A) MVIIA (green) showing the positions of the four structural loops and (B) SVIB (pink) structures. Disulphide bonds are shown in yellow. The structures were superimposed over the backbone atoms of residues 1 to 20 (average RMSD = 0.94 Å) to obtain a similar view. The lower view is related to the original view by a $90°_z$-$90°_x$ set of rotations.

values (~7 to 8 Hz) which reflect conformational averaging.

Description of local geometry

A Ramachandran analysis of local geometry confirms the qualitative deductions about secondary structure made earlier. In particular, the β-sheet regions of the two peptides are almost identical, as are the deviations from ideal secondary structure, i.e. at residues 6–7 and 20, which form part of the triple-stranded β-sheet but are in the β_P region of the Ramachandran plot.

Similar turn types in MVIIA and SVIB occur at residues 3 to 6, which form a $\beta_P\gamma$ β-turn (using the nomenclature of Wilmot & Thornton, 1990) and residues 15 to 18 (αα type). The greatest differences in turn types are in loops 2 and 4. In MVIIA, the

Table 1. Geometric and energetic statistics for 20 structures of MVIIA and SVIB

	MVIIA	SVIB
Pairwise RMSD for C^α, N, C atoms (Å)	0.59	0.77
RMSD from distance restraints (Å)	0.016 ± 0.001	0.016 ± 0.002
RMSD from dihedral restraints (°)	0.37 ± 0.13	0.22 ± 0.09
RMSD from idealised geometry:		
Bonds (Å)	0.007 ± 0.00	0.008 ± 0.001
Angles (°)	2.00 ± 0.04	2.14 ± 0.04
Impropers (°)	0.16 ± 0.01	0.18 ± 0.02
Energies (kcal mol^{-1}):		
E_{NOE}	2.68 ± 0.47	3.13 ± 0.64
E_{cdih}	0.15 ± 0.12	0.09 ± 0.07
$E_{L\text{-}J}$	−98.2 ± 3.8	−105.6 ± 3.4
$E_{bond} + E_{angle} + E_{improper}$	402 ± 1.7	47.4 ± 1.6

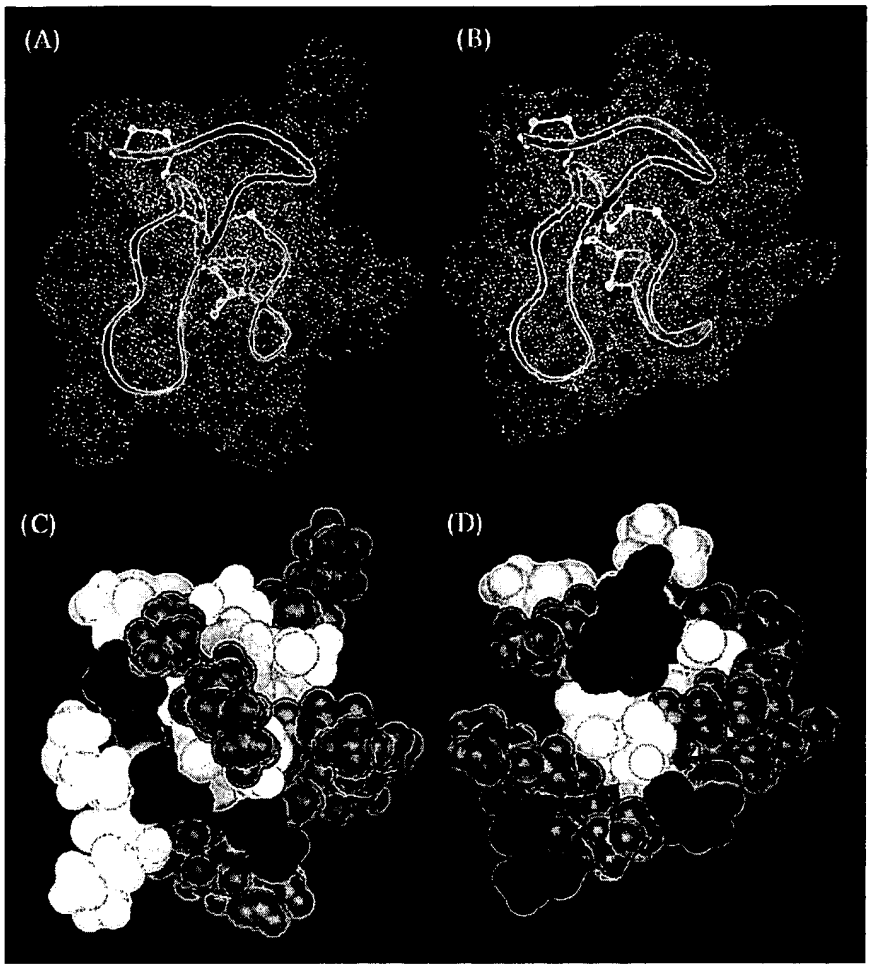

Figure 7. Surface views of the lowest energy structures for (A) MVIIA and (B) SVIB. Colour coding is as follows: Connolly surface (white dots), backbones (blue ribbon) and the disulphide bridges (yellow). The same views are given in (C) and (D) where the surfaces are colour coded: positively charged residues (blue); negatively charged residues (red); polar residues (green); hydrophobic residues (yellow) and glycine residues (white).

β-turn in loop 4 (residues 21 to 24) adopts a γγ conformation while the corresponding five-residue turn in SVIB (residues 21 to 25) adopts a αγγ conformation, and forms part of a G1-type β-bulge, similar to what is observed in GVIA (Pallaghy *et al.*, 1993). The turns in loop 2 are more difficult to classify as there is no unambiguous demarcation between them. However, on the basis of established distance criteria (Lewis *et al.*, 1973) a β-turn involving residues 9 to 12 is present in both peptides.

In the 3D structures there are differences between the H-bonding patterns of loop 2 for SVIB and MVIIA, particularly with respect to possible acceptors for the NH proton of Asp14. However, it is difficult to reliably quantify this since the broad linewidths observed at residues 11 to 13 are a limiting factor to the analysis. The broad linewidths suggest that conformational exchange occurs in this region, perhaps as a flip between different turn types or as a shifting of turn loci. The uncertainty in the conformation of this region is highlighted by a comparison of our MVIIA structures with those described by Kohno *et al.* (1995), where there are minor conformational differences for residues 9 to 14. The structural differences between MVIIA and SVIB in loop 2 may arise from local effects due to variance in amino acid composition or possibly from longer range effects due to the different relative positioning of residues on loop 4.

Surface profile

Small biologically active polypeptides such as the ω-conotoxins have functional groups exposed on their surface for interaction with their receptor. Therefore, to gain information on which residues contribute to activity it is important to investigate the surface profile of these peptides. This includes the surface shape, charge/hydrophobicity distribution and solvent accessibility of individual residues. The surface shapes of MVIIA and SVIB are similar, as is evident in Figure 7(A) and (B), indicating that the N/P/Q-subfamily of VSCCs have related ω-conotoxin macrosites. In contrast, the distributions of charged, hydrophobic and polar

residues on the surface are dissimilar (Figure 7(C) and (D) and are likely to form the basis of the different specificities. In general, the hydrophobic residues are less exposed than the polar and charged residues, so that both peptides form a hydrophobic core and a highly charged polar surface. However, there are some exceptions; most notably Leu11 in MVIIA and, to a lesser degree Leu3, in SVIB are solvent exposed. The former, at least, is known to contribute strongly to the binding interaction of MVIIA with its receptor (Nadasdi *et al.*, 1995). Other exposed hydrophobic residues are Cys1 and Cys16, which form a disulphide bridge. It is notable that the corresponding disulphide bridge in the structurally related "squash" peptides (Pallaghy *et al.*, 1994) is not considered important for the peptide's ability to fold and is the first bridge to open under reducing conditions (Le-Nguyen *et al.*, 1993). The other cysteine residues form the core of MVIIA and SVIB, consistent with a role in maintaining 3D structure *via* involvement in disulphide bridges. Polar and charged residues, which are less exposed to solvent, include Ser9 and Asp14 in MVIIA, and Ser12 and Asp14 in SVIB. The relative shielding of these residues suggests that they may play a role in maintaining the structure of loop 2, thereby placing the functionally more important side-chains in optimum positions for receptor interactions. In general, residues which have been shown to be important for the binding of MVIIA to the N-type VSCC (Nadasdi *et al.*, 1995) have increased solvent accessibility compared to the core residues. Residue 17, a polar residue, is notable for its high degree of exposure in both peptides; however, its contribution to activity is not known.

Solvent effects

Different solvents were used to study the structural integrity of the ω-conotoxins, particularly to investigate the possibility of alternate conformations in loops 2 and 3. MVIIA and SVIB have several H^{α}-NH_{i+2} NOEs in these loops (Figure 2) and, while these have been interpreted in terms of a series of overlapping turns, their presence is also a feature of nascent helical structures, which generally form a stabilised helix in the presence of structure-promoting solvents such as TFE (Sönnichsen *et al.*, 1992). Furthermore, a region of α-helix for residues 12 to 20 is consistently predicted in a hydrophobic environment for the ω-conotoxins shown in Figure 1 (data not shown). This has not been detected in any of the ω-conotoxins studied to date; however, there have been no reports on their structures in solvents other than water. Here, MVIIA was examined by ^1H NMR in 20% CD_3CN/80% H_2O and 50% TFE/50% H_2O solvent mixtures, and in aqueous solution in the presence of salt (2 mM $CaCl_2$). H^{α} shifts were chosen to compare the peptide conformation in the four solvents as they are relatively insensitive to external conditions but are good indicators of changes in secondary structure (Pastore & Saudek, 1990). The hydrophobic solvents have no effect on the H^{α} shifts, nor does the presence of salt, even in the region predicted to form helix. Thus, the conformation of MVIIA appears to be stable. This is an important result as it shows that this class of peptide is relatively impervious to environmental conditions and hence supports the suggestion that the receptor-bound conformation may be similar to that observed in solution. However, the possibility of specific receptor-induced conformational changes in the peptide cannot be completely discounted.

Discussion

It is important to identify structural similarities amongst the ω-conotoxins to aid in determining a generalised picture of the features that contribute to their activities in blocking VSCCs. From this study and previous reports on GVIA (Pallaghy *et al.*, 1993; Davis *et al.*, 1993; Skalicky *et al.*, 1993; Sevilla *et al.*, 1993), MVIIC (Nemoto *et al.*, 1995; Farr-Jones *et al.*, 1995) and, more recently, MVIIA (Basus *et al.*, 1995; Kohno *et al.*, 1995), emerges a canonical structure of ω-conotoxins that includes the triple-stranded β-sheet/disulphide knot motif described by Pallaghy *et al.* (1994). This provides a stable base from which critical side-chains are anchored. The structures also have in common a β-turn preceding the first β-strand followed by a series of turns. The high degree of structural similarity found for these peptides, despite their different activities, supports the notion that the ω-conotoxin macrosites on the N and P/Q-type VSCCs are related.

Having established the similarities, structural differences can be examined and correlated to function. These are potentially more interesting as they may provide information on what contributes to VSCC subtype specificity. It has been shown here that differences in backbone conformation are minimal but may include the conformation of loop 2 and the relative orientation of loop 4. However, the greatest determinant is likely to be the positions of the charged, polar and hydrophobic side-chains on the surface of the peptides.

Charge and polarity distribution

In contrast to Na^+ and K^+ channels, little is known about the structural features of the Ca^{2+} channel which make it susceptible to toxin blockage. A recent study on the interactions of GVIA with chimeric proteins combining individual motifs from the N-type VSCC has shown that a cluster of residues on a putative large extracellular loop contributes to toxin binding (Ellinor *et al.*, 1994). Mutations at several sites along this loop, particularly Glu → Lys and Gln → Arg substitutions, caused significant decreases in the rate of toxin block, indicating that a negative charge, or the electron-acceptor properties of the amino acid

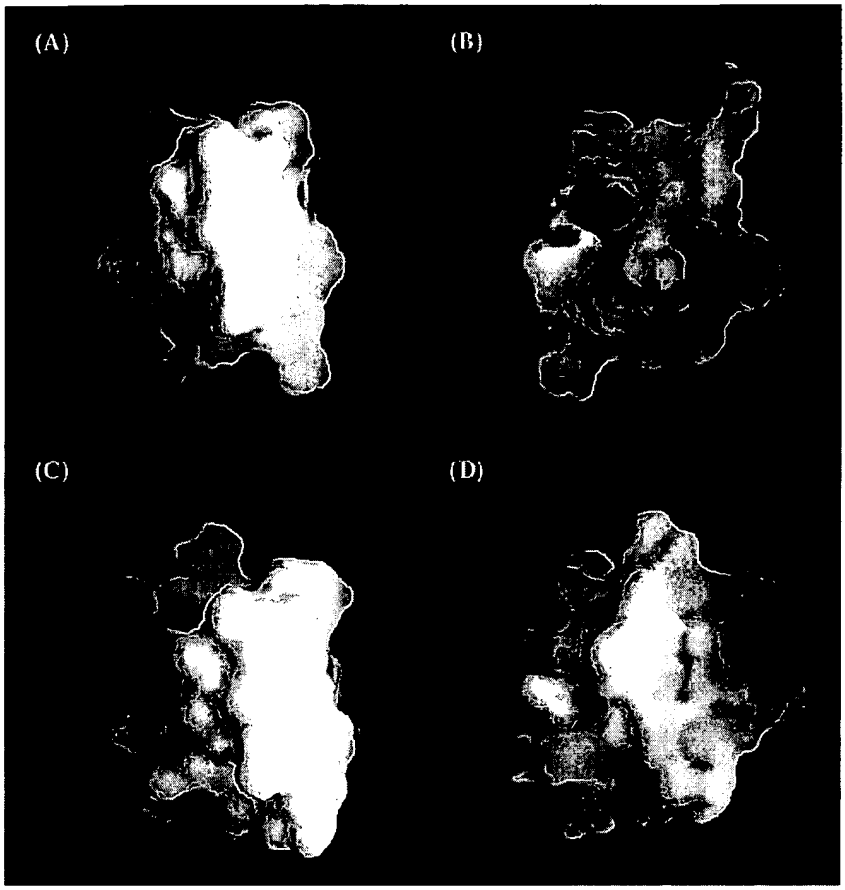

Figure 8. Surface charge distributions of MVIIA and SVIB. The lowest energy MVIIA structure coloured according to charge (blue for positive, red for negative) showing (A) the neutral face and (B) the same structure rotated by 180°. The corresponding views of SVIB are shown in (C) and (D). Figures were generated using GRASP (Nicholls *et al.*, 1991).

side-chain are important prerequisites for the receptor at these sites. Not surprisingly, the ω-conotoxins are rich in strategically placed positively charged (Arg, Lys) and hydroxylated (Thr, Ser, Tyr, Hyp) residues. The distribution of formal charges on the surface (Figure 8) shows that while one face of both MVIIA and SVIB is neutral, the other face has a strong, positive electrostatic potential which may form the basis of the initial attraction to the VSCC ω-conotoxin macrosite.

The relative contribution of the individual positive charges to N-type VSCC inhibition in MVIIA has been investigated using Ala substitutions or, in the case of the N terminus, N-acetylation (Nadasdi *et al.*, 1995). The results show that the order of importance is: Lys2 > Arg10 > N terminus > Arg21 > Lys7 > Lys4 > Lys24, with the latter three substitutions having little effect on potency. In the 3D structure of MVIIA, the functionally important positive charges are not clustered in one region, emphasising that no one site forms the ω-conotoxin/VSCC binding interface. Instead, in binding to the VSCC macrosite these peptides are likely to form points of attachment at several microsites, each making significant contributions to optimal binding (Olivera *et al.*, 1994). In MVIIA, the positive charges of Lys2 and the N terminus are near to one another, as are those of Arg21 and Arg10, but these two clusters of charge are diametrically opposed. Figure 9 shows the positions of these side-chains on the MVIIA structures and compares them with their counterparts in SVIB. The N-terminal and Lys2 charges are placed identically in both peptides, indicating that this is may be an important generic feature for ω-conotoxins binding to VSCCs.

Of other important positive charges in MVIIA, Arg21 is shifted by one residue and Arg10 is replaced by Lys10 in SVIB. As mentioned in the Results, there are apparent conformational differences between Arg21 in MVIIA and Arg22 in SVIB in loop 4 which, in concert with the middle segment, may play a role in determining VSCC specificity. Surprisingly, Arg21 in MVIIA occupies approximately the same region of space as Arg22 in SVIB, despite the sequence displacement and the fact that these residues form different elements of secondary structure. This is an important result as it indicates that a positive charge in this relative position may be conducive to binding to the N/P/Q-subfamily of VSCCs but has little influence on subtype differentiation. Thus, the confor-

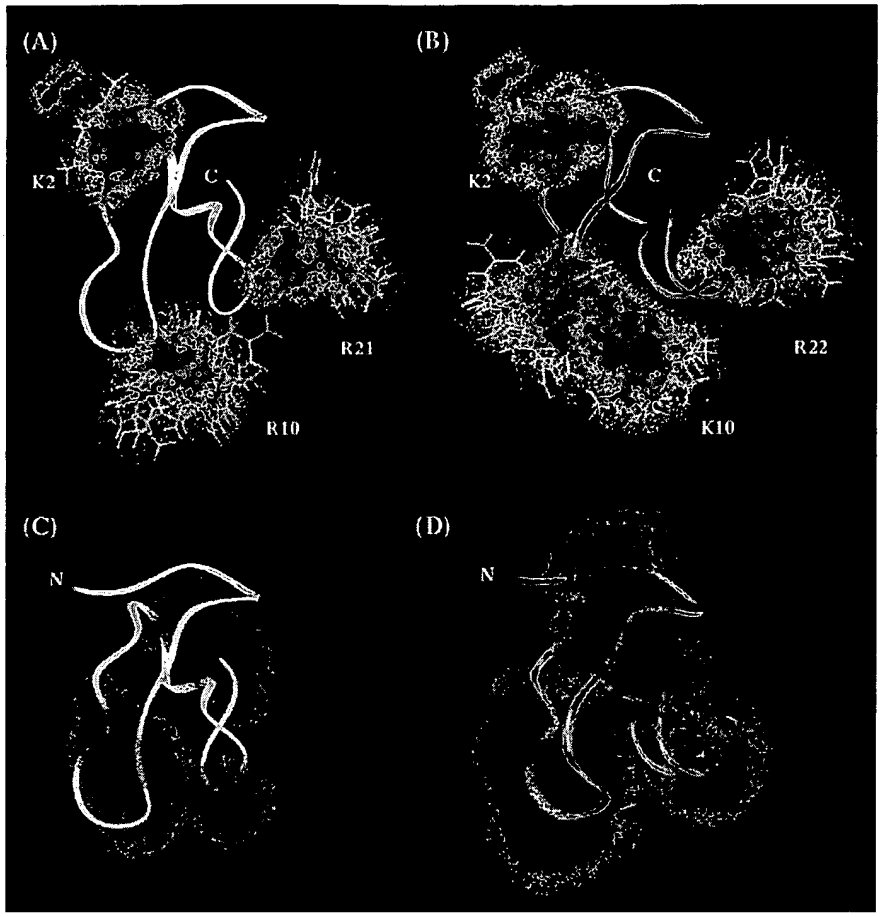

Figure 9. Surface distributions of charged and polar amino acids. The lowest energy structure of (A) MVIIA (yellow ribbon) and (B) SVIB (pink ribbon) in equivalent views showing the positions of selected positive charges (blue) for all 20 structures. The same views in (C) and (D) show the positions of the polar side-chains (green).

mational difference between MVIIA and SVIB at loop 4 is likely to reflect the fulfilment of a charge requirement. Also indicated in Figure 9(B) is the extra charge on SVIB at position 10. This may be important for VSCC subtype differentiation, as all known ω-conotoxins with P/Q-type VSCC selectivity (SVIB, MVIIC and MVIID) carry two consecutive positive charges at positions 9–10, in contrast to specific N-type VSCC blockers that are charged at position 9 and prefer a serine at position 10.

The large numbers of hydroxyl-bearing residues in the ω-conotoxins, and in the μ-conotoxins, which target voltage-gated sodium channels, may also play a significant role in receptor binding. Apart from the hydroxyl group on Tyr13, their role has not been examined by structure-activity studies. However, it is conceivable that they may influence the binding of ω-conotoxins to their receptor by participation in H-bonding interactions or by increasing the overall surface polarity. Hydroxyl-bearing side-chains are also potential sites for post-translational modifications but this has not been reported to date for ω-conotoxins. For MVIIA and SVIB the distribution of surface exposed hydroxyl groups differs (Figure 9(C) and (D)). While every polar residue on the surface of MVIIA has a counterpart in SVIB, there are many more polar residues on the surface of the latter peptide. However, there are no specific trends in primary structure, nor are there activity data available on ω-conotoxins which do not target N-type VSCCs that would explain this observation.

Loop 2

In the MVIIA structures, loop 2 is exposed, with the side-chains of Arg10, Leu11 and Tyr13 oriented towards the solvent. Therefore, it is feasible that these residues are critical for binding to the VSCC. By specific amino acid substitutions, Nadasdi *et al.* (1995) found that the phenolic group on Tyr13 contributes strongly to binding affinity, as does the Leu11 side-chain (although a Thr at this position is also tolerated). A Tyr at position 13 is generally but not always present in ω-conotoxins with N or P/Q-type VSCC specificity. This residue is replaced by Arg in GVIIA and GVIIB, both N-type VSCC blockers with low potencies, and in SVIA by Ile (not active). Interestingly, these peptides all have a Tyr in loop 4 which, judging from the GVIA and MVIIA

structures, is also likely to be exposed, in principle providing a different microsite interaction at the VSCC macrosite.

Recently, a 49-residue peptide, SNX-325, isolated from the venom of the spider, *Segestria florentina*, was found to a be a selective N-type VSCC antagonist (Newcomb *et al.*, 1995). The sequence of SNX-325 has been compared to MVIIA and found to contain a middle segment, Ser-Arg-Ser-Met-Lys-Asn, which bears a strong resemblance to residues 9 to 14 of the ω-conotoxins with N-type VSCC specificity (Newcomb *et al.*, 1995). This indicates that there is possibly some macrosite overlap on the N-type VSCC among these peptides. In SNX-325, Tyr13 is replaced by a positively charged Lys, similar to the Arg replacement in GVIIA and GVIIB, and, in addition, there is a Tyr at position 44 that may correspond to Tyr22 in these two peptides. However, the 3D structure determination of SNX-325 is required to confirm this suggestion.

Loop 2 is indisputably important for the binding of the ω-conotoxins to either N or P/Q-type VSCCs. This is demonstrated by the fact that SVIA, which has several sequence changes and lacks a residue at position 14, is a poor binder to either of these channel subtypes. The functional role of Asp14 is unclear. In MVIIA, its substitution by Ala leads to a 75% reduction in the binding affinity (Nadasdi *et al.*, 1995); however, this residue is not highly exposed on the surface (~25%) and may be important for structural interactions with the side-chain of Ser9 in MVIIA or with Ser12 in SVIB, which are also not highly exposed. Thus, Asp14 may have a role in directing the conformation of loop 2, which appears to differ, albeit in a subtle way, amongst the ω-conotoxins studied here.

Comparison of MVIIA structures

Although there has been no previous report on the structures of SVIB and SNX-202, two structures of MVIIA were reported while the manuscript was in preparation (Basus *et al.*, 1995; Kohno *et al.*, 1995). These structures, calculated by independent means, are in general agreement with ours. The structures described by Basus *et al.* (1995) and Kohno *et al.* (1995) were based on the observation of fewer NOEs than reported here. In the study of Kohno *et al.* (1995), low RMSD values were reported, but these reflect the fact that only 13/100 structures (i.e. 13% of the total calculated structures) converged to the same fold. The reason for this low rate of convergence is not clear. In our case the convergence rate was much higher; we chose 20/50 structures on the basis of low energy to represent MVIIA, although more than 80% of the total calculated structures converged to the same fold. The analysis of Basus *et al.* (1995) was also based on a majority (61%) of calculated structures. However, the quality of their structures was significantly improved (i.e. the RMSD dropped from 0.85 Å to 0.59 Å) by the introduction of non-NOEs (approximately 24% of the total NOEs). In general, our preference is to calculate structures based on the positive observation of NOEs rather than on their absence, since other factors, including local motion, may inhibit the observation of NOEs for proximal protons (Kuntz *et al.*, 1989). The use of non-NOEs becomes more uncertain where large amplitudes of motion are present; however, the rigidity of MVIIA suggests that their use may be acceptable in the case of ω-conotoxins.

Conclusion

Marine molluscs of the Family Conidae (~500 species) have evolved a cocktail of bioactive peptides, used in the capture of their prey (either fish, molluscs or worms). The peptides are synthesised in a venom duct and delivered through a hollow, barbed radula tooth. One class of conopeptides, the ω-conotoxins from piscivorous *Conus* spp., are highly potent and selective blockers of voltage-sensitive calcium channels (VSCCs) that have proved valuable research tools to help unravel the role played by the different VSCCs in cellular processes such as transmitter release. The present work describes the solution structures of MVIIA, SVIB and a synthetic hybrid SNX-202. Comparison of these structures reveals features important for their different specificities for the various VSCC subtypes.

Using MVIIA as a model, we confirm that the ω-conotoxins are rigid peptides with a structure that is likely to be little altered on changing the environment. Rigidity is conferred by three disulphide bonds which direct the folding of the ω-conotoxins into a class of four-loop peptides that possess almost identical secondary structure, despite considerable differences in primary structure. Structural similarities among the ω-conotoxins suggest that this class of peptide binds to a common VSCC macrosite that varies slightly amongst the different VSCC subtypes. Several other classes of four-loop peptides from *Conus* spp. have activity at less related sites, including the δ-conotoxins, which delay inactivation of voltage sensitive sodium channels, and the μO-conotoxins and κ-conotoxins, which block the sodium and potassium channels, respectively. From this work, it is evident that these too will adopt similar structures to the ω-conotoxins. However, the positioning of positively and negatively charged and hydrophobic amino acids is quite different amongst these classes of peptides. Thus, the four-loop framework appears an efficient template upon which to develop small bioactive peptides and as such is an attractive starting point for combinatorial library development.

The structure of the ω-conotoxin family of peptides comprises a triple-stranded β-sheet and several turns. Detailed comparison of the 3D structures of MVIIA (specific for N-type VSCC) and SVIB (specific for P/Q-type VSCC) reveal remarkable structural similarities, with the only differences being subtle changes in backbone conformation in loops 2 and 4. These peptides, parti-

cularly MVIIA, are being exploited as leads to new neuroprotective drugs for the treatment of diseases such as stroke. The structures presented here are refined models for peptidomimetic VSCC blocker development. We have shown that the location of side-chains important for ω-conotoxin binding are well defined but widely distributed. The challenge will be to produce small molecule peptidomimetics of the ω-conotoxins that correctly present these groups for selective binding to VSCC subtypes. The extent to which molecular rigidity is important to the ability of the ω-conotoxins to bind and block the VSCC is unclear.

Materials and Methods

Synthesis of MVIIA, SVIB and SNX-202

All amino acids were obtained from the Peptide Institute Company. p-MBHA resin was obtained from Peninsula Laboratories. Other reagents were of peptide synthesis grade. Linear peptides were synthesised using solid phase BOC-chemistry methodology on an Applied Biosystems 430A synthesiser (MVIIA), or with manual HBTU *in-situ* coupling techniques (SVIB and SNX-202), starting from p-MBHA resin using a p-MeBzl group for protection of the SH groups on cysteine residues. After HF cleavage, the crude peptides were purified using preparative HPLC on a Vydac C18 2.2 cm × 25 cm column. The cyclised products were obtained by air oxidation in 0.33 M NH_4OAc/0.5 M GnHCl (pH 7.8, 0.5 mM) in the presence of reduced (GSH), oxidised (GSSG) glutathione (molar ratio of peptide: GSH:GSSG was 1:100:10). The reaction mixture was stirred at 4°C for three days, monitored by HPLC and stopped by lowering the pH to 1 with TFA. The crude cyclised product was purified by preparative HPLC. Purity was confirmed by analytical HPLC (Waters Delta pak C18 300A 3.9 mm × 30 cm column), and the correct mass for the oxidised products was obtained using a PE Sciex API triple quadrupole mass spectrometer.

NMR data

All NMR spectra were recorded on a Bruker ARX 500 spectrometer equipped with a *z*-gradient unit. Peptide concentrations were in the range 1 to 3 mM (pH 3 to 3.5) in 95% H_2O/5% ^2H_2O and 100% ^2H_2O for MVIIA, SVIB and SNX-202 and, additionally, in 20% CD_3CN/80% H_2O; 2 mM $CaCl_2$ in 95% H_2O/5% ^2H_2O and 50% d_3-TFE/50% H_2O (v/v) for MVIIA. ^1H NMR experiments run were DQF-COSY (Rance *et al.*, 1983), NOESY (Jeener *et al.*, 1979; Kumar *et al.*, 1980), with mixing times of 400, 200, 100 and 50 ms, TOCSY (Bax & Davis, 1985) with a mixing time of 65 ms, and E-COSY (Greisinger *et al.*, 1987). All spectra were recorded at 293 K with additional NOESY spectra recorded at 283 K. Temperature coefficients were measured by from a series of TOCSY spectra at 5 K intervals from 283 to 303 K.

Spectra were recorded over 6024 Hz with 4096 data points, 512 to 600 FIDs, 16 to 64 scans and a recycle delay of one second (1.5 seconds for DQF-COSY and E-COSY). In NOESY and TOCSY experiments, the solvent was suppressed using the WATERGATE sequence (Piotto *et al.*, 1992). Spectra were processed using UXNMR. FIDS were multiplied by a polynomial function and apodised using a 60° or 90° shifted sine-bell function in both dimensions prior to Fourier transformation. Baseline correction using a fifth order polynomial was applied and chemical shifts were referenced externally to DSS at 0.00 ppm. $^3J_{NH\text{-}H^\alpha}$ coupling constants were measured from high resolution 1D spectra (32 K) and compared to those obtained from the DQF-COSY spectra, which were strip transformed to 8192 × 1024 and extracted using the Lorentzian line-fitting routine in the program Aurelia (Bruker GMBH). $^3J_{H^\alpha\text{-}H^\beta}$ coupling constants were measured directly from E-COSY spectra, strip transformed to high digital resolution (8192 × 1024).

Distance restraints and structure calculations

Peak volumes in NOESY spectra were classified as strong, medium, weak and very weak corresponding to upper bounds on interproton distances of 2.7, 3.5, 5.0 and 6.0 Å, respectively. Lower distance bounds were set to 1.8 Å. Appropriate pseudo-atom corrections were made (Wüthrich *et al.*, 1983) and distances of 1.5 Å and 2.0 Å were added to the upper limits of restraints involving methyl and phenyl protons, respectively. $^3J_{NH\text{-}H^\alpha}$ coupling constants were used to determine ϕ dihedral angle restraints (Pardi *et al.*, 1984), and $^3J_{H^\alpha\text{-}H^\beta}$ coupling constants together with relevant NOESY peak strengths were used to determine χ_1 dihedral angle restraints (Wagner *et al.*, 1987). Where there was no diastereospecific assignment for a prochiral pair of protons, the larger upper bound for the two restraints was used but where stereospecific assignments were established, the distances were specified explicitly.

Structures were calculated (co-ordinates have been deposited with the Brookhaven Protein Databank: ID codes 1MVI and 1MVJ) using the simulated annealing protocol in X-PLOR (Brünger *et al.*, 1986; Brünger, 1992) version 3.1 using the geometric forcefield, parallhdg.pro. Starting structures were generated using random (ϕ, ψ) dihedral angles and energy minimised (500 steps) to produce structures with correct local geometry. The structures were subjected to a total of 30 ps of high temperature molecular dynamics before cooling to 0 K and final energy minimization (1000 steps). Structure refinements were performed using energy minimization (2000 steps) under the influence of the CHARMM forcefield (Brooks *et al.*, 1983).

Data analysis

Structures were compared using pairwise and average RMSD values for the C^α, C and N atoms (X-PLOR version 3.1) and by calculating angular order parameters for the backbone dihedral angles (Pallaghy *et al.*, 1993; Hyberts *et al.*, 1992). Solvent accessibility calculations and structure visualisation were done using INSIGHTII (Biosym technology inc.). Structure predictions were carried out using the program ALB (Ptitsyn & Finkelstein, 1983), which simulates the secondary structures of proteins based on primary structure in aqueous, partial hydrophobic and hydrophobic environments.

Acknowledgements

This work was supported by a GIRD grant from the Department of Industry, Science and Tourism, and AMRAD Corporation Ltd. D.J.C. is the holder of an

Australian Research Council Senior Fellowship. The authors thank Bruker Australia Pty Ltd for a generous donation of NMR time, and Peter Andrews, Michael Dooley, Mark Smythe, Dianne Alewood, John Gehrmann and Jenny Martin for advice.

References

Adams, M. E., Bindokas, V. P., Hasegawa, L. & Venema, V. J. (1990). ω-Agatoxins: novel calcium channel antagonists of two subtypes from funnel web spider (*Agelenopsis aperta*) venom. *J. Biol. Chem.* **265**, 861–878.

Basus, V. J., Nadasdi, L., Ramachandran, J. & Miljanich, G. P. (1995). Solution structure of ω-conotoxin MVIIA using 2D NMR spectroscopy. *FEBS Letters*, **370**, 163–169.

Bax, A. & Davis, D. G. (1985). MLEV-17 based two-dimensional homonuclear magnetization transfer spectroscopy. *J. Magn. Reson.* **65**, 355–360.

Bindokas, V. P. & Adams, M. E. (1989). ω-Aga-I: a presynaptic calcium channel antagonist from venom of the funnel web spider, *Agelenopsis aperta*. *J. Neurobiol.* **20**, 171–188.

Bindokas, V. P., Venema, V. J. & Adams, M. E. (1991). Differential antagonism of transmitter release by subtypes of ω-agatoxins. *J. Neurophysiol.* **66**, 590–601.

Bowersox, S. S., Valentino, K. L. & Luther, R. R. (1994). Neuronal voltage-sensitive calcium channels. *Drugs News Perspect.* **7**, 261–268.

Brooks, B., Bruccoleri, R., Olafson, B. O., States, D., Swaminathan, S. & Karplus, M. (1983). CHARMM: a program for macromolecular enegy, minimization, and dynamics calculations. *J. Comput. Chem.* **4**, 187–217.

Brünger, A. T. (1992). X-PLOR version 3.1. In *A System for X-ray Crystallography and NMR*. Yale University, New Haven, CT.

Brünger, A. T., Clore, G. M., Gronenborn, A. M. & Karplus, M. (1986). Three-dimensional structure of proteins determined by molecular dynamics with interproton distance restraints: application to crambin. *Proc. Natl Acad. Sci. USA* **83**, 3801–3805.

Davis, J. H., Bradley, E. K., Miljanich, G. P., Nadasdi, L., Ramachandran, J. & Basus, V. J. (1993). Solution structure of ω-conotoxin GVIA using 2-D NMR spectroscopy and relaxation matrix analysis. *Biochemistry*, **32**, 7396–7405.

Ellinor, P. T., Zhang, J-F., Horne, W. A. & Tsien, R. W. (1994). Structural determinants of the blockade of N-type calcium channels by a peptide neurotoxin. *Nature*, **372**, 272–275.

Farr-Jones, S., Miljanich, G. P., Nadasdi, L., Ramachandran, J. & Basus, V. J. (1995). Solution structure of ω-conotoxin MVIIC, a high affinity ligand of P-type calcium channels, using ^{1}H NMR spectroscopy and complete relaxation matrix analysis. *J. Mol. Biol.* **248**, 106–124.

Greisinger, C., Sørenson, O. W. & Ernst, R. R. (1987). Practical aspects of the E. COSY technique. Measurements of scalar spin-spin coupling constants in peptides. *J. Magn. Reson.* **75**, 474–492.

Haack, J., Kinser, P., Yoshikami, D. & Olivera, B. (1993). Biotinylated derivatives of ω-conotoxins GVIA and MVIID: probes for neuronal calcium channels. *Neuropharmacology*, **32**, 1151–1159.

Hillyard, D. R., Monje, V. D., Mintz, I. M., Bean, B. P. & Nadasdi, L. (1992). A new *Conus* peptide ligand for mammalian presynaptic Ca^{2+} channels. *Neuron*, **9**, 69–77.

Hyberts, S. G., Goldberg, M. S., Havel, T. S. & Wagner, G. (1992). The solution structure of eglin C based on the measurement of many NOEs and coupling constants and its comparison with X-ray structures. *Protein Sci.* **1**, 736–751.

Jeener, J., Meier, B. H., Bachmann, P. & Ernst, R. R. (1979). Investigation of chemical exchange processes by two-dimensional NMR spectroscopy. *J. Chem. Phys.* **71**, 4546–4553.

Kim, J.-I., Takahashi, M., Ogura, A., Kohno, T., Kudo, Y. & Sato, K. (1994). Hydroxyl group of Tyr^{13} is essential for the activity of ω-conotoxin GVIA, a peptide toxin for N-type calcium channel. *J. Biol. Chem.* **269**, 23876–23878.

Kim, J.-I., Takahashi, M., Ohtake, A., Wakamiya, A. & Sato, K. (1995). Tyr^{13} is essential for the activity of ω-conotoxin MVIIA and GVIA specific N-type calcium channel blockers. *Biochem. Biophys. Res. Commun.* **206**, 449–454.

Kohno, T., Kim, J. I., Kobayashi, K., Kodera, Y., Maeda, T. & Sato, K. (1995). Three-dimensional structure in solution of the calcium channel blocker ω-conotoxin MVIIA. *Biochemistry*, **34**, 10256–10265.

Kumar, A., Ernst, R. R. & Wüthrich, K. (1980). A two-dimensional nuclear Overhauser enhancement (2D NOE) experiment for the elucidation of complete proton-proton cross-relaxation networks in biological macromolecules. *Biochem. Biophys. Res. Commun.* **95**, 1–6.

Kuntz, I. D., Thomason, J. F. & Oshiro, C. M. (1989). Distance Geometry. In *Methods in Enzymology* (Oppenheimer, N. J. & James, T. L., eds), vol. 177, pp. 159–204, Academic Press, Inc., San Diego.

Lampe, R. A., Lo, M. M. S., Keith, R. A., Horn, B. M., McLane, M. W., Herman, J. L. & Spreen, R. C. (1993). Effects of site-specific acetylation on ω-conotoxin GVIA binding and function. *Biochemistry*, **32**, 3255–3260.

Le-Nguyen, D., Heitz, A., Chiche, L., El Hajji, M. & Castro, B. (1993). Characterization and 2D NMR study of the stable (9–21, 15–27) 2 disulphide intermediate in the folding of the 3 disulphide trypsin inhibitor EETI II. *Protein Sci.* **2**, 165–174.

Lewis, P. N., Momany, F. A. & Scheraga, H. A. (1973). Chain reversals in proteins. *Biochim. Biophys. Acta*, **303**, 211–229.

Miljanich, G. P. & Ramachandran, J. (1995). Antagonists of neuronal calcium channels: structure, function and therapeutic implications. *Annu. Rev. Pharmacol. Toxicol.* **35**, 707–734.

Miljanich, G. P., Bowersox, S. S., Fox, J. A., Valentino, K. L., Bitner, R. S. & Yamashiro, D. H. (1993) In *Compositions for Delayed Treatment of Ischemia-related Neuronal Damage*. International Patent application no. PCT/US92 09766; Classification, C07K 7/10, A61K 37/02.

Nadasdi, L., Yamashiro, D., Chung, D., Tarczyhornoch, K., Adriaenssens, P. & Ramachandran, J. (1995). Structure-activity analysis of a *Conus* peptide blocker of N-type neuronal calcium channels. *Biochemistry*, **34**, 8076–8081.

Nemoto, N., Kubo, S., Yoshida, T., Chino, N., Kimura, T., Sakakibara, S., Kyogoku, Y. & Kobayashi, Y. (1995). The solution structure of ω-conotoxin MVIIC determined by NMR. *Biochem. Biophys. Res. Commun.* **207**, 695–700.

Newcomb, R., Palma, A., Fox, J., Gaur, S., Lau, K., Chung, D., Cong, R., Bell, J. R., Horne, B., Nadasdi, L. & Ramachandran, J. (1995). SNX-325, A novel calcium antagonist from the spider *Segrestria florentina*. *Biochemistry*, **34**, 8341–8347.

Nicholls, A., Sharp, K. A. & Honig, B. (1991). Protein folding and association: insights from the interfacial and thermodynamic properties of hydrocarbons. *Proteins: Struct. Funct. Genet.* **11**, 281–296.

Olivera, B. M., McIntosh, J. M., Cruz, L. J., Luque, F. A. & Gray, W. R. (1984). Peptide neurotoxins from fish-hunting cone snails. *Biochemistry*, **23**, 5087–5090.

Olivera, B. M., Gray, W. R., Zeikus, R., McIntosh, J. M. & Varga, J. (1985). Peptide neurotoxins from fish-hunting cone snails. *Science*, **230**, 1338–1343.

Olivera, B. M., Miljanich, G. P., Ramachandran, J. & Adams, M. E. (1994). Calcium channel diversity and neurotransmitter release: the ω-conotoxins and ω-agatoxins. *Annu. Rev. Biochem.* **63**, 823–867.

Pallaghy, P. K., Duggan, B. M., Pennington, M. W. & Norton, R. S. (1993). Three-dimensional structure in solution of the calcium channel blocker ω-conotoxin. *J. Mol. Biol.* **234**, 405–420.

Pallaghy, P. K., Nielsen, K. J., Craik, D. J. & Norton, R. S. (1994). A common structural motif incorporating a cysteine knot and a triple-stranded β-sheet in toxic and inhibitory polypeptides. *Protein Sci.* **3**, 1833–1839.

Pardi, A., Billeter, M. & Wüthrich, K. (1984). Calibration of the angular dependence of the amide proton-C^{α} proton coupling constants, $^{3}J_{NH\alpha}$ in globular protein. *J. Mol. Biol.* **180**, 741–751.

Pastore, A. & Saudek, V. (1990). The relationship between chemical shift and secondary structure in proteins. *J. Magn. Reson.* **90**, 165–176.

Piotto, M., Saudek, V. & Sklenár, V. (1992). Gradient-tailored excitation for single quantum NMR spectroscopy of aqueous solutions. *J. Biomol. NMR*, **2**, 661–665.

Ptitsyn, O. B. & Finkelstein, A. V. (1983). Theory of protein secondary structure and algorithm of its prediction. *Biopolymers*, **22**, 15–25.

Ramilo, C. A., Zafaralla, G. C., Nadasdi, L., Hammerland, L. G. & Yoshikami, D. (1992). Novel α- and ω-conotoxins from *Conus striatus* venom. *Biochemistry*, **31**, 9919–9926.

Rance, M., Sørenson, O. W., Bodenhausen, G., Wagner, G., Ernst, R. R. & Wüthrich, K. (1983). Improved spectral resolution in COSY ^{1}H NMR spectra of proteins *via* double quantum filtering. *Biochem. Biophys. Res. Commun.* **177**, 479–485.

Sato, K., Park, N.-G., Kohno, T., Maeda, T., Kim, J.-I., Kato, R. & Takahashi, M. (1993). Role of basic residues for the binding of ω-conotoxin GVIA to N-type calcium channels. *Biochem. Biophys. Res. Commun.* **194**, 1292–1296.

Sevilla, P., Bruix, M., Santoro, J., Gago, F., Garcia, A. G. & Rico, M. (1993). Three-dimensional structure of ω-conotoxin GVIA determined by ^{1}H NMR. *Biochem. Biophys. Res. Commun.* **192**, 1238–1244.

Skalicky, J. J., Metzler, W. J., Ciesla, D. J., Galdes, A. & Pardi, A. (1993). Solution structure of the calcium channel antagonist ω-conotxin GVIA. *Protein Sci.* **2**, 1591–1603.

Sönnichsen, F. D., van Eyk, J. E., Hodges, R. S. & Sykes, B. D. (1992). Effect of trifluoroethanol on protein secondary structure: an NMR and CD study using a synthetic actin peptide. *Biochemistry*, **31**, 8790–8798.

Venema, V. J., Swiderek, K. M., Lee, T. D., Hathaway, G. M. & Adams, M. E. (1992). Antagonism of synaptosomal calcium channels by subtypes of ω-agatoxins. *J. Biol. Chem.* **267**, 2610–2615.

Wagner, G., Braun, W., Havel, T. F., Schaumann, T., Go, N. & Wüthrich, K. (1987). Protein structures in solution by nuclear magnetic resonance and distance geometry. The polypeptide fold of the basic pancreatic trypsin inhibitor determined by two different algorithms, DISGEO and DISMAN. *J. Mol. Biol.* **196**, 611–639.

Wilmot, C. M. & Thornton, J. M. (1990). β-turns and their distortions: a proposed new nomenclature. *Protein Eng.* **3**, 479–493.

Wishart, D. S., Sykes, B. D. & Richards, F. M. (1991). Relationship between nuclear magnetic resonance chemical shift and protein secondary structure. *J. Mol. Biol.* **222**, 311–333.

Wishart, D. S., Bigam, C. G, Holm, A., Hodges, R. S. & Sykes, B. D. (1995). ^{1}H, ^{13}C and ^{15}N random coil NMR chemical shifts of the common amino acids. I. Investigations of nearest-neighbor effects. *J. Biomol. NMR*, **5**, 67–81.

Wüthrich, K. (1986). *NMR of Proteins and Nucleic Acids*. Wiley-Interscience, New York.

Wüthrich, K., Billeter, M. & Braun, W. (1983). Pseudo structures for the 20 common amino acids for use in studies of protein conformations by measurements of intramolecular proton-proton distance constraints with nuclear magnetic resonance. *J. Mol. Biol.* **169**, 949–961.

Edited by P. E. Wright

(Received 8 March 1996; received in revised form 11 June 1996; accepted 26 July 1996)

Supplementary material for this paper, comprising one Table and one Figure is available from JMB Online

Solution structure and proposed binding mechanism of a novel potassium channel toxin κ-conotoxin PVIIA

Martin J Scanlon[1]*, David Naranjo[2], Linda Thomas[1], Paul F Alewood[1], Richard J Lewis[1] and David J Craik[1]

Background: κ-PVIIA is a 27-residue polypeptide isolated from the venom of *Conus purpurascens* and is the first member of a new class of conotoxins that block potassium channels. By comparison to other ion channels of eukaryotic cell membranes, voltage-sensitive potassium channels are relatively simple and methodology has been developed for mapping their interactions with small-peptide toxins. PVIIA, therefore, is a valuable new probe of potassium channel structure. This study of the solution structure and mode of channel binding of PVIIA forms the basis for mapping the interacting residues at the conotoxin–ion channel interface.

Results: The three-dimensional structure of PVIIA resembles the triple-stranded β sheet/cystine-knot motif formed by a number of toxic and inhibitory peptides. Subtle structural differences, predominantly in loops 2 and 4, are observed between PVIIA and other conotoxins with similar structural frameworks, however. Electrophysiological binding data suggest that PVIIA blocks channel currents by binding in a voltage-sensitive manner to the external vestibule and occluding the pore. Comparison of the electrostatic surface of PVIIA with that of the well-characterised potassium channel blocker charybdotoxin suggests a likely binding orientation for PVIIA.

Conclusions: Although the structure of PVIIA is considerably different to that of the αK scorpion toxins, it has a similar mechanism of channel blockade. On the basis of a comparison of the structures of PVIIA and charybdotoxin, we suggest that Lys19 of PVIIA is the residue which is responsible for physically occluding the pore of the potassium channel.

Addresses: [1]Centre for Drug Design and Development, University of Queensland, St. Lucia, 4072, Australia and [2]Department of Biophysics, Instituto de Fisiologia Celular, UNAM, AP 70-253, CP 04510, Mexico DF, Mexico.

*Corresponding author.
E-mail: m.scanlon@mailbox.uq.edu.au

Key words: charybdotoxin, electrophysiology, NMR spectroscopy, potassium-channel blockers

Received: **21 August 1997**
Revisions requested: **18 September 1997**
Revisions received: **13 October 1997**
Accepted: **15 October 1997**

Structure 15 December 1997, 5:1585–1597
http://biomednet.com/elecref/0969212600501585

Introduction

Voltage-gated ion channels, which span eukaryotic plasma membranes, directly mediate the flow of monovalent and divalent ions (e.g. Na^+, K^+ and Ca^{2+}) that regulate the electrical and biochemical activity of cells. A mechanistic understanding of the factors which govern the conductance and selectivity of these channels, therefore, is of great importance. Like nearly all integral membrane proteins, however, the voltage-gated ion channels are poorly defined at the level of molecular structure. This is largely due to the fact that the nature of these membrane-bound proteins makes them difficult to study by crystallographic or NMR spectroscopic methods. One approach to this problem has been the use of small peptide toxins with well-defined structures as probes of the structure and function of ion channels [1–3].

The venoms from marine snails of the genus *Conus* are a rich source of such toxins [4]. Conotoxins are small (8–35 residues) conformationally constrained molecules which bind with high affinity and specificity to ion channels and receptors in the mammalian neuromuscular system [5]. Although conotoxins are remarkably diverse, both in terms of their sequence and pharmacological properties, many of these peptides fall into distinct structural and activity classes, namely the α, μ, δ and ω conotoxins, which specifically interact at acetylcholine, sodium (two sites) or calcium channels, respectively [6]. Conotoxins have also been classified on the basis of characteristic arrangements of cysteine residues which give rise to two-, three- and four-loop frameworks, the loops being defined by the backbone segments between cysteine residues. An individual structural class can contain multiple pharmacological families, such that the ω, μO and δ conotoxins, which target various subtypes of calcium channels or sodium channels, have four-loop frameworks with remarkably similar folds. Residue substitutions at critical positions in the sequence result in the formation of the required toxin surface for highly potent and selective interactions with their receptors.

The ability of conotoxins to distinguish between different receptor subtypes has made them indispensable tools to unravel many physiological processes. There has also been considerable interest in these toxins as structural probes,

because a knowledge of their three-dimensional structure may be used to map the functional surface of their respective receptors [1]. Several structures of conotoxins from different receptor-binding classes have now been reported [7–13]; however, their use as probes of receptor structure has been hampered by a lack of detailed experimental data on how they interact with their respective ion channels at the molecular level. For this reason, the recent identification of the toxin κ-conotoxin PVIIA in the venom of the piscivorous snail *Conus purpurascens* is an exciting development. PVIIA is a four-loop conotoxin that is active at vertebrate K^+ channels and has been shown to block K^+ conductance in oocytes expressing the cloned K^+ channel encoded by the *Shaker* locus in *Drosophila* [14]. By comparison to other ion channels of eukaryotic cell membranes, voltage-sensitive potassium channels (VSKCs) are relatively simple as they can be assembled from four identical subunits. Through the combined use of recombinant DNA manipulation of the channel sequences and high resolution electrophysiological analysis with peptide toxins, the gross architecture of the active site of K^+ channels is beginning to become apparent. It is known, for example, that VSKCs are tetramers organised in axial fourfold symmetry around the K^+-selective pore [15] and that the most crucial determinants of ion selectivity are found in a short stretch of sequence between the fifth and sixth transmembrane helical domains [16–18].

Studies with scorpion toxins have established methodology for defining the complementary interacting surfaces of the pore loops of VSKCs and peptide toxins of known structure [1–3]. Identification of new ion-channel probes with different binding surfaces and channel subtype specificity will aid in the improved characterisation of VSKCs. Recently, the structure [19] and binding surface [20] of a novel potassium channel toxin, ShK, from the sea anemone *Stichodactyla helianthus* have been reported. κ-Conotoxin PVIIA is significantly different, both in size and sequence, to either the αK scorpion toxins or sea anemone toxins and as such represents the first member of a new class of structural probes of VSKCs. The discovery of novel potassium channel ligands such as ShK and PVIIA will probably provide new insights into the structural factors that govern ion channel subtype specificity.

A knowledge of the structure of PVIIA is an essential prerequisite for binding studies aimed at gaining new topographical information about K^+ channels. Information obtained regarding its mode and orientation of binding to the potassium channel may facilitate the development of similar models of the voltage-sensitive sodium and calcium channels which are targeted by other conotoxins with similar structural frameworks.

In this study, we report the solution structure of PVIIA as well as preliminary electrophysiological data aimed at identifying its mechanism of action. These data suggest that PVIIA blocks the pore of the channel, but binding is mediated through a different set of complementary interactions than those observed with scorpion toxins. On the basis of a comparison of our structure of PVIIA with that of the αK scorpion toxin charybdotoxin (CTX), which binds to the outer vestibule of the Shaker K^+ channel and blocks ion currents by physically occluding the pore [21], we propose a mode of binding for PVIIA.

Results

Peptide synthesis

PVIIA was prepared by solid-phase peptide synthesis and the disulfide bonds formed by air oxidation in the presence of reduced and oxidised glutathione. The peptide was purified using analytical reverse-phase HPLC, and its purity and molecular weight were confirmed by electrospray ionisation mass spectrometry.

Resonance assignments

Resonances were assigned to specific protons using standard sequential assignment procedures [22]. Spectra recorded at different temperatures were used to confirm assignments in cases of peak overlap or coincidence with the water resonance. Figure 1 shows the fingerprint region of a DQF–COSY and a 250 ms mixing time NOESY spectrum recorded in 90% H_2O/10% ^2H_2O. A summary of the short and medium range NOE connectivities along with $^3J_{HNH\alpha}$ coupling constant and amide proton exchange data is presented in Figure 2.

Structure determination and analysis

Structures were generated using a restraint set consisting of 320 inter-proton distances inferred from NOE intensities, 21 backbone and 15 sidechain dihedral angles. Stereospecific assignments were made for ten β-methylene pairs along with all five pairs of sidechain amide protons of asparagine and glutamine residues. The inter-proton restraints, from which redundancies based on the covalent geometry had been eliminated, consisted of 64 intra-residue, 110 sequential, 58 medium-range and 88 long-range distances.

Initial structures were calculated in X-PLOR [23], using a dynamical simulated annealing protocol in a geometric force field. These were energy minimised using a modified CHARMm [24] force field. From the final round of calculations, a family of 20 structures (from a total of 50) with the lowest energies and least residual violations of the experimental restraints were chosen to represent the structure of PVIIA. A summary of the structural statistics for this family is given in Table 1. The structures have no violations of distance or dihedral angle restraints greater than 0.15 Å or 2°, respectively, they have good covalent geometry, as indicated by the small deviations from ideal bond lengths and bond angles, and they have favourable

Figure 1

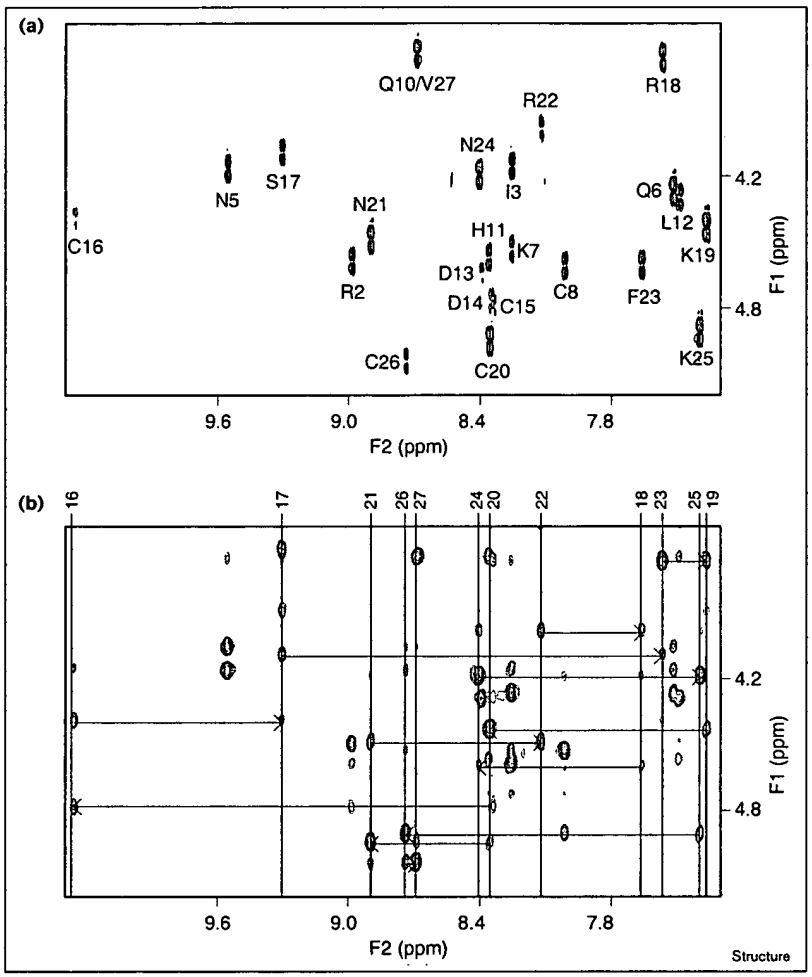

Fingerprint regions of NMR spectra of PVIIA. **(a)** DQF–COSY spectrum of PVIIA recorded in 90% H_2O/10% ^2H_2O at 750 MHz, 298K and pH 3.0. Cross peaks are labelled according to the one-letter amino acid code and numbers indicate the position in the sequence of PVIIA. **(b)** 250 ms mixing time NOESY spectrum recorded in 90% H_2O/10% ^2H_2O. Vertical lines indicate the amide proton resonance positions of residues 15–27 and sequential $H\alpha$–NH_{i+1} connectivities are shown by arrows for these residues.

non-bonded contacts, indicated by the low values of the mean Lennard–Jones potential.

The root mean square deviations (rmsds) for the coordinates of the backbone heavy atoms, when the final 20 structures are superimposed over the entire sequence, are shown as a function of residue number in Figure 3a. These data indicate that the structure is generally well defined, with the least ordered region being loop 2 (residues 9–14). Backbone angular order parameters (Figure 3b–c) are > 0.96 for the entire molecule and > 0.99 for all residues outside loop 2. Mean pairwise rmsds, over the whole molecule, for the backbone heavy atoms (N, Cα and C) and all heavy atoms are 0.38 (± 0.10) Å and 1.52 (± 0.19) Å, respectively. Corresponding values when loop 2 is excluded are 0.27 (± 0.08) Å and 1.40 (± 0.21) Å, respectively. The relative disorder in loop 2 is reflected in decreased sidechain order parameters (Figure 3d).

A stereoview of the final 20 structures superimposed over the backbone heavy atoms is shown in Figure 4. The positions of the three disulfide bonds, which make up the hydrophobic core of the molecule, are indicated. Analysis of the family of structures in PROCHECK [25] reveals that 73% of residues lie in the most favoured regions of the Ramachandran plot with the remaining 27% in the additionally allowed region.

Description of the structure

Elements of secondary structure were identified using the program PROMOTIF [26]. PVIIA contains three β strands, encompassing residues 6–8, 19–21 and 24–27. According to the criteria of Kabsch and Sander [27], these elements do not formally constitute a β sheet as there are only two hydrogen bonds present between each pair of strands as shown Figure 5. A similar structural element, however, has been identified in a number of other conotoxins and

Figure 2

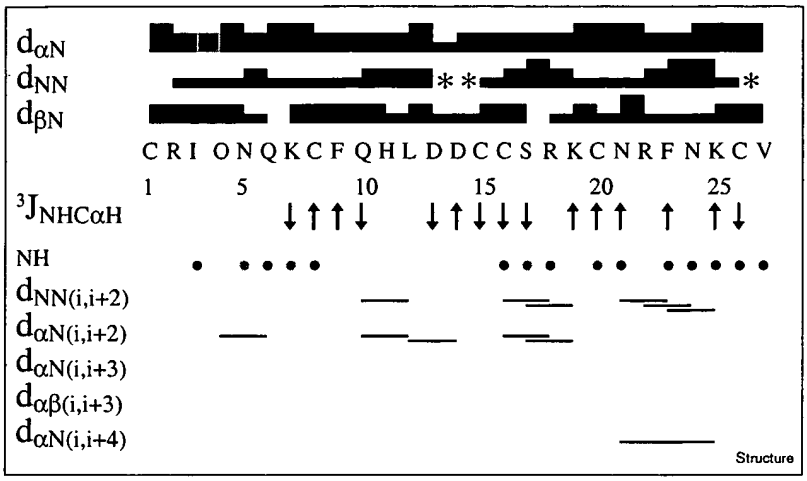

Summary of the NMR data used for sequence-specific assignments and identification of secondary structure in PVIIA. Shaded bars indicate sequential connectivities observed in a 250 ms mixing time NOESY spectrum at 298K and pH 3.0, with the height of the bars indicating their strength. Medium range connectivities are also shown. ↓ indicates values of $^3J_{HNH\alpha} \leq 5$ Hz; ↑ indicates values of $^3J_{HNH\alpha} \geq 8$ Hz. Grey circles indicate backbone NH protons that were still observed in TOCSY spectra of PVIIA 4 h after dissolution in ^2H_2O; black circles indicate backbone NH protons that were not fully exchanged after 24 h.

classified as an antiparallel triple stranded β sheet with +2x, –1 topology. An isolated β bridge involving Arg2 and Cys16 is also present, containing hydrogen bonds as shown in Figure 5.

Five β turns are present in the loops of PVIIA: residues Ile3–Gln6 form a type II β turn, residues Phe9–Leu12 and residues Gln10–Asp13 form overlapping type IV turns, and residues Cys15–Arg18 and Asn21–Asn24 form type I turns. A hydrogen bond was consistently found for the turns 3–6 and 21–24, in structures calculated in the absence of hydrogen-bonding restraints. In addition, an inverse γ-turn is present between residues Leu12–Asp14. In two of the final structures, the overlapping turns between Phe9–Asp14 are classified as a short stretch of 3_{10} helix.

Table 1

Statistics for the family of 20 PVIIA structures*.

Mean rmsd from experimental restraints	
NOE (Å)	0.0125 ± 0.00054
dihedrals (°)	0.43 ± 0.044
Mean rmsd from idealised covalent geometry†	
bonds (Å)	0.0075 ± 0.0003
angles (°)	2.20 ± 0.021
impropers (°)	0.152 ± 0.010
Restraint violations	
mean NOE violations per structure > 0.1 Å	1.3 ± 0.5
maximum NOE violation (Å)	0.13
mean dihedral angle violations per structure > 1°	2.5 ± 0.9
maximum angle violation (°)	1.84
Mean energies (kJ mol^{-1})	
E_{NOE}‡	2.05 ± 0.18
E_{cdih}‡	0.20 ± 0.04
E_{L-J}§	–154.27 ± 6.57
E_{bond}	3.70 ± 0.26
$E_{improper}$	0.49 ± 0.07
E_{angle}	56.6 ± 1.13
E_{total}	–84.7 ± 7.02

*The values in the table are given as means ± standard deviation. †Idealised geometry is defined by the CHARMm force field as implemented within X-PLOR. ‡Force constants for the calculation of square well potentials for the NOE and dihedral angle restraints were 50 kcal mol^{-1} Å^{-2} and 200 kcal mol^{-1} rad^{-2}, respectively. §The Lennard–Jones van der Waals energy was calculated with the CHARMm empirical energy function.

The elements of secondary structure identified in the calculated structures of PVIIA account reasonably well for the amide protons which were found to be in slow exchange with ^2H_2O. Only Ile3 and Arg18 lack clearly defined hydrogen-bonding partners, although in three of the final structures a hydrogen bond is present in the 15–18 β turn. A number of hydrogen bonds involving sidechain acceptors have also been identified and these include: Ser17 NH–Ser17 OG (19/20 structures), Lys19 NH–Ser17 OG (14/20 structures), Cys20 NH–Asp13 OD2 (8/20 structures), Phe23 NH–Asn20 OD1 (10/20 structures) and Lys25 NH–Asn20 OD1 (10/20 structures).

The Cys15–Cys26 disulfide bond forms a left-hand spiral (χSS = –88°, χ1/Cys15 = –43° and χ1/Cys26 = –75°), whereas the other two disulfide bonds have non-standard conformations (χSS = –77°, χ1/Cys1 = 100° and χ1/Cys16 = –149°; χSS = –127°, χ1/Cys8 = 59° and χ1/Cys20 = –70°). Like other four-loop conotoxins, the three disulfides in PVIIA form a cystine knot in which the Cys15–Cys26 bond passes through a ring formed by the other two disulfides and their connecting segments of the backbone.

Electrophysiology

Two-electrode voltage clamp (TEVC) recordings on whole oocytes were used to measure the effects of κ-conotoxin

Figure 3

Parameters for the family of 20 structures chosen to represent the solution conformation of PVIIA. **(a)** Rmsds from the average structure for the backbone heavy atoms (N, Cα and C). **(b–d)** Angular order parameters [8] for the backbone dihedral angles ϕ and ψ and the sidechain angle χ1.

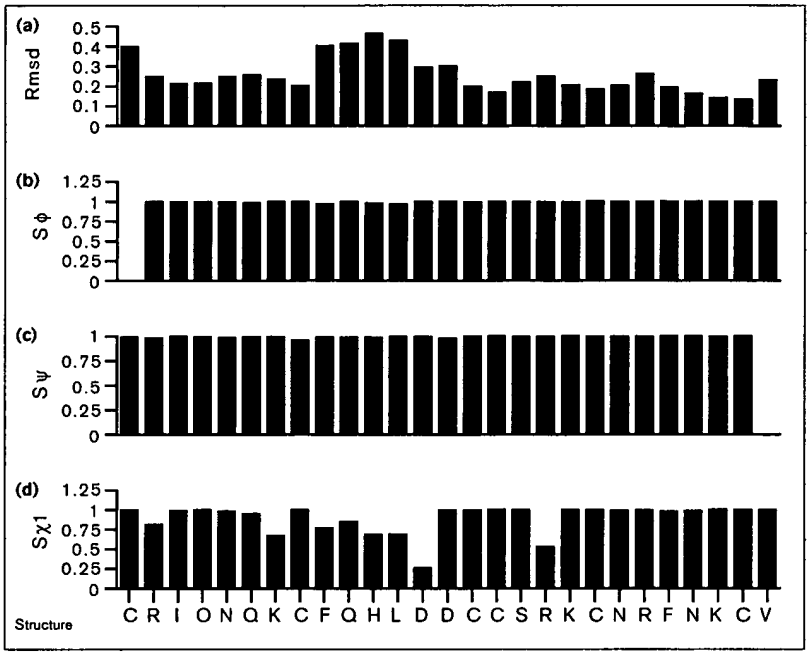

PVIIA on Shaker K^+ channel currents. To determine the effect of voltage on toxin blockade, currents were recorded as the oocytes were depolarised to increasingly positive voltages. Figure 6a shows the currents elicited in response to a series of depolarisations from a holding potential of –90 mV to –60 mV and in 10 mV steps to +50 mV in the absence of toxin. Figure 6b shows the same type of records when the experiments were recorded in the presence of 33 nM PVIIA. The apparent change in kinetics is due to relaxation of the voltage-dependent blockade as the command voltage is made more positive. The normalised inhibition time courses ($I_{PVIIA}/I_{control}$) were calculated from point-by-point division of the data in Figure 6b by the control family in Figure 6a and plotted (Figure 6c) to describe toxin inhibition. To avoid interference from activation kinetics, only those results obtained at voltages > 0 mV are shown. In order to undertake kinetic analysis of these data, it was necessary to modify the approach of Goldstein and Miller [21], to take account of the fast off-rate of PVIIA. The normalised data were fit to a single exponential function of the form:

$$f(t) = m-(m-n)*\exp(-t/\tau) \quad (1)$$

Equation 1 describes the relaxation of a first order (or pseudo-first order) equilibrium in response to a pulse-like perturbation: m is the asymptotic new equilibrium following the perturbation, n is the equilibrium state preceding the perturbation, t is the time after the perturbation and τ is the time constant of the current relaxation. Such an analysis is applicable to toxins with off-rates in the tens of millisecond timescale and allows resolution of kinetic processes that are faster than the solution exchange rate. The solid lines in Figure 6c correspond to a fit of the normalised inhibition time course to Equation 1. Note that the fitted lines converge at the beginning of the pulse, indicating the same level of prepulse inhibition. The time constants for current relaxation obtained from the solutions of this equation at different voltages were used to calculate the effective valence (zδ) of the voltage dependence according to Equation 2 ([21]; Figure 6d).

$$\tau = \tau(0)*\exp(z\delta FV/RT) \quad (2)$$

The values of zδ for PVIIA (0.48–0.55) are similar to the corresponding value for charybdotoxin (CTX; [21]) which indicates that blockade by PVIIA is similarly voltage sensitive. In CTX, the voltage sensitivity arises from the fact that the η-group of Lys27 interacts with potassium ions in the conduction pathway. Thus, a similar voltage dependency supports a similar mechanism of interaction for PVIIA.

If the mechanism of PVIIA blockade is indeed similar to that of the αK scorpion toxins, it would be expected that

Figure 4

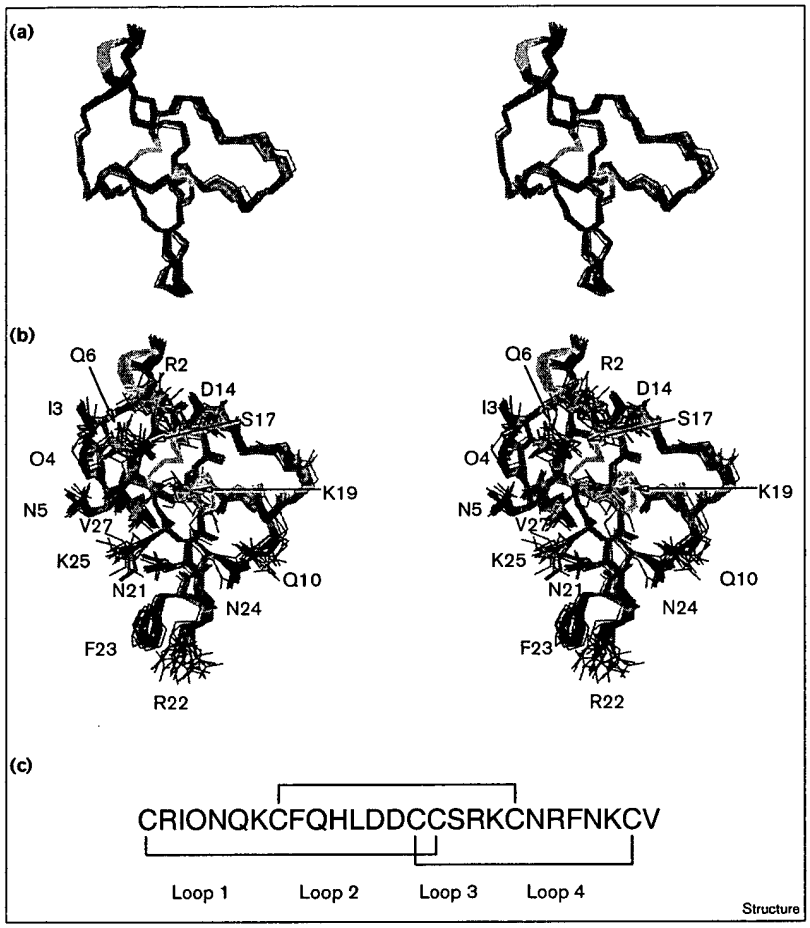

The solution structure of PVIIA. **(a)** Stereoview of the superimposed backbone heavy atoms (N, Cα and C) of the final 20 structures of PVIIA. The three disulfide bonds are shown in yellow. **(b)** Stereoview of the final structures in the same orientation. Backbone atoms (N, Cα and C) are shown in green, sidechain heavy atoms for the cysteine residues are shown in yellow and other well-defined sidechains ($S\chi1 > 0.8$) are shown in magenta. **(c)** The primary sequence and disulfide connectivity for PVIIA (O = γ-trans-L-hydroxyproline).

the tetraethylammonium ion (TEA), a specific K^+ channel pore blocker, would compete with PVIIA for binding, as is the case with CTX [28]. In order to test this hypothesis, toxin inhibition was studied by measuring whole cell currents in the presence and absence of external TEA. Figure 7a shows the currents elicited in response to a 100 ms depolarisation to 0 mV in the absence and presence of 100 nM PVIIA. Figure 7b shows the same type of records when the currents were recorded with 20 mM TEA in the external solution. In the absence of toxin, 20 mM TEA inhibited ~50% of the channel current at 0 mV, indicating that this concentration of TEA is close to its dissociation constant [28]. Normalised inhibition time courses are shown in Figure 7c. The continuous lines in Figure 7c are single exponential fits of the data to Equation 1, in which the time constants are 40 ms and 32 ms for 0 and 20 mM TEA, respectively. Addition of 20 mM TEA to the extracellular solution resulted in a ~50% weaker inhibition produced by 100 nM PVIIA. For the data shown in Figure 7c, apparent dissociation constants for PVIIA were calculated by measuring ($I_{PVIIA}/I_{control}$) values at the end of the 100 ms depolarisation pulse (using Equation 3), and they were found to be 360 and 700 nM in the absence and presence of TEA (20 mM), respectively.

$$I_{PVIIA}/I_{control} = \{1+[PVIIA]/K_d\}^{-1} \quad (3)$$

On average, with depolarisations to 0 mV, 20 mM TEA increased the apparent K_d of PVIIA by 2.3 ± 0.23 (mean ± sd; n = 3 separate experiments). These values are consistent with a competitive scheme in which the apparent K_d for the toxin is expected to be doubled when the concentration of its competitor is near its own K_d.

Discussion

The ability of conotoxins to distinguish between different receptor subtypes has resulted in their widespread

Figure 5

Schematic diagram of the secondary structural elements in PVIIA showing NOEs between β strands (double headed arrows) and the position of proposed hydrogen bonds (broken lines).

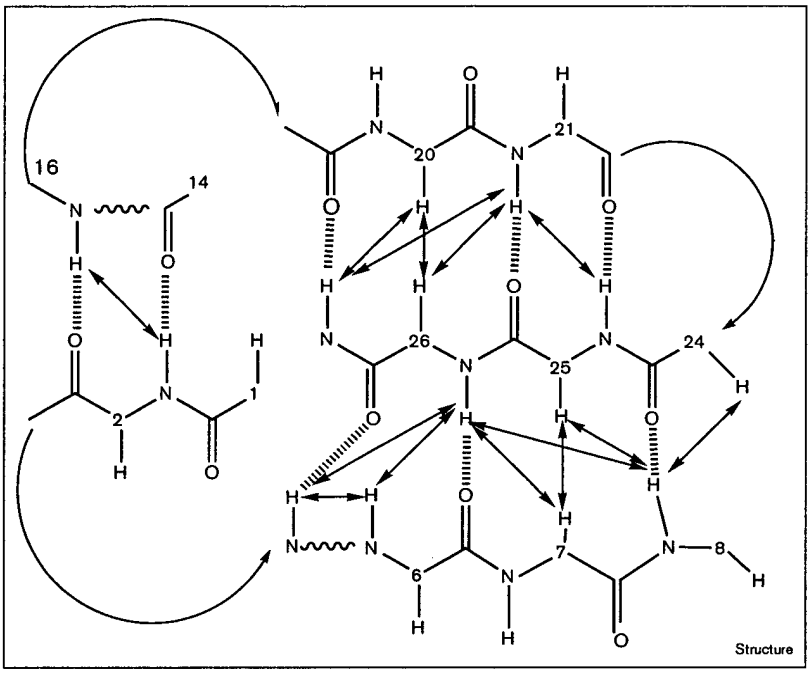

use as pharmacological probes of ion channels. For the same reasons, conotoxins have the potential to be used as templates for the development of ion channel therapeutics which combine high affinity with low toxicity. Detailed

Figure 6

Two-electrode voltage clamp (TEVC) records of currents elicited in response to a series of depolarisations from a holding potential of −90 mV to −60 mV and in 10 mV steps to +50 mV in the absence **(a)** and presence **(b)** of 33 nM PVIIA. **(c)** Point by point division of the data recorded in the presence of toxin (b) by the control family (a). The panel only shows those results obtained at voltages > 0 mV to avoid interference from activation kinetics. **(d)** Voltage dependency of the relaxation time constant obtained from the traces in (c).

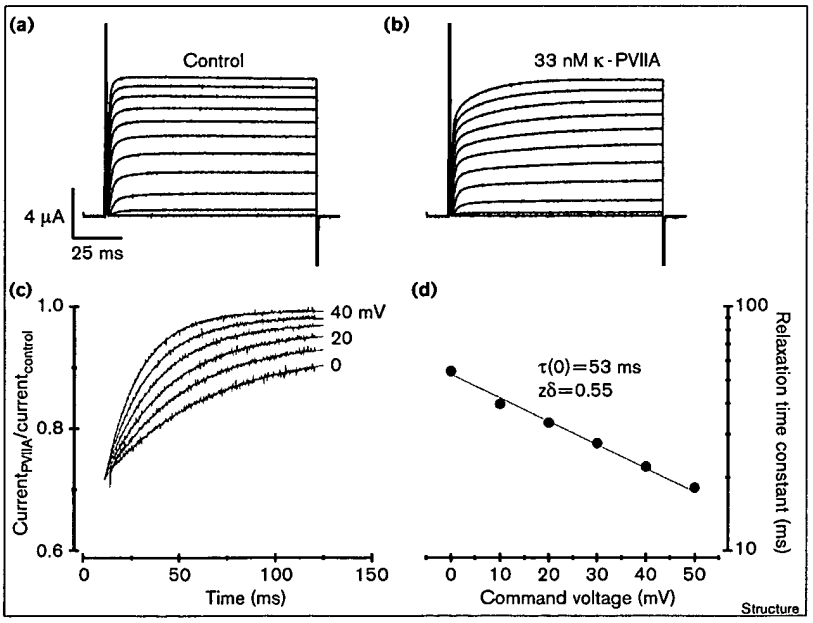

Figure 7

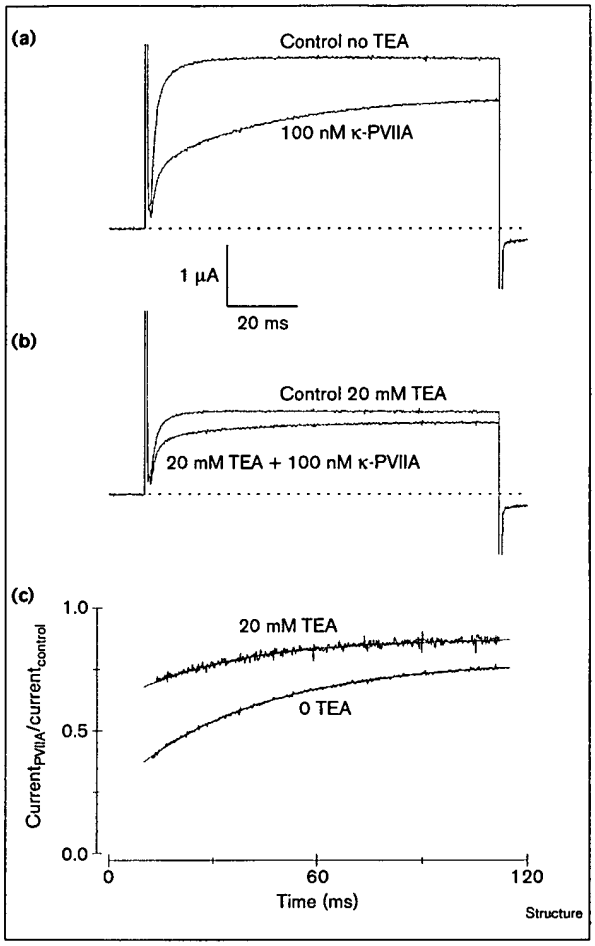

Toxin inhibition in the presence of TEA. **(a)** TEVC records of currents elicited in response to a 100 ms depolarisation to 0 mV under control conditions and in the presence of 100 nM PVIIA. **(b)** The same records measured after addition of TEA (20 mM) to the extracellular solution. **(c)** Normalised inhibition time course in the presence and absence of 20 mM TEA.

experimental data on how individual conotoxins interact with ion channels is currently lacking, however.

PVIIA is a recently identified conotoxin, found in the venom of the piscivorous snail *C. purpurascens*, which binds at nM concentrations to the Shaker K^+ channel [14]. This is the first conotoxin that has been identified with K^+ channel activity and as such represents the first member of the κ-class of conotoxins.

We have determined the structure of PVIIA at high resolution as a starting point from which to identify the residues necessary for high affinity interaction with the Shaker channel. PVIIA belongs to the four-loop class of conotoxins, containing six cysteine residues which form three disulfide bonds. This structural class displays diverse pharmacological activities and includes PVIIA, ω-conotoxins that block calcium channels, δ-conotoxins that delay the inactivation of sodium channels and conotoxin GS that blocks sodium channels. Solution structures have been previously reported for several ω-conotoxins [8,9,13] and conotoxin GS [12], which all share the same topology, comprising a triple stranded antiparallel β sheet with +2x, −1 topology linked by a cystine knot. This structural motif has now been reported for a number of toxic and inhibitory peptides [12,13,29–31].

Comparison of the structures of κ-PVIIA with ω-GVIA and conotoxin GS reveals that despite differences in the three sequences, the overall fold is remarkably similar (Figure 8). Indeed, the six Cα atoms of the conserved cysteine residues superimpose with an rmsd of 0.97 Å between ω-GVIA and κ-PVIIA and 1.27 Å between conotoxin GS and κ-PVIIA. The most notable differences between the three structures are in the size and relative orientation of loops 2 and 4. These structural differences are of particular interest because loop 2 of the ω-conotoxins is thought to be involved in calcium-channel binding and subtype discrimination [13]. Although the electrostatic profiles presented by the binding surfaces of the different conotoxins is likely to be the principal determinant of their specificity, the importance of the conformational differences observed among different classes of conotoxins is currently unclear. Without a knowledge of the binding orientation of the toxins on their respective channels and the mechanism of channel blockade, however, it is difficult to speculate on the importance of the observed structural differences.

We have investigated the binding of PVIIA to Shaker K^+ channels using electrophysiology and find that TEA ions compete with PVIIA and blockade by PVIIA is voltage sensitive. Although this result is apparently in conflict with those of Terlau *et al.* [14], we believe that this is due to their use of a channel with an attached inactivation domain. Inactivation kinetics mask the change in the toxin's binding affinity, which occurs as the membrane is stepped to depolarising potentials to open the channels. Furthermore, mutations in the K^+ channel vestibule were found to affect the binding affinity of PVIIA. For example, the channel mutation Lys427Glu increased toxin affinity by ~fivefold (data not shown). These results also indicate that the binding specificity of PVIIA is different to that of CTX. The affinity of CTX for the Shaker channel is increased > 2000-fold by the channel mutation Phe425Gly [32]; however, the same channel mutation makes PVIIA binding undetectable up to 5 μM. Taken together, these data strongly suggest that, like a number of αK scorpion toxins, PVIIA binds to

Figure 8

Comparison of the solution structures of **(a)** ω-conotoxin-GVIA **(b)** κ-conotoxin-PVIIA and **(c)** conotoxin-GS. The structures were aligned by superimposition over the Cα atoms of the six conserved half cysteines. Backbone heavy atoms (N, Cα and C) as well as the sidechain heavy atoms of the cysteine residues (yellow) are shown. Coordinates for GVIA (PDB accession code 1OMC; [9]) were obtained from the PDB. Coordinates for GS (PDB accession code 1AG7) were kindly provided by Justine Hill.

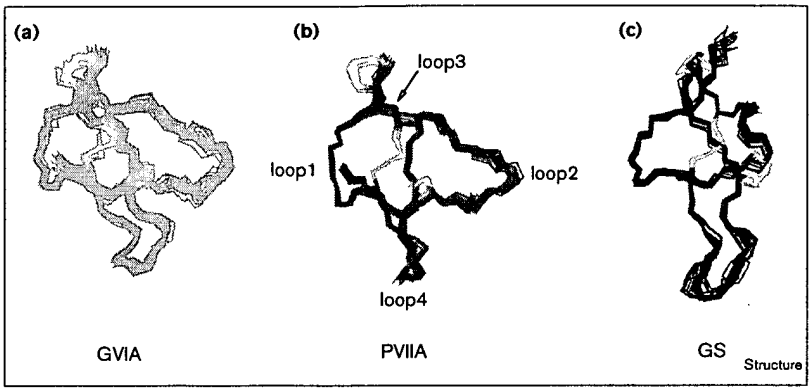

the external vestibule of the Shaker channel and blocks currents by physically occluding the pore.

Several studies have been reported that reveal details of interactions between CTX and the Shaker channel; therefore, a comparison of the structures of CTX and PVIIA represents a logical starting point from which to identify the possible orientation for PVIIA binding. Scanning mutagenesis experiments with CTX have revealed that binding is mediated by electrostatic interactions between the toxin and the channel [33]. CTX mutants in which each of the nine charge bearing residues were individually neutralised have revealed that only three charged residues, Arg25, Lys27 and Arg34, are crucial for toxin binding and blockade [34]. In addition, residues Lys11 and Lys31 in CTX have been shown to have unfavourable electrostatic interactions with the positively charged channel residue Lys427. The mutation Lys427Glu increases the affinity of CTX for the Shaker channel by ~50-fold [35]. Furthermore, Lys27 directly interacts with K^+ ions in the pore of the Shaker channel, conferring high affinity binding and voltage dependency to the dissociation rate [21]. Substitution of this residue for an arginine results in a marked reduction in affinity, while neutralisation of Lys27 to asparagine or glutamine drastically reduces the voltage sensitivity [21]. As PVIIA displays a similar voltage dependency of blockade to that of CTX, it would be expected that one of the three lysine residues in PVIIA binds within the pore of the channel and contributes significantly to the affinity of the interaction.

Comparison of the structure of PVIIA with that of CTX reveals a remarkable similarity in their folds (Figure 9a). CTX has a βαβ structure consisting of a triple-stranded antiparallel β sheet in which the first and second strands are linked by a loop containing an α helix. The residues that interact with the pore region of the K^+ channel are located on the second and third β strands and at the end of the α helix, which together form a relatively flat surface on one side of the molecule. Lys27, the residue which occludes the pore of the channel, is located on the second β strand. PVIIA, which also contains a triple-stranded antiparallel β sheet, has a considerably shorter sequence than CTX and lacks the α helix between the first and second β strands. As shown in Figure 9a, there is a striking similarity between CTX and PVIIA in the backbone fold of the remainder of the molecule, however. Furthermore, as shown in Figure 9b, when the backbone of Lys19 in PVIIA is superimposed over Lys27 in CTX, a number of positively charged residues in PVIIA align with positive charges in CTX that mediate binding to the Shaker channel. In this orientation, like CTX, PVIIA presents a flat surface which appears to be a prerequisite for toxins, interacting within the flat floor of the vestibule of the K^+ channel, to block ion flow. The majority of residues which contribute to this surface are contained in loop 4 of PVIIA, suggesting that the observed structural differences between conotoxins from different pharmacological classes may have functional significance. In this orientation, the sidechain of Lys19 in PVIIA overlaps that of Lys27 in CTX. Lys19 is therefore the residue which we suggest binds in the pore and confers voltage dependency to blockade of channel currents by PVIIA.

This model for PVIIA binding to the Shaker K^+ channel can now be used to direct a rational approach to mutational analysis aimed at identifying interacting pairs of residues on PVIIA and the Shaker channel. As we have demonstrated, the specificity of PVIIA is clearly different to that of any of the previously identified scorpion toxins. It is expected, therefore, that the data obtained from such mutational studies will enhance the currently available models of the selectivity-determining pore of the K^+ channel vestibule.

Figure 9

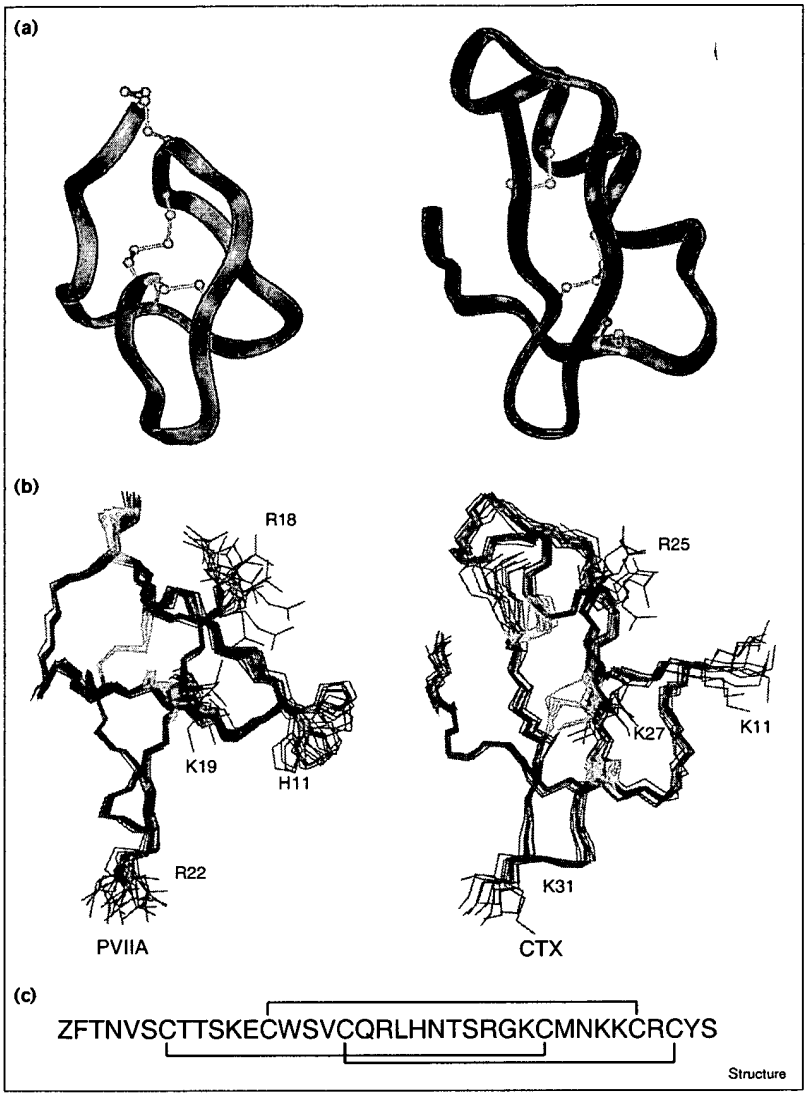

A comparison of the structures of PVIIA and CTX. **(a)** Comparison of Cα ribbon representations of the structures of PVIIA (blue) and CTX (green). Sidechain heavy atoms of the cysteine residues are shown in yellow. **(b)** Comparison of the structures of PVIIA and CTX. The alignment is based on superposition of the backbone heavy atoms (N, Cα and C) of Lys19 of PVIIA and Lys27 of CTX. Positively charged sidechains of CTX which have been found to mediate binding to the Shaker channel are shown in blue, as are selected positively charged sidechains of PVIIA. **(c)** The primary sequences and disulfide connectivity of charybdotoxin (Z = pyroglutamate).

Biological implications

Venomous marine snails of the genus *Conus* produce many small, disulfide-rich, peptide toxins with potent biological activities. Several of these conotoxins have been found to be highly selective blockers of mammalian ion channels. Such channels control a variety of biological processes and represent important therapeutic targets. Like other membrane proteins, however, ion channels are beyond the scope of direct structure determination by currently available methods. One solution to this problem has been the use of small molecules with well-defined structures to probe the complementary structure of their receptors. Although conotoxins would seem to be ideal for this purpose, their use as structural probes has been hampered by a lack of detailed experimental data on how they interact with their respective ion channels at the molecular level.

In this study, we have determined the structure of κ-conotoxin PVIIA. PVIIA is the first member in a new class of conotoxins that block voltage-sensitive potassium channels (VSKCs). By comparison to other ion channels of eukaryotic cell membranes, VSKCs have relatively simple architecture and a methodology has been devised for mapping their interactions with small peptide toxins. Our electrophysiological data for PVIIA

suggest that it binds to the external vestibule of the Shaker K^+ channel and blocks currents by physically occluding the pore. Furthermore, blockade by PVIIA has similar voltage dependency to blockage by charybdotoxin (CTX). Comparison of the structures of PVIIA and CTX suggest a likely binding orientation in which Lys19 of PVIIA is the residue which confers voltage dependency to the channel blockage. In this orientation, PVIIA binding to the outer vestibule of the Shaker K^+ channel is mediated through a different set of interactions to those of previously characterised toxins. Identification of those residues on the surface of PVIIA that interact with the VSKC, therefore, will enhance current models of the channel pore.

Knowledge of the structural basis for channel blockade by PVIIA may assist in the development of similar models describing blockade of voltage-sensitive sodium and calcium channels that are targeted by other conotoxins with the same structural framework. Such models should prove useful as guides to the development of novel selective and therapeutically useful ion channel modulating agents.

Materials and methods

Peptide synthesis

Boc-L-amino acids were obtained from Novabiochem (Läufelfingen, Switzerland) or the Peptide Institute (Osaka, Japan); t-Boc-Val-OCH_2-PAM-resin (substitution value 0.77 mmol g^{-1}) was obtained from Perkin Elmer (Brisbane, Australia). 2-(1H-benzotriazol-1-yl)-1,1,3,3,-tetramethyluronium hexafluorophosphate (HBTU) was obtained from Richelieu Biotechnologies (Quebec, Canada). Other reagents were of peptide synthesis grade from Auspep (Melbourne, Australia).

Stepwise synthesis (0.5 mmol scale, 0.649 g resin) was conducted manually using *in situ* BOC SPPS [36], starting from Boc-PAM-Val resin. The average coupling was 99.80 as determined by ninhydrin assay [37]. The peptide was cleaved from the resin using HF:*p*-cresol:*p*-thiocresol (18:1:1) at −10–0°C for 1 h. Peptide was precipitated with cold ether, collected by filtration on a sinter funnel, washed with cold ether and dissolved in 50% AcOH, diluted with water and lyophilised. The crude peptide was purified by preparative chromatography (Vydac C18 column, 2.2 × 25 cm), using a 1% gradient (100% A to 80% B, 80 min; A = 0.1% TFA in H_2O, B = 0.09% TFA, 10% H_2O, 90% CH_3CN) to give reduced peptide in 34% yield.

The folded product was obtained by dissolving reduced peptide (10 mg) in aqueous 0.33 M NH_4OAc/0.5 M GnHCl (154 ml), with pH adjusted to 7.8 using 0.01 M NH_4OH. The solution was stirred at 4°C for 5 days, in the presence of reduced and oxidised glutathione (molar ratio of peptide:GSH:GSSG was 1:100:10). The oxidation was terminated by lowering the pH to 2–3 with TFA (5 ml). The reaction mixture was loaded onto a preparative HPLC column (Vydac C18 column, 2.2 × 25cm) (8 ml min^{-1}) and washed with 0.1% TFA until all oxidation buffer had eluted. A 1% gradient (100% A to 80% B, 80 min) was applied and pure oxidised κ-PVIIA was isolated in 95% yield. Electrospray ionisation mass spectra recorded on a PE Sciex API III triple quadrupole mass spectrometer were used to confirm the purity and molecular weights of the synthetic peptides.

NMR Spectroscopy. NMR samples contained ~1.5 mM peptide in either 90% H_2O/10% ^2H_2O or ^2H_2O at pH 3.0. pH values are meter readings at 295K, uncorrected for deuterium isotope effects. Spectra were recorded on a Bruker DRX 750 spectrometer with sample temperatures of 280K, 298K or 313K. In all experiments, the carrier was set at the centre of the spectrum on the water resonance frequency and quadrature detection was used in both dimensions. Spectra were recorded in phase sensitive mode using TPPI [38]. The following homonuclear 2D NMR spectra were recorded: double quantum filtered (DQF) COSY [39], TOCSY [40] with MLEV17 [41] isotropic mixing periods of 50 and 80 ms, ECOSY [42] and NOESY [43] with mixing times of 80 ms, 150 ms and 250 ms. Water suppression was achieved using selective low power irradiation of the water resonance during the relaxation delay of 1.8 s and during the mixing period in NOESY experiments. Slowly exchanging amide protons were identified by recording a series of 1D and TOCSY spectra on a fully protonated sample of PVIIA immediately following dissolution in ^2H_2O.

Spectra were processed on a Silicon Graphics Indigo 2 R8000 using UXNMR (Bruker). Data were processed as described previously [13]. Processed data were analysed using AURELIA (Bruker) and plots for the figures were generated using Felix 2.3 (Biosym).

Structure calculations

Distance constraints were derived from the intensity of cross peaks in NOESY spectra recorded in 90% H_2O/10% ^2H_2O and ^2H_2O with a mixing time of 250 ms. Cross peaks were classified as strong, medium, weak or very weak and assigned corresponding upper bounds of 2.7 Å, 3.5 Å, 5.0 Å or 6.0 Å, respectively. Pseudoatom corrections were added to distance constraints where necessary and a further 0.5 Å was added to the upper bound of restraints involving methyl protons.

Backbone dihedral φ angles were derived from $^3J_{HNH\alpha}$ coupling constants measured from either 1D NMR spectra or from lineshape analysis of the antiphase crosspeak splitting in a high digital resolution 2D DQF–COSY spectrum. Dihedral angle constraints were applied as follows: $-120° \pm 30°$ for $^3J_{HNH\alpha} > 8$ Hz; $-60° \pm 30°$ for $^3J_{HNH\alpha} < 5$ Hz. Additional f angle restraints of $-100° \pm 80°$ were applied in cases where the intra residue dαN(i,i) NOE was clearly weaker than the sequential dαN(i,i+1) NOE.

Positive φ angle restraints of $+60° \pm 30°$ were used for residues where $6 \text{ Hz} < {}^3J_{HNH\alpha} < 8$ Hz and the intra residue dαN(i,i) NOE was strong. In preliminary structure calculations, in which no positive φ angle restraints were included, these residues angles converged to a positive value in the majority of cases.

Stereospecific assignment of the β-methylene protons and χ1 dihedral angle restraints were derived using $^3J_{\alpha\beta}$ coupling constants measured form ECOSY spectra, together with dαβ(i,i) and dNβ(i,i) NOE intensities [44]. χ1 angles were restrained to values of 60°, 180° or −60°, as appropriate, with a range of ± 30°. Additional χ1 restraints were obtained for Ile3 and Val27 from measurement of $^3J_{\alpha\beta}$ in the ECOSY spectrum.

Structures were calculated using a dynamic simulated annealing protocol in X-PLOR 3.1 [23] using a geometric force field. Starting structures were generated using random (φ,ψ) dihedral angles and energy minimised (500 steps) to produce structures with the correct local geometry. A soft square well potential [45] was used for NOE and dihedral constraints and bond lengths were fixed during the high temperature and cooling stages. The structures were subjected to 30 ps of high temperature molecular dynamics at 1000 K before cooling to 0 K and final energy minimisation over 15 ps. Structure refinements were performed using energy minimisation under the influence of the CHARMm forcefield [24].

The final 20 structures with the lowest overall energies which had no violations of NOE restraints > 0.15 Å or dihedral angle restraints > 2.0° were retained for analysis. Structures were visualised using InsightII (Biosym) and analysed using the program PROMOTIF [26].

Molecular biology

In vitro cRNA synthesis and expression of Shaker channel mutants Phe425Gly and Lys427Glu were undertaken as described by Goldstein *et al.* [34].

Electrophysiology

Oocytes from *Xenopus laevis* were injected with 0.05–0.5 ng of total RNA [32], coding for the inactivation removed Shaker K^+ channel (Δ6–46) [46]. Currents were recorded using two electrode voltage clamp (TEVC) recordings on whole oocytes at room temperature [47]. Extracellular solution consisted of 96 mM NaCl, 2 mM KCl, 0.3 mM $CaCl_2$, 10 mM HEPES (pH 7.6) and bovine serum albumin (25 mg ml^{-1}). Current and voltage electrode pipettes (0.2–0.5 MΩ) were filled with a solution of 3 mM KCl, 5 mM EGTA and 10 mM HEPES (pH 7.0). During the experiments the oocytes were maintained at a holding potential of −90 mV. TEVC records were obtained of currents elicited in response to 100 or 110 ms depolarisations to −60 mV to +50 mV in 10 mV steps. The time course of toxin inhibition was obtained from point-by-point division of records obtained in the presence of PVIIA (33–100 nM) from control records obtained in its absence. Kinetic analysis of these time courses was undertaken by fitting the data to a single exponential function (equation 1) as described in the text.

To determine the effect of external TEA ions on channel blockade, experiments were undertaken, essentially as described above, in the absence and presence of PVIIA and repeated after the addition of TEA (20 mM) to the extracellular solution. Apparent dissociation constants (K_d) for PVIIA were estimated from the standard one-site inhibition equation, given by Equation 3.

In the presence of TEA, the toxins apparent K_d is given by:

$$K_d = K_{d(0)} * \{1 + [TEA]/K_{d(TEA)}\} \quad (4)$$

in which $K_{d(0)}$ is the dissociation constant in the absence of TEA.

Accession numbers

Coordinates for PVIIA have been submitted to the Protein Data Bank with the accession code 1AV3.

Supplementary material

The supplementary material available with the Internet version of this paper contains a table of Chemical shift assignments (ppm) for PVIIA in 90% H_2O/10% ^2H_2O at 298K and pH 3.0.

Acknowledgements

This work was supported in part by a grant from the Australian Research Council to DJC. DN was partially supported by grant DGAPA–UNAM IN200397. We thank Chris Miller for helpful discussions and allowing parts of this work to be undertaken in his laboratory.

References

1. Miller, C. (1995). The charybdotoxin family of K^+ channel blocking peptides. *Neuron* **15**, 5–10.
2. Aiyar, J., *et al.*, & Chandy, K.G. (1995). Topology of the pore region of a K^+ channel revealed by the NMR-derived structures of scorpion toxins. *Neuron* **15**, 1169–1181.
3. Ranganathan, R., Lewis, J.H. & Mackinnon, R. (1996). Spatial localisation of the K^+ channel selectivity filter by mutant cycle-based structure analysis. *Neuron* **16**, 131–139.
4. Bingham, J.P., Jones, A., Lewis, R.J., Andrews, P.R. & Alewood, P.F. (1996). *Conus* venom peptides (conopeptides): inter-species, intra-species and within individual variation revealed by ionspray mass spectrometry. In *Biochemical Aspects of Marine Pharmacology*, (Lazarovici, P., ed.), pp 13–27, Alaken, Colorado.
5. Myers, R.A., Cruz, L.J., Rivier, J.E. & Olivera, B.M. (1993). *Conus* peptides as chemical probes for receptors and ion channels. *Chem. Rev.* **93**, 1923–1936.
6. Lewis, R.J., *et al.*, & Andrews, P. (1996). Secrets of the cone shell. *Life Sci.* **8**, 16–24.
7. Ott, K.H., Becker, S., Gordon, R.D. & Rüterjans, H. (1991). Solution structure of μ-conotoxin GIIIA analysed by 2D-NMR and distance geometry calculations. *FEBS Letters* **278**, 160–166.
8. Pallaghy, P.K., Duggan, B.M., Pennington, M.W. & Norton, R.S. (1993). Three-dimensional structure in solution of the calcium channel blocker ω-conotoxin. *J. Mol. Biol.* **234**, 405–420.
9. Davis, J.H., Bradley, E.K., Miljanich, G.P., Nadasdi, L., Ramachandran, J. & Basus, V.J. (1993). Solution structure of ω-conotoxin GVIA using 2-D NMR spectroscopy and relaxation matrix analysis. *Biochemistry* **32**, 7396–7405.
10. Farr-Jones, S., Miljanich, G.P., Madasdi, L., Ramachandran, J. & Basus, V.J. (1995). Solution structure of ω-conotoxin MVIIC, a high affinity ligand of P-type calcium channels using ^1H NMR spectroscopy and complete relaxation matrix analysis. *J. Mol. Biol.* **248**, 106–124.
11. Hill, J.M., Alewood, P.F. & Craik, D.J. (1996). Three-dimensional solution structure of μ-conotoxin GIIIB, a specific blocker of skeletal muscle sodium channels. *Biochemistry* **35**, 8824–8835.
12. Hill, J.M., Alewood, P.F. & Craik, D.J. (1997). Solution structure of the sodium channel antagonist conotoxin GS: a new molecular calliper for probing sodium channel geometry. *Structure* **5**, 571–583.
13. Nielsen, K.J., Thomas, L., Lewis, R.J., Alewood, P.F. & Craik, D.J. (1996). A consensus structure for ω-conotoxins with different selectivities for voltage sensitive calcium channel subtypes: comparison of MVIIA, SVIB and SNX-202. *J. Mol. Biol.* **263**, 297–310.
14. Terlau, H., Shon, K.-J., Grilley, M., Stocker, M., Stühmer, W. & Olivera, B.M. (1996). Strategy for rapid immobilisation of prey by a fish-hunting marine snail. *Nature* **381**, 148–151.
15. Mackinnon, R. (1991). Determination of the subunit stoichiometry of a voltage-activated potassium channel. *Nature* **350**, 232–235.
16. Miller, C. (1991). 1990: *Annus mirabilis* of potassium channels. *Science* **252**, 1092–1096.
17. Sigworth, F.J. (1994). Voltage gating of ion channels. *Quart. Rev. Biophys.* **27**, 1–40.
18. Mackinnon, R. (1995). Pore loops: an emerging theme in ion channel structure. *Neuron* **14**, 889–892.
19. Tudor, J.E., Pallaghy, P.K., Pennington, M.W. & Norton, R.S. (1996). Solution structure of ShK toxin, a novel potassium channel inhibitor from a sea anemone. *Nature Struct. Biol.* **3**, 317–320.
20. Pennington, M.W., Mahnir, V.M., Khaytin, I., Zaydenburg, I., Byrnes, M.E. & Kem, W.R. (1996). An essential binding surface for ShK toxin interaction with rat brain potassium channels. *Biochemistry* **35**, 16407–16411.
21. Goldstein, S.A.N. & Miller, C. (1993). Mechanism of charybdotoxin block of a voltage-gated K^+ channel. *Biophys. J.* **65**, 1613–1619.
22. Wüthrich, K. (1986). *NMR of proteins and nucleic acids.* John Wiley & Sons Inc., New York.
23. Brünger, A.T. (1992). *X-PLOR Version 3.1. A system for X-ray crystallography and NMR.* Yale University Press, New Haven, CT.
24. Brooks, B.R., Bruccoleri, R.E., Olafson, B.D., States, D.J., Swaminathan, S. & Karplus, M. (1983). CHARMm: A program for macromolecular energy minimisation and dynamics calculations. *J. Comp. Chem.* **4**, 187–217.
25. Laskowsi, R.A., MacArthur, M.W., Moss, D.S. & Thornton, J.M. (1993). PROCHECK: a program to check the stereochemical quality of protein structure coordinates. *J. Appl. Cryst.* **26**, 283–291.
26. Hutchinson, E.G. & Thornton, J.M. (1996). PROMOTIF: a program to identify and analyse structural motifs in proteins. *Protein Sci.* **5**, 212–220.
27. Kabsch, W. & Sander, C. (1983). Dictionary of protein secondary structure: pattern recognition of hydrogen-bonded and geometrical features. *Biopolymers* **22**, 2577–2637.
28. Miller, C. (1988). Competition for block of a Ca^{2+} activated K^+ channel by charybdotoxin and tetraethylammonium. *Neuron* **1**, 1003–1006.
29. Pallaghy, P.K., Nielsen, K.J., Craik, D.J. & Norton, R.S. (1994). A common structural motif incorporating a cystine knot and a triple-stranded β-sheet in toxic and inhibitory peptides. *Protein Sci.* **3**, 1833–1839.
30. Narasimhan, L., Singh, J., Humblet, C., Guruprasad, K. & Blundell, T. (1994). Snail and spider toxins share a similar tertiary structure and 'cystine motif'. *Nat. Struct. Biol.* **1**, 850–852.
31. Fletcher, J.L., *et al.*, & King G.F. (1997). The structure of a novel insecticidal neurotoxin, atracotoxin-HVI, from the venom of an Australian funnel web spider. *Nat. Struct. Biol.* **4**, 559–566.
32. Goldstein, S.A.N. & Miller, C. (1992). A point mutation in a *Shaker* K^+ channel changes its charybdotoxin binding site from low to high affinity. *Biophys. J.* **62**, 5–7.

33. Park, C.S. & Miller, C. (1992). Mapping function to structure in a channel-blocking peptide: electrostatic mutants of charybdotoxin. *Biochemistry* **31**, 7749–7755.
34. Goldstein, S.A.N., Pheasant, D.J. & Miller, C. (1994). The charybdotoxin receptor of a *Shaker* K^+ channel: peptide and channel residues mediating molecular recognition. *Neuron* **12**, 1377–1388.
35. Stocker, M. & Miller, C. (1994). Electrostatic distance geometry in a K^+ channel vestibule. *Proc. Natl. Acad. Sci. USA* **91**, 9509–9513.
36. Schnolzer, M., Alewood, P.F., Jones, A., Alewood, D. & Kent, S.B.H. (1992). *In situ* neutralisation in Boc-chemistry solid phase peptide synthesis. *Int. J. Pept. Protein Res.* **40**, 180–193.
37. Sarin, V., Kent, S.B.H., Tan, J.P. & Merrifield, R.B. (1981). Quantitative monitoring of solid phase peptide synthesis by the ninhydrin reaction. *Anal. Biochemistry* **117**, 147–157.
38. Marion, D. & Wüthrich, K. (1983). Application of phase sensitive two dimensional correlated spectroscopy (COSY) for measurement of ^1H–^1H spin–spin couplings in proteins. *Biochem. Biophys. Res. Comm.* **113**, 967–974.
39. Rance, M., Sørenson, O.W., Bodenhausen, G., Wagner, G., Ernst, R.R. & Wüthrich, K. (1983). Improved spectral resolution in COSY ^1H NMR spectra of proteins via double quantum filtering. *Biochem. Biophys. Res. Comm.* **117**, 479–485.
40. Braunschweiler, L. & Ernst, R.R. (1983). Coherence transfer by isotropic mixing: application to proton correlation spectroscopy. *J. Magn. Reson.* **53**, 521–528.
41. Bax, A. & Davis, D.G. (1985). MLEV-17 based two dimensional homonuclear magnetisation transfer spectroscopy. *J. Magn. Reson.* **65**, 355–360.
42. Greisinger, C., Sørenson, O.W. & Ernst, R.R. (1987). Practical aspects of the E.COSY technique: measurement of scalar spin-spin coupling constants in peptides. *J. Magn. Reson.* **88**, 177–185.
43. Kumar, A. Ernst, R.R. & Wüthrich, K. (1980). A two-dimensional nuclear Overhauser enhancement (2D NOE) experiment for elucidation of complete proton–proton cross relaxation networks in biological macromolecules. *Biochem. Biophys. Res. Comm.* **95**, 1–6.
44. Wagner, G. (1990). NMR investigations of protein structure. *Prog. NMR Spectroscopy* **22**, 101–139.
45. Nilges, M., Gronenborn, A.M., Brünger, A.T. & Clore, G.M. (1988). Determination of three-dimensional structures of proteins by simulated annealing with interproton distance constraints. Application to crambin, potato carboxypeptidase inhibitor and barley serine proteinase inhibitor 2. *Protein Eng.* **2**, 27–38.
46. Hoshi, T., Zagotta, W.N. & Aldrich, R.W. (1990). Biophysical and molecular mechanisms of *Shaker* potassium channel inactivation. *Science* **250**, 533–538.
47. Naranjo, D. & Miller, C. (1996). A strongly interacting pair of residues on the contact surface of charybdotoxin and a *Shaker* K^+ channel. *Neuron* **16**, 123–130.

ELSEVIER

Journal of Neurological Sciences 153 (1997) 25–31

JOURNAL OF THE NEUROLOGICAL SCIENCES

SNX-111, a novel, presynaptic N-type calcium channel antagonist, is neuroprotective against focal cerebral ischemia in rabbits

Miguel A. Perez-Pinzon[1], Midori A. Yenari, Guo H. Sun, David M. Kunis, Gary K. Steinberg*

Department of Neurosurgery and Stanford Stroke Center, Stanford University Medical Center, Stanford, CA 94305, USA

Received 6 February 1997; received in revised form 1 July 1997; accepted 5 August 1997

Abstract

Cytosolic Ca^{2+} overload has been proposed as a main cause of neuronal injury during cerebral ischemia. SNX-111, a synthetic product of the naturally occurring ω-conotoxin MVIIA, is a novel, presynaptic N-type Ca^{2+} channel antagonist and has been reported to be neuroprotective against cerebral ischemia. We studied the neuroprotective effects of SNX-111 in a rabbit model of focal cerebral ischemia. New Zealand white male rabbits (2.5–3.5 kg) were given 1 mg/kg/h i.v. SNX-111 ($n=8$) or normal saline ($n=8$) 10 min after onset of a 2-h period of transient focal cerebral ischemia induced by occlusion of the left middle cerebral, anterior cerebral and internal carotid arteries followed by 4 h reperfusion. SNX-111 significantly attenuated overall cortical ischemic neuronal damage by 44% (saline, 38.7±3.0%; SNX-111, 21.5±6.0%, $P<0.05$) and regions of hyperintensity on T2-weighted MRI by 30% (saline, 70.6±4.0%; SNX-111, 49.3±11.0%, $P<0.05$). No significant difference in (regional cerebral blood flow) rCBF or MAP (mean arterial blood pressure) was found between SNX-111- and saline-treated rabbits suggesting that neuroprotection is due to a cellular effect. We conclude that SNX-111 reduces ischemic injury in this model. Its use as a clinical neuroprotective agent for cerebrovascular surgery or stroke should be investigated further. © 1997 Elsevier Science B.V.

Keywords: Calcium; Excitotoxicity; Focal cerebral ischemia; Conopeptides; Stroke; Rabbit; MVIIA

1. Introduction

Cytosolic Ca^{2+} overload has been proposed as one of the main cellular processes leading to neuronal death during cerebral ischemia (Siesjo, 1981). This hypothesis proposes that calcium influx during cerebral ischemia occurs when voltage-dependent calcium channels open as a result of the fall in ATP levels and membrane depolarization (Schurr and Rigor, 1992). Other mechanisms resulting in this overload include glutamate-induced NMDA receptor hyperactivation (Rothman and Olney, 1986), reversal of the Na^{+}–Ca^{2+} exchanger (Stys et al., 1991) and inhibition of the Ca^{2+}-ATPase (Lipton and Lobner, 1990). In vitro studies confirm that increased intracellular Ca^{2+} is a major detrimental factor in hypoxic-ischemic cell damage (Lipton and Lobner, 1990; Schurr and Rigor, 1992). In addition, hippocampal slices are fully protected against neuronal damage when superfused in a low calcium solution during hypoxia (Schurr et al., 1991). In vivo studies have shown voltage-gated calcium channel antagonists to be successful as neuroprotective agents when given prior to or immediately following cerebral ischemia (Jacewicz et al., 1990; Sauter and Rudin, 1990; Bielenberg and Beck, 1991; Roda et al., 1995). However, post-ischemic administration of L-type calcium channel blockers have failed as neuroprotectants (Steen et al., 1984; Snape et al., 1993).

Another approach has been to block the N-type calcium channel, which is believed to control Ca^{2+}-dependent transmitter release in brain (Tsien et al., 1988). Since

*Corresponding author. Department of Neurosurgery, Room R109, SUMC, Stanford University, Stanford, CA 94305, USA. Tel.: +1 650 7235575; fax: +1 650 7232815.

[1]Present address: Department of Neurology, D4-5, University of Miami, School of Medicine, Miami, FL 33101, USA.

PII S0022-510X(97)00196-2

N-type Ca^{2+} channels control presynaptic Ca^{2+} uptake and release of glutamate, it has been hypothesized that blockade of the N-type Ca^{2+} channel could reduce glutamate-induced ischemic injury. The synthetic peptide SNX-111, corresponding to the ω-conopeptide MVIIA from *Conus magus* is a selective N-type Ca^{2+} antagonist that blocks the N-subtype Ca^{2+} channel (Olivera et al., 1987; Wagner et al., 1988; Obaid et al., 1989). SNX-111 was found to reduce neuronal injury in animal models of global and focal ischemia (Buchan et al., 1994; Zhao et al., 1994).

As previous studies of Ca^{2+} channel antagonists suggest that the protective mechanism is due to enhancement of collateral blood supply, this study examined the neuroprotective effects of SNX-111 with attention to regional cerebral blood flow (rCBF) and mean arterial blood pressure (MAP).

2. Materials and methods

2.1. Animal preparation for in vivo ischemia

Following approval from the Institutional Administrative Panel on Laboratory Animal Care (APLAC), male New Zealand white rabbits (2.5–3.5 kg) were sedated with 1 cc i.m. xylazine/acepromazine maleate (3:1) and anesthetized with 3–4% halothane delivered by mask. Tracheostomy was performed and anesthesia maintained during the entire experiment using mechanical ventilation with 1% halothane in 0.5 l/min O_2, 4.5 l air. End-tidal CO_2 was measured with a capnograph (Puritan-Bennett, Teaksburg, MA, USA) and controlled at 30–40 mmHg. Catheters were inserted into the right femoral vein and artery for blood pressure monitoring, blood sampling and drug administration. Mean arterial pressure (MAP), rectal temperature, and heart rate were monitored continuously. MAP was maintained at 50–60 mmHg throughout the clipping period and at 60–70 mmHg throughout the reperfusion period using small boluses of saline and phenylephrine (1 cc in 50 cc normal saline) as necessary. A hole was drilled 1 cm lateral from the bregma, in the contralateral hemisphere, and a 33-gauge thermocouple lowered 4 mm into the brain in order to measure brain temperature. Brain temperature was controlled at 37.5–38.5°C with a heating lamp. Arterial blood gases (178 pH/blood gas analyzer; Ciba-Corning, Medfield, MA, USA), plasma glucose levels (One Touch glucose monitor; Lifescan, Milpitas, CA, USA) and hematocrit were measured intermittently throughout the experiment; blood gases were maintained in the physiological range by adding sodium bicarbonate or adjusting the ventilator settings.

2.2. Somatosensory-evoked potentials

Median nerve somatosensory-evoked potentials (SEP) were recorded over both hemispheres using skull screws positioned 5 mm to either side of the sagittal suture at bregma. Square wave stimuli (10 mA and 0.25 ms) duration were delivered to the median nerves at a frequency of 2.1 Hz. Evoked potentials were recorded and stored using the Nicolet Pathfinder II Electrodiagnostic System (Madison, WI, USA). Thirty responses were averaged for each measurement using a band pass filter of 30–1500 Hz. The amplitude of the SEP wave was measured from the peak of the major positive deflection to the trough of the negative deflection (Steinberg et al., 1986). For purposes of analysis, SEP amplitudes were expressed as a percentage of pre-ischemic amplitudes. In order to confirm consistent ischemia, we only used animals in this experiment whose SEP amplitude decreased to <25% of the pre-ischemic values within the first 10 min after arterial occlusion. SEP were recorded pre-ischemia, at 15 min intervals during the 2-h ischemic period and at 30-min intervals during reperfusion.

2.3. Cerebral blood flow measurements

A 1-mm diameter Laser-Doppler flow probe (TSI BPM 403 A, St. Paul, MN, USA) was placed over an approximately 2-mm diameter hole drilled in the skull (dura left intact), 10 mm to the left of bregma. The probe was lowered using a micromanipulator and advanced under microscopic guidance to the surface of the dura. Care was taken not to damage the brain while adjusting the probe position. Since the Laser-Doppler method has been demonstrated to provide accurate measurements of rCBF changes, but not absolute flow (Dirnagl et al., 1989), all measurements were expressed as relative percentages of pre-ischemic values. In order to confirm consistent ischemia, we only used animals in this experiment whose rCBF decreased below 20% after arterial occlusion.

2.4. Ischemia model

The model was modified from previous studies (Steinberg et al., 1989, 1991). In the present study, using a retro-orbital approach, three vessels were occluded (left anterior cerebral artery, left internal carotid artery, left middle cerebral artery), with miniature temporary Yasargil clips (Steinberg et al., 1991). The three vessels were occluded for 2 h, followed by removal of the clips and 4 h of reperfusion. Ten minutes after the onset of arterial occlusion, rabbits were administered i.v. either 1 mg/kg/h SNX-111 ($n=8$) or an equivalent volume of normal saline ($n=8$), in a blinded fashion. Drug or normal saline was continued for the duration of the experiment.

Six hours following the onset of arterial occlusion, animals were sacrificed with an i.v. overdose of pentobarbital 100 mg/kg and perfused transcardially with 300 cc saline followed by 300 cc buffered formalin (pH 7.4). Brains were left in the skulls to fix overnight, removed the next day and allowed to sit in formalin for at least another

5 days before magnetic resonance imaging (MRI) scanning and histological processing.

All investigators involved in animal surgery and data analysis were blinded to treatment groups.

2.5. Magnetic resonance imaging

MRI scans of the fixed brains were obtained using a 1.5-Tesla GE Signa Scan magnet with a 6-inch diameter saddle coil positioned at magnetic isocenter, a 16-cm field of view and a 256×256 matrix (0.625 mm pixel diameter) and two excitations/projection. Three-mm thick, spin echo T2-weighted MRI scans (T2W) were obtained using a repetition time (TR) of 2500 ms and an echo time (TE) of 80 ms. We have previously shown a high correlation (>85%) between in vivo MRI images and postmortem images (DeLaPaz et al., 1991). High-intensity regions, representing increased brain water content, were measured using an image analyzing system (Jandel Sigma and IBM PC XT computer). The image corresponding to histological level 1 (see below) was selected to compute the % area of T2W hyperintensity as this represents the region of maximum injury and the ischemic core in this model (Steinberg et al., 1988, 1991).

2.6. Histopathology

Histopathology was performed on paraffin-embedded, coronal 10-mm sections stained with hematoxylin and eosin. Three standard coronal sections were analyzed corresponding to: level 1, 3 mm anterior to the anterior commissure (AC); level 2, at the AC; and level 3, 3 mm posterior to the AC. Areas containing neurons with early ischemic neuronal damage (IND) were measured on each of the standard sections using an image-analyzing system. Ischemic damage was determined when neurons showed moderate to severe shrinkage, increased nuclear basophilia, and a pyknotic nucleus. Similar criteria have been used in previous studies (Ginsberg et al., 1978; Steinberg et al., 1988, 1991). Percentage area of IND for each animal was calculated for the left cortex and striatum by summing the total area of IND for left cortex or striatum divided by the total area of left cortex or striatum on three coronal sections.

2.7. Statistical analysis

Student's t-tests were used to determine significant differences between SNX-111 and saline groups for IND and T2W lesion areas. Two-factor ANOVA with repeated measure design and compensation for multiple comparisons were used for CBF and SEP data. Data are expressed as mean values±SEM. P values <0.05 were considered significant.

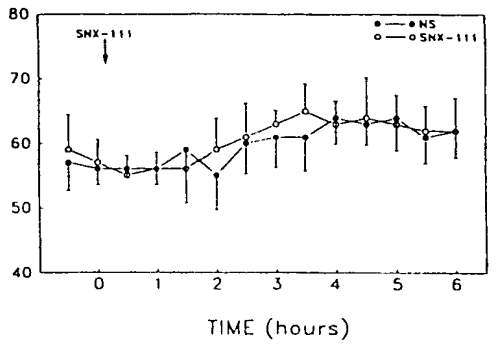

Fig. 1. Mean arterial blood pressure (MAP) measured with catheters inserted into the right femoral artery prior to, during and following 2 h of focal ischemia in rabbits treated with vehicle or SNX-111 (administered at 1 mg/kg/h i.v., 10 min after onset of ischemia). SNX-111, $n=8$, and saline, $n=8$.

3. Results

3.1. Systemic parameters

Physiological parameters throughout the experiment did not show significant differences between groups. In particular, there was no significant difference between groups in MAP (Fig. 1) and the volume of saline or phenylephrine infused during the experiment.

3.2. Ischemic neuronal damage

Histological analysis showed that SNX-111 attenuated overall cortical IND by 44% (saline, 38.7±3.0%, $n=8$ vs. SNX-111, 21.5±6.0%, $n=8$, $P<0.05$) (Fig. 2). In sections 1 and 2, SNX-111 reduced cortical IND by 40 and 34% ($P<0.05$), respectively. SNX-111 reduced hemispheric IND (sections 1–3) by 56% (saline, 30.4±3.0 vs. SNX-111, 13.4±4.0, $P<0.01$). No significant neuroprotection by SNX-111 was found in basal ganglia (Fig. 2), although

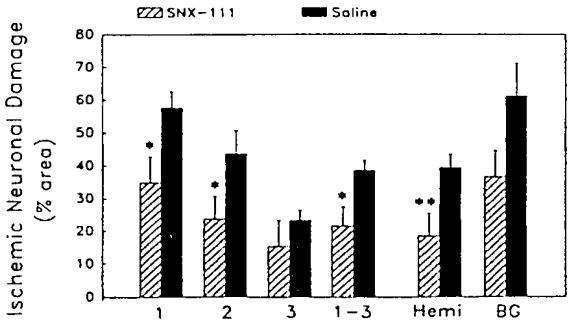

Fig. 2. Percentage area of ischemic neuronal damage (IND) in cerebral cortex in three coronal levels: levels 1–3, combined, hemisphere and basal ganglia. SNX-111 administered at 1 mg/kg/h i.v., starting 10 min after onset of ischemia; $n=8$ for SNX-111 and $n=8$ for saline. *$P<0.05$, **$P<0.01$; Student's t-test.

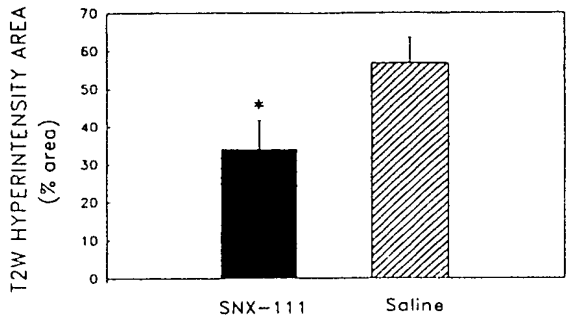

Fig. 3. Percentage area of hyperintense regions observed on T2-weighted MRI scans. SNX-111 administered at 1 mg/kg/h i.v., starting 10 min after onset of ischemia; $n=8$ for SNX-111 and $n=8$ for saline. *$P<0.05$; Student's t-test; MRI, magnetic resonance imaging.

a trend towards protection was found (IND was 61.2±10.0% in the saline vs. 36.5±8.0% in the SNX-111 group, $P=0.172$).

3.3. Magnetic resonance imaging

SNX-111 decreased T2W hyperintensity area within the cortex by 30% (saline, 70.6±4.0%, $n=8$ vs. SNX-111, 49.3±11.0%, $n=8$, $P<0.05$) (Fig. 3). SNX-111 was also effective in reducing T2W hyperintensity area within the hemisphere by 40% (saline, 56.8±7.0%; SNX-111, 34.1±8.0%, $P<0.05$).

3.4. Cerebral blood flow

Measurements of cerebral blood flow in the left hemisphere (hemisphere undergoing focal ischemia) are shown in Fig. 4. In the SNX-111 group, CBF dropped to 10.0±1.3% of pre-ischemic values ($P<0.001$; $n=8$), and in the saline group, CBF dropped to 11.1±2.3% of pre-ischemic values ($P<0.001$; $n=8$). No statistical difference in CBF was found between the two treatment groups at any time during the experiment.

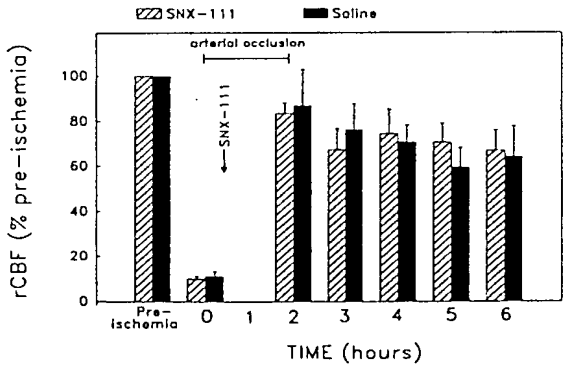

Fig. 4. Percent change from pre-ischemic values in cerebral blood flow during focal ischemia and reperfusion in both saline ($n=8$) and SNX-111 ($n=8$) rabbits. SNX-111 (1 mg/kg/h i.v.) administered 10 min after arterial occlusion. rCBF, regional cerebral blood flow as measured by laser Doppler.

3.5. Somatosensory-evoked potentials

SEP in the left hemisphere for both groups during ischemia and during the reperfusion phase are shown in Fig. 5A. In the SNX-111 group, SEP within the ischemic hemisphere fell to 8.2±3.5% of pre-ischemic values ($n=8$), whereas in the saline group, SEP dropped to 5.7±3.0% of pre-ischemic values ($n=8$). A significant difference was found between groups at 1 h of reperfusion (3 h after the onset of occlusion) with significantly better recovery of the SEP in the SNX-111 group (saline, 24.3±7.4%, vs. SNX-111, 55.8±12.7%, $P<0.05$) (Fig. 5A).

In the right (non-ischemic) hemisphere, no significant differences in the SEP amplitudes were found between groups at any time (Fig. 5B).

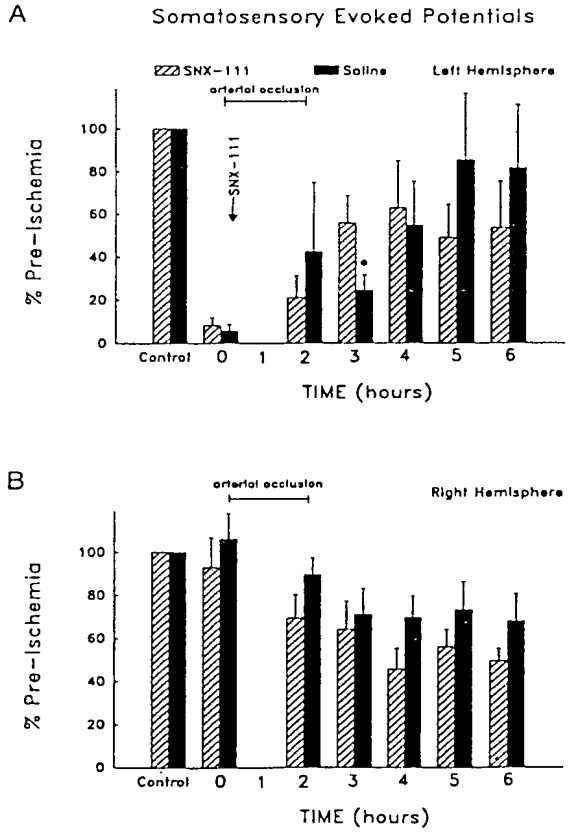

Fig. 5. SNX-111 treatment improves recovery of somatosensory-evoked potentials (SEPs) 1 h after reperfusion (3 h after the onset of ischemia). Percent change from control in SEPs during focal ischemia and reperfusion in saline ($n=8$) and SNX-111 ($n=8$) treated rabbits. (A) Left (ischemic) hemisphere. (B) Right (non-ischemic) hemisphere. *$P<0.05$; ANOVA with compensation for multiple comparisons) SNX-111 (1 mg/kg/h i.v.) administered 10 min after arterial occlusion.

4. Discussion

Intracellular calcium accumulation plays a pivotal role in the pathophysiology of cerebral ischemia (Siesjo, 1981), and while the NMDA receptor is a major site of Ca^{2+} entry during ischemia (Cheng and Mattson, 1992), Ca^{2+} influx also occurs through non-NMDA receptors (Gibbons et al., 1993) and voltage-activated Ca^{2+} channels (Mattson et al., 1988). Among Ca^{2+} channels, the N-type is thought to play an important role in the onset of calcium accumulation, since pre-synaptic Ca^{2+} uptake is mediated by this channel. The N-type calcium channels are high threshold and dihydropyridine insensitive that exhibit voltage-dependent inactivation and that are blocked by ω-conopeptides (McCleskey et al., 1987; Hillyard et al., 1992; Ramilo et al., 1992). They are found in cell bodies and nerve terminals and are the dominant Ca^{2+} channel subclass governing the release of small molecule neurotransmitters, such as glutamate. The synthetic ω-conopeptides SNX-111 (MVIIA), SNX-230 (MVIIC) and SNX-124 (GVIA) have been used to selectively block N-type calcium channels.

The present study demonstrated that SNX-111 is neuroprotective in this model of transient focal ischemia, significantly reducing cortical edema by 30% in the ischemic core and ischemic neuronal damage by 44%. These results support previous findings which showed that SNX-111 is neuroprotective in different models of cerebral ischemia. For example, Takizawa et al. (1995) found reduction in cortical infarction (by 60%) in normotensive rats during focal cerebral ischemia. Zhao et al. (1994), also utilizing a focal ischemia rat model, showed 82% attenuation of cortical infarction using SNX-111 (5 mg/kg, 15 min after occlusion and 48 h of reperfusion). However, in the latter study hypothermia occurred in the SNX-111 group, likely accounting for some of the neuroprotective effect. Evidence in other models of ischemia suggest that SNX-111 is also neuroprotective against delayed neuronal damage. Buchan et al. (1994) using rat models of both global and focal ischemia, demonstrated robust neuroprotection even when administered after prolonged reperfusion times. A single dose of SNX-111 (5 mg/kg) administered 6 or 24 h after reperfusion, reduced CA1 neuronal injury by 45 and 64%, respectively, in rats subjected to 10 min of forebrain ischemia followed by 7 days of reperfusion. Significant neuroprotection (55–60%) was obtained in hypertensive rats subjected to transient occlusion of the right middle cerebral artery for 1.5 or 2 h duration with 24-h survival. Smith and Siesjo (1992), using a global ischemia model, demonstrated that SNX-111 administered 6 h after onset of recirculation, reduced neocortical damage, both after 10 and 15 min of ischemia, but significant CA1 protection was only observed after 10 min (but not 15 min) of ischemia. Valentino et al. (1993) showed that SNX-111 protected pyramidal neurons in the CA1 subfield of the rat hippocampus from damage caused by transient forebrain ischemia, when SNX-111 was administered as late as 24 h after onset of recirculation. These results are in contrast to L-type Ca^{2+} channel blockers, such as dihydropyridines, which fail to protect neurons when administered after the ischemic episode (Steen et al., 1984; Milde et al., 1986; Snape et al., 1993). Other calcium channel blockers have shown conflicting evidence of neuroprotection (Berger et al., 1984; Sakaki et al., 1993).

The reduction in ischemic injury achieved by SNX-111 in our model of focal ischemia was not as robust as we have observed with various NMDA antagonists (CGS 19755, CGP 40116, dextrorphan, dextromethorphan, MK-801) (Steinberg et al., 1989, 1991; Maier et al., 1993; Perez-Pinzon et al., 1995). These observations are in line with those of Pringle et al. (1996) who used organotypic hippocampal slice models and found that while SNX-111 and SNX-230 (MVIIC) were both protective against hypoxia, neither compound afforded protection against ischemic injury.

The mechanism of neuroprotection with N-type calcium channel antagonists is not well characterized. Although one recent study in a rat model of focal ischemia demonstrated that SNX-111 inhibited glutamate release by 50% (Takizawa et al., 1995), other evidence suggests that this may not explain SNX-111's neuroprotective effects (Valentino et al., 1993). In fact, blockade of N-type VDCCs does not necessarily result in neuroprotection. Although N-type channels control release of excitatory amino acids, SNX-230, a more potent inhibitor of glutamate release, does not appear to have neuroprotective properties against global ischemia compared to SNX-111 (Valentino et al., 1993). Madden et al. (1990) studied another N-type VDCC antagonist, SNX-124 (GVIA) and did not find improvement in neurological outcome following treatment in a model of spinal cord ischemia. They also found less attenuation of cell death by SNX-124 compared to ketamine (an NMDA antagonist) against in vitro hypoxia. In the latter study, animals could not be given SNX-124 in doses ranges shown to be neuroprotective in cell culture due to systemic toxicity. This could, in part, explain the lack of efficacy seen in Madden's study.

Previous reports have shown that SNX-111 administered i.v. can dose-dependently decrease MAP in rats (Bowersox et al., 1992) and induce hypothermia (Smith and Siesjo, 1992; Zhao et al., 1994). Buchan et al. (1994) showed that a bolus infusion of SNX-111 (5 mg/kg) provoked a reduction in CBF and MAP that persisted during ischemia and reperfusion, and that recovered after 24 h. However, slow infusion (over 30 min) caused only mild reductions in CBF and MAP. In the rabbit model used in the present study, SNX-111 given as a continuous infusion over 6 h had no significant effect on MAP (Fig. 1) nor did it require additional phenylephrine. This was also the case in the study by Valentino et al. (1993) in a model of global ischemia where a similar dosing regimen was used. Brain temperature was strictly controlled, excluding hypothermia

as a protective mechanism. Prior studies have suggested that neuroprotection against ischemia using various Ca^{2+} antagonists may arise from improvement of collateral blood flow during and after ischemia; however, in this study there was no change in rCBF. Neuroprotection was also observed in hippocampal slice models, further suggesting that SNX-111's mechanism of action is probably due to direct cellular actions (Pringle et al., 1996). One limitation of the present study is the relatively short reperfusion period (4 h), so the outcome is determined 6 h after onset of ischemia. While the histological criteria we employed for early ischemic neuronal injury (shrunken, angular basophilic neurons with dark staining nuclei) are suggestive of cerebral infarction, delayed neuronal damage may progress for up to 2 months in the case of global ischemia and up to 2 weeks under certain conditions of focal ischemia (Pulsinelli et al., 1982; Dirnagl et al., 1989; Dereski et al., 1993). It is possible that the reduction in ischemic injury afforded by SNX-111 is merely delaying the time course of ischemic neuronal death but does not alter the final outcome at a later time in our model. Unfortunately, it is not possible to conduct long-term stroke studies in rabbits due to the high mortality rate. However, using a rat model of focal cerebral ischemia, our group found early transient neuroprotection with SNX-111 which was subsequently lost by 24 h (Yenari et al., 1996).

In conclusion, we report here that continuous administration of SNX-111 was efficacious against a focal ischemic insult, decreasing ischemic neuronal damage and T2W hyperintensity without affecting rCBF or MAP. These results suggest that attenuation of ischemic injury is primarily due to actions at the cellular level, rather than improved collateral blood flow or protection through systemic effects in this model. We conclude that SNX-111 reduces focal cerebral ischemic injury in this model by blocking N-type calcium channels, however, its precise mechanism remains undefined. Clinical safety and efficacy trials of SNX-111 in stroke patients are currently being planned.

Acknowledgements

This study was supported by funding from NIH NINDS Grant # RO1 NS 27292 (G.K.S.), NIH NINDS Grant # K08 NS01860 (M.A.Y.), Neurex Corporation (Menlo Park, CA, USA), Bernard and Ronni Lacroute and the William Randolph Hearst Foundation (G.K.S.). Neurex Corp. also supplied SNX-111.

References

Berger, J.R., Busto, R., Ginsberg, M.D., 1984. Verapamil: failure of metabolic amelioration following global forebrain ischemia in the rat. Stroke 15, 1029–1032.

Bielenberg, G.W., Beck, T., 1991. The effects of dizocilpine (MK-801), phencyclidine, and nimodipine on infarct size 48 h after middle cerebral artery occlusion in the rat. Brain Res. 552, 338–342.

Bowersox, S.S., Singh, T., Nadasdi, L., Zukowska-Grojec, Z., Valentino, K., Hoffman, B.B., 1992. Cardiovascular effects of omega-conopeptides in conscious rats: mechanisms of action. J. Cardiovasc. Pharmacol. 20, 756–764.

Buchan, A.M., Gertler, S.Z., Li, H., Xue, D., Huang, Z.G., Chaundy, K.E., Barnes, K., Lesiuk, H.J., 1994. A selective N-type Ca(2+)-channel blocker prevents CA1 injury 24 h following severe forebrain ischemia and reduces infarction following focal ischemia. J. Cereb. Blood Flow Metab. 14, 903–910.

Cheng, B., Mattson, M.P., 1992. IGF-I and IGF-II protect cultured hippocampal and septal neurons against calcium-mediated hypoglycemic damage. J. Neurosci. 12, 1558–1566.

DeLaPaz, R.L., Shibata, D., Steinberg, G.K., Zarnegar, R., George, C., 1991. Acute cerebral ischemia in rabbits: correlation between MR and histopathology. Am. J. Neuroradiol. 12, 89–95.

Dereski, M.O., Chopp, M., Knight, R.A., Rodolosi, L.C., Garcia, J.H., 1993. The heterogeneous temporal evolution of focal ischemic neuronal damage in the rat. Acta Neuropathol. (Berlin) 85, 327–333.

Dirnagl, U., Kaplan, B., Jacewicz, M., Pulsinelli, W., 1989. Continuous measurement of cerebral cortical blood flow by laser-Doppler flowmetry in a rat stroke model. J. Cereb. Blood Flow Metab. 9, 589–596.

Gibbons, S.J., Brorson, J.R., Bleakman, D., Chard, P.S., Miller, R.J., 1993. Calcium influx and neurodegeneration. Ann. NY Acad. Sci. 679, 22–33.

Ginsberg, M.D., Budd, M.W., Welsh, F.A., 1978. Diffuse cerebral ischemia in the cat: I. Local blood flow during severe ischemia and recirculation. Ann. Neurol. 3, 482–492.

Hillyard, D.R., Monje, V.D., Mintz, I.M., Bean, B.P., Nadasdi, L., Ramachandran, J., Miljanich, G., Azimi-Zoonooz, A., McIntosh, J.M., Cruz, L.J., Imperial, J.S., Baldomero, O.M., 1992. A new Conus peptide ligand for mammalian presynaptic Ca2+ channels. Neuron 9, 69–77.

Jacewicz, M., Brint, S., Tanabe, J., Wang, X.J., Pulsinelli, W.A., 1990. Nimodipine pretreatment improves cerebral blood flow and reduces brain edema in conscious rats subjected to focal cerebral ischemia. J. Cereb. Blood Flow Metab. 10, 903–913.

Lipton, P., Lobner, D., 1990. Mechanisms of intracellular calcium accumulation in the CA1 region of rat hippocampus during anoxia in vitro. Stroke 21, III60–64.

Madden, K.P., Clark, W.M., Marcoux, F.W., Probert, Jr. A.W., Weber, M.L., Rivier, J., Zivin, J.A., 1990. Treatment with conotoxin, an 'N-type' calcium channel blocker, in neuronal hypoxic-ischemic injury. Brain Res. 537, 256–262.

Maier, C., Steinberg, G.K., Sun, G.H., Zhi, G.T., Maze, M., 1993. Neuroprotection by the alpha 2-adrenoreceptor agonist dexmedetomidine in a focal model of cerebral ischemia. Anesthesiology 79, 306–312.

Mattson, M.P., Guthrie, P.B., Kater, S.B., 1988. Intracellular messengers in the generation and degeneration of hippocampal neuroarchitecture. J. Neurosci. Res. 21, 447–464.

McCleskey, E.W., Fox, A.P., Feldman, D.H., Cruz, L.J., Olivera, B.M., Tsien, R.W., Yoshikami, D., 1987. Omega-conotoxin: direct and persistent blockade of specific types of calcium channels in neurons but not muscle. Proc. Natl. Acad. Sci. USA 84, 4327–4331.

Milde, L.N., Milde, J.H., Michenfelder, J.D., 1986. Delayed treatment with nimodipine improves cerebral blood flow after complete cerebral ischemia in the dog. J. Cereb. Blood Flow Metab. 6, 332–337.

Obaid, A.L., Flores, R., Salzberg, B.M., 1989. Calcium channels that are required for secretion from intact nerve terminals of vertebrates are sensitive to omega-conotoxin and relatively insensitive to dihydropyridines. Optical studies with and without voltage-sensitive dyes. J. Gen. Physiol. 93, 715–729.

Olivera, B.M., Cruz, L.J., de Santos, V., LeCheminant, G.W., Griffin, D., Zeikus, R., McIntosh, J.M., Galyean, R., Varga, J., Gray, W.R., Rivier,

J., 1987. Neuronal calcium channel antagonists. Discrimination between calcium channel subtypes using omega-conotoxin from *Conus magus* venom. Biochemistry 26, 2086–2090.

Perez-Pinzon, M.A., Maier, C.M., Yoon, E.J., Sun, G.H., Giffard, R.G., Steinberg, G.K., 1995. Correlation of CGS 19755 neuroprotection against in vitro excitotoxicity and focal cerebral ischemia. J. Cereb. Blood Flow Metab. 15, 865–876.

Pringle, A., Benham, C., Sim, L., Kennedy, J., Iannotti, F., Sundstrom, L., 1996. Selective N-type calcium channel antagonist omega conotoxin MVIIA is neuroprotective against hypoxic neurodegeneration in organotypic hippocampal-slice cultures. Stroke 27, 2124–2130.

Pulsinelli, W.A., Brierley, J.B., Plum, F., 1982. Temporal profile of neuronal damage in a model of transient forebrain ischemia. Ann. Neurol. 11, 491–498.

Ramilo, C.A., Zafaralla, G.C., Nadasdi, L., Hammerland, L.G., Yoshikami, D., Gray, W.R., Kristipati, R., Ramachandran, J., Miljanich, G., Olivera, B.M., Cruz, L.J., 1992. Novel alpha- and omega-conotoxins from *Conus striatus* venom. Biochemistry 31, 9919–9926.

Roda, J.M., Carceller, F., Diez-Tejedor, E., Avendano, C., 1995. Reduction of infarct size by intra-arterial nimodipine administered at reperfusion in a rat model of partially reversible brain focal ischemia. Stroke 26 (10), 1888–1892.

Rothman, S.M., Olney, J.W., 1986. Glutamate and the pathophysiology of hypoxic–ischemic brain damage. Ann. Neurol. 19, 105–111.

Sakaki, T., Tsujimoto, S., Sasaoka, Y., Tsunoda, S., Shintomi, K., 1993. The effect of a new calcium antagonist, TA3090 (clentiazem), on experimental transient focal cerebral ischemia in cats. Stroke 24, 872–878.

Sauter, A., Rudin, M., 1990. Calcium antagonists for reduction of brain damage in stroke. J. Cardiovasc. Pharmacol. 15, S43–47.

Schurr, A., Rigor, B.M., 1992. The mechanism of cerebral hypoxic-ischemic damage. Hippocampus 2, 221–228.

Schurr, A., West, C.A., Rigor, B.M., 1991. Neurotoxicity of quinolinic acid and its derivatives in hypoxic rat hippocampal slices. Brain Res. 568, 199–204.

Siesjo, B.K., 1981. Cell damage in the brain: a speculative synthesis. J. Cereb. Blood Flow Metab. 1, 155–185.

Smith, M.-L., Siesjo, B.K., 1992. Postischemia treatment with the omega-conopeptide SNX-111 protects the rat brain against ischemic damage. In: Krieglstein, J., Oberpilcher, H. (Eds.), Pharmacology of Cerbral Ischemia Stuttgart. Germany, Wissenschaftliche Verlagsgesellshft, pp. 161–167.

Snape, M.F., Baldwin, H.A., Cross, A.J., Green, A.R., 1993. The effects of chlormethiazole and nimodipine on cortical infarct area after focal cerebral ischaemia in the rat. Neuroscience 53, 837–844.

Steen, P.A., Newberg, L.A., Milde, J.H., Michenfelder, J.D., 1984. Cerebral blood flow and neurologic outcome when nimodipine is given after complete cerebral ischemia in the dog. J. Cereb. Blood Flow Metab. 4, 82–87.

Steinberg, G.K., Gelb, A.W., Lam, A.M., Manninen, P.H., Peerless, S.J., Rassi Neto, A., Floyd, P., 1986. Correlation between somatosensory evoked potentials and neuronal ischemic changes following middle cerebral artery occlusion. Stroke 17, 1193–1197.

Steinberg, G.K., George, C.P., DeLaPaz, R., Shibata, D.K., Gross, T., 1988. Dextromethorphan protects against cerebral injury following transient focal ischemia in rabbits. Stroke 19, 1112–1118.

Steinberg, G.K., Saleh, J., Kunis, D., DeLaPaz, R., Zarnegar, S.R., 1989. Protective effect of *N*-methyl-D-aspartate antagonists after focal cerebral ischemia in rabbits. Stroke 20, 1247–1252.

Steinberg, G.K., Kunis, D., Saleh, J., DeLaPaz, R., 1991. Protection after transient focal cerebral ischemia by the *N*-methyl-D-aspartate antagonist dextrorphan is dependent upon plasma and brain levels. J. Cereb. Blood Flow Metab. 11, 1015–1024.

Stys, P.K., Waxman, S.G., Ransom, B.R., 1991. Na(+)-Ca2+ exchanger mediates Ca2+ influx during anoxia in mammalian central nervous system white matter. Ann. Neurol. 30, 375–380.

Takizawa, S., Matsushima, K., Fujita, H., Nanri, K., Ogawa, S., Shinohara, Y., 1995. A selective N-type calcium channel antagonist reduces extracellular glutamate release and infarct volume in focal cerebral ischemia. J. Cereb. Blood Flow Metab. 15, 611–618.

Tsien, R.W., Lipscombe, D., Madison, D.V., Bley, K.R., Fox, A.P., 1988. Multiple types of neuronal calcium channels and their selective modulation. Trends Neurosci. 11, 431–438.

Valentino, K., Newcomb, R., Gadbois, T., Singh, T., Bowersox, S., Bitner, S., Justice, A., Yamashiro, D., Hoffman, B.B., Ciaranello, R., Miljanich, G., Ramachandran, J., 1993. A selective N-type calcium channel antagonist protects against neuronal loss after global cerebral ischemia. Proc. Natl. Acad. Sci. USA 90, 7894–7897.

Wagner, J.A., Snowman, A.M., Biswas, A., Olivera, B.M., Snyder, S.H., 1988. Omega-conotoxin GVIA binding to a high-affinity receptor in brain: characterization, calcium sensitivity, and solubilization. J. Neurosci. 8, 3354–3359.

Yenari, M., Palmer, J., Sun, G., de Crespigny, A., Moseley, M., Steinberg, G., 1996. Time-course and treatment response with SNX-111, an N-type calcium channel blocker, in a rodent model of focal cerebral ischemia using diffusion-weighted MRI. Brain Res. 739, 36–45.

Zhao, Q., Smith, M.L., Siesjo, B.K., 1994. The omega-conopeptide SNX-111, an N-type calcium channel blocker, dramatically ameliorates brain damage due to transient focal ischaemia. Acta Physiol. Scand. 150, 459–461.

Exhibit "D"

Clinical Journal of Pain

Volume 13(3) September 1997 pp 256-259

Use of Intrathecal SNX-111, a Novel, N-Type, Voltage-Sensitive, Calcium Channel Blocker, in the Management of Intractable Brachial Plexus Avulsion Pain

[Case Report]

Brose, William G. M.D.*; Gutlove, David P. M.D.*; Luther, Robert R. M.D.†; Bowersox, S. Scott Ph.D.†; McGuire, Dawn M.D.†‡

*Department of Anesthesia, Stanford University Medical Center, Palo Alto, California; †Neurex Corporation, Menlo Park, California; and ‡Department of Neurology, University of California at San Francisco, San Francisco, California, U.S.A.

Manuscript submitted August 7, 1996; revision received January 30, 1997; accepted for publication April 14, 1997.

Address correspondence and reprint requests to Dr. Dawn McGuire, 3760 Haven Avenue, Menlo Park, CA 94025, U.S.A.

All of the authors received either study stipends, consultancy fees, or salary from the sponsor, Neurex Corporation, during the time the present study was conducted and reported.

Outline

Graphics

Abstract:

Objective: The objective was to assess the analgesic, antihyperesthesic, and antiallodynic properties of SNX-111 in neuropathic pain.

Design: We describe a patient with refractory, severe deafferentation pain successfully treated with SNX-111 in an open-label, baseline-controlled Phase I/II trial.

Setting: The patient was hospitalized for treatment and observation.

Patient: The patient was a 43-year-old man with intractable deafferentation pain of 23 years' duration secondary to brachial plexus avulsion.

Intervention: SNX-111, the first neuron-specific, N-type, voltage-sensitive calcium

channel blocker developed for clinical use, was administered by continuous, constant-rate, intrathecal infusion via an indwelling cervical catheter.

Outcome Measures: The primary outcome measures were the Visual Analog Scales of Pain Intensity (VASPI) and Pain Relief (VASPR).

Results: The patient experienced complete pain relief (VASPI = 0.0 cm and VASPR = 10.0 cm) with elimination of hyperesthesia and allodynia.

Conclusions: SNX-111, administered intrathecally by continuous, constant-rate infusion, produced dose-dependent pain relief in a 43-year-old male patient with a 23-year history of intractable deafferentation and phantom limb pain secondary to brachial plexus avulsion and subsequent amputation. Dizziness, blurred vision, and lateral-gaze nystagmus were dose-dependent side effects that resolved with decreasing dose levels. Complete pain relief was achieved in this patient without side effects after dose adjustment. We conclude that SNX-111 is a potent analgesic, antihyperesthesic, and antiallodynic agent. Controlled studies of SNX-111 in patients with malignant and nonmalignant pain syndromes are warranted and are under way.

SNX-111 is the first selective neuronal voltage-sensitive calcium channel (VSCC) blocker to enter clinical development. SNX-111 specifically blocks N-type VSCCs, which are found at presynaptic nerve terminals. Binding studies with radiolabeled SNX-111 in rats have demonstrated specific binding sites for SNX-111 in the superficial laminae of the dorsal horn of the spinal cord, the site of primary nociceptive afferent synapses. The presumed mechanism of action of SNX-111 in analgesia is the blockade of neurotransmitter release at the primary afferent nerve terminal.

Nerve injury can result in deafferentation pain, and patients typically describe a constant burning with superimposed paroxysms of lancinating or electrical shock-like pain, usually developing within days or weeks of the triggering injury. In brachial plexus injury, lesions proximal to the dorsal root ganglia and avulsion of multiple roots are associated with the development of chronic, severe deafferentation pain for which conventional treatments have proved to be of limited usefulness. In this report, a patient with refractory, severe deafferentation pain from brachial plexus avulsion successfully treated with SNX-111 is described.

CASE REPORT

A 43-year-old man with left upper extremity pain due to brachial plexus avulsion was admitted to the Stanford Pain Management Service. This patient had a 23-year history of intractable pain, described as a constant burning and aching of his left upper extremity, with episodic lancinating pains. Brachial plexus avulsion had been confirmed at the time of injury by myelography. One year after the injury, above-the-elbow, left arm amputation was performed because of recurrent injury to the flail limb. The amputation did not alter the nature or severity of his pain in the phantom limb or the remaining stump. Multiple treatment modalities were attempted and had failed, including nonsteroidal anti-inflammatory drugs, systemic opiates, tricyclic antidepressants, anticonvulsants, transcutaneous electrical nerve stimulation, somatic and sympathetic blockade, and intrathecally administered opiates. After informed consent had been obtained, the patient was enrolled in a Stanford University Medical Center IRB-approved protocol for an open-label, baseline-controlled, Phase I/II trial of SNX-111 (Neurex Corporation, Menlo Park, CA) administered by continuous intrathecal infusion. SNX-111 is being evaluated clinically under an active US IND# 45,718.

On examination, the patient appeared anxious, intermittently grimacing and rubbing his left upper extremity stump. Marked hyperesthesia and allodynia were present over the upper arm. The remainder of his physical examination was remarkable only for mild hypertension and tachycardia.

After placement of an intrathecal cervical catheter (Burron 20-gauge polyamide) in the C6-C7 interspace, SNX-111 was administered by continuous infusion beginning at a dose of 0.3 ng/kg/hour, with upward titration every 24 hours. Pain evaluations, including Visual Analog Scale of Pain Intensity (VASPI), Visual Analog Scale of Pain Relief (VASPR), and a binary Satisfaction/Dissatisfaction assessment were recorded at 4-hour intervals.

The initial VASPI score was 8.5 cm (where 0 = no pain and 10 = worst pain ever experienced), and the initial VASPR score was 0 cm (where 0 = no pain relief and 10 = complete pain relief). On the second day of treatment, no significant improvement in pain control had been achieved, and the infusion was increased to 1 ng/kg/hour. At this dose, the patient experienced less frequent episodes of lancinating pain and complete elimination of the hyperesthesia and allodynia. Overall pain control, however, remained unsatisfactory. On the third day of treatment, the SNX-111 infusion was increased to 3 ng/kg/hour. Ten hours after initiation of this dosage level, the patient reported complete pain relief, with a score of 0 cm on the VASPI and 10 cm on the VASPR. Because this and higher dosage levels were associated with moderate dizziness, blurred vision, and lateral-gaze nystagmus, the dose of SNX-111 was decreased. On the eighth day of treatment, the patient was receiving SNX-111 at a dosage level of 2 ng/kg/hour, at which level he was pain-free and experienced no side effects. During up and down titration, single-blinded (to the patient) dose alterations were made between the 1 ng/kg/hour and the 2 ng/kg/hour dosage levels. The patient's pain and pain relief reporting demonstrated consistent and concordant changes with dose, with return of pain at doses less than 2 ng/kg/hour. These results indicate a specific, dose-related analgesic effect (Fig. 1).

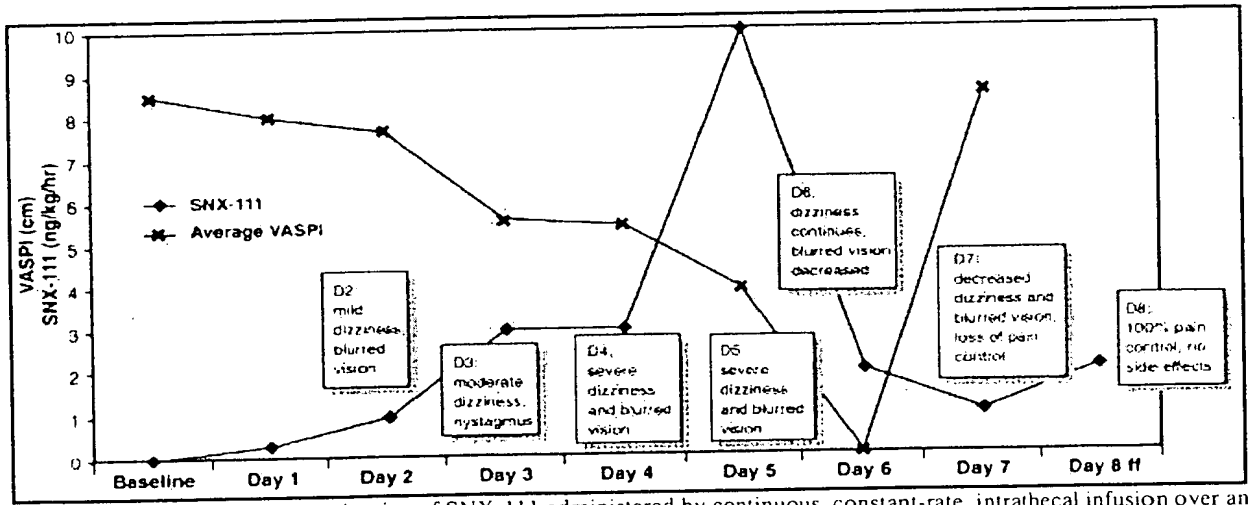

FIG. 1. The patient's response to titration of SNX-111 administered by continuous, constant-rate, intrathecal infusion over an 8-day period is summarized. SNX-111 dose level (ng/kg/hour), VASPI scores (cm), and side effects are shown.

DISCUSSION

Nerve injury can result in persistent, spontaneous ectopic discharges in primary afferent nociceptors and in altered central processing of afferent inputs.[1] Loeser and Ward,[2] using microelectrode recordings in the dorsal horn of cats after dorsal rhizotomy, demonstrated markedly abnormal spontaneous discharges in chronically deafferented sections. Both continuous and burst patterns of firing were observed. Large numbers of hyperactive units

were found in the superficial layers of the dorsal horn. Afferent evoked discharges were also abnormal and characterized by high frequency bursts lasting more than 100 msec, in contrast to the briefer (<35 msec) discharges evoked in normal dorsal horn sections under similar conditions. Abnormal firing patterns were not observed immediately after rhizotomy, but were present by day 14, implicating secondary changes rather than the immediate loss of afferent input in the development of abnormal neuronal excitability. These spontaneous discharges, in both chronic and burst patterns, have been demonstrated by intraneuronal recordings from transected nerves in patients with phantom limb pain and may be the physiologic correlate of clinical dysesthesias after nerve transection or other injury.3 In brachial plexus injury, lesions proximal to the dorsal root ganglia and avulsion of multiple roots are associated with the development of chronic, severe deafferentation pain for which conventional treatments have proved to be of limited usefulness.4

Calcium channels have been implicated in the maintenance of spontaneous ectopic discharges in injured primary afferent nociceptors 5 and in mediating persistent tactile allodynia after nerve injury.6 Omega-conopeptide MVIIA, the naturally occurring form of SNX-111, is a 25-amino acid residue peptide found in the venom of the piscivorous marine snail *Conus magus*. SNX-111 has been demonstrated to bind selectively and with high affinity to the neuronal, N-type, voltage-sensitive calcium channels in mammalian nervous systems.7 These calcium channels are localized to presynaptic nerve terminals where they control depolarization-induced neurotransmitter release.8 N-type calcium channels are present in highest density in the superficial layers (Rexed laminae I and II) of the dorsal horn, the site of primary afferent nociceptive junctions.9 In contrast, L-type calcium channels are located on cardiac and vascular smooth muscle and are blocked by agents such as the dihydropyridines.

SNX-111 may modify nociception by preventing neurally evoked release of neurotransmitters from primary nociceptive afferents and associated spinal interneurons. SNX-111 has demonstrated to be a safe and effective analgesic when administered intrathecally in a variety of rodent models of acute, chronic, and neuropathic pain.10,11 Unlike opiate analgesics, continuous intrathecal infusion of SNX-111 does not result in the development of tolerance during 7 days of continuous treatment in rats.11 Although high doses of SNX-111 have been associated with gross body tremors in animal models, analgesic doses producing minimal or no motor disturbances have been readily achieved. The mechanism producing the shaking/tremors in animals has not been elucidated, but this effect is reversible after discontinuation of treatment and tends to diminish in intensity with continued treatment. SNX-111 has been thoroughly evaluated in drug safety studies in rats, dogs, and cynomolgus monkeys in which SNX-111 has been administered intravenously and intrathecally by continuous, constant-rate infusion and by bolus injection.12,13 The maximum tolerated dose of SNX-111 administered by continuous, constant-rate, intrathecal infusion exceeds 1,000 ng/kg/hour in rats and dogs.13

A feasibility study of SNX-111, in which this patient was a subject, evaluated open-label, continuous intrathecal infusions of SNX-111 at doses ranging from 0.3 to 300 ng/kg/hour.14 Of the 23 evaluable patients who received SNX-111 for at least 3 days, 83% showed improvement ranging from partial to complete pain relief and concomitant opioid use decreased by 50% to 100% in two thirds of all patients.

CONCLUSIONS

We report the successful treatment of intractable brachial plexus avulsion pain with the novel, N-type, calcium channel blocker, SNX-111. Administered intrathecally by continuous infusion, SNX-111 provided complete pain relief in a dose-dependent fashion in a 43-year-old male patient with a 23-year history of deafferentation and intractable phantom limb pain

secondary to brachial plexus avulsion. Dizziness, blurred vision, and lateral-gaze nystagmus were dose-dependent side effects that resolved with decreasing dose. Complete pain relief was achieved in this patient without side effects following dose adjustment. These clinical results support the hypothesis that SNX-111 is a potent analgesic, antihyperesthesic, and antiallodynic agent when administered by continuous, constant-rate intrathecal infusion. Controlled studies of SNX-111 in patients with malignant and nonmalignant neuropathic pain syndromes are warranted and currently are under way.

Acknowledgment: This study was supported by Neurex Corporation, Menlo Park, California, U.S.A.

REFERENCES

1. Gracely RH, Lynch S, Bennett GJ. Painful neuropathy: altered central processing, maintained dynamically by peripheral input. *Pain* 1992;51:175-94. [Context Link]

2. Loeser JD, Ward AA. Some effects of deafferentation on neurons of the cat spinal cord. *Arch Neurol* 1967;17:629-36. [Context Link]

3. Nystrom B, Hagbarth KE. Microelectrode recordings from transected nerves in amputees with phantom limb pain. *Neurosci Lett* 1981;27:211-6. [Context Link]

4. Wynn Parry CB. Pain in avulsion lesions of the brachial plexus. *Pain* 1980;9:41-53. [Context Link]

5. Xie Y, Xiao W, Li H. The relationship between new ion channels and ectopic discharges from a region of nerve injury. *Sci China B* 1993;35:68-74. Bibliographic Links [Context Link]

6. Chaplan SR, Pogrel JW, Yaksh TL. Role of voltage-dependent calcium channel subtypes in experimental tactile allodynia. *J Pharmacol Exp Ther* 1994;269:1117-23. Bibliographic Links [Context Link]

7. Cruz LJ, Johnson DS, Olivera BM. Characterization of the [omega]-conotoxin target. *Biochemistry* 1987;26:820-4. Bibliographic Links [Context Link]

8. Kerr LM, Yoshikami D. A venom peptide with a novel presynaptic blocking action. *Nature* 1984;308:282-4. [Context Link]

9. Takemura M, Kyama H, Fukui H, Tohyama M, Wada H. Distribution of the [omega]-conotoxin receptor in rat brain: an autoradiographic mapping. *Neuroscience* 1989;32(2):405-16. Bibliographic Links [Context Link]

10. Malmberg AB, Yaksh TL. Effect of continuous intrathecal infusion of [omega]-conopeptides, N-type calcium-channel blockers, on behavior and antinociception in the formalin and hot-plate tests in rats. *Pain* 1995;60:83-90. Bibliographic Links [Context Link]

11. Malmberg AB, Yaksh TL. Voltage-sensitive calcium channels in spinal nociceptive processing: blockade on N- and P-type channels inhibits formalin-induced nociception. *J Neurosci* 1994;14:4882-90. Bibliographic Links [Context Link]

12. Bowersox SS, Luther RR. SNX-111: N-type voltage-sensitive calcium channel antagonist. *Drugs Future* 1994;19(2):128-30. Bibliographic Links [Context Link]

13. Neurex Scientific Report Nos. 5509-M009-94 and 54156 (unpublished data). [Context Link]

14. Brose WG, Pfeifer BL, Hassenbusch SJ, Burchiel KJ, Byas-Smith M, Krames E, McGuire D, Tich N, Luther RR. Analgesia produced by SNX-111 in patients with morphine-resistant pain. Abstract presented at 15th Annual Scientific Meeting American Pain Society, November 14-17, 1996. [Context Link]

Key Words: SNX-111; Calcium channel blocker; Analgesia; Neuropathic pain; Deafferentation pain; Brachial plexus avulsion; Allodynia; Hyperesthesia

Accession Number: 00002508-199709000-00012

Exhibit "E"

Display Abstract Show: 20 Sort Send to Text

1: Neurol Res. 1997 Jun;19(3):334-9.

Related Articles, Li

Mitochondrial dysfunction after experimental and human brain injury and its possible reversal with a selective N-type calcium channel antagonist (SNX-111).

Verweij BH, Muizelaar JP, Vinas FC, Peterson PL, Xiong Y, Lee CP.

Department of Neurosurgery, School of Medicine, Wayne State University, Detroit, MI, USA.

We have recently demonstrated in a rat model that traumatic brain injury induces perturbation of cellular calcium homeostasis with an overload of cytosolic calcium and excessive calcium adsorbed on the mitochondrial membrane, consequently the mitochondrial respiratory chain-linked oxidativ phosphorylation was impaired. We report the effect of a selective N-type calcium channel blocker, SNX-111 on mitochondrial dysfunction induced by controlled cortical impact. Intravenous administration of SNX-111 at varying times post injury was made. The concentration titration profile revealed SNX 111 at 4 mg kg-1 to be optimal, and the time window to be administration at h post-injury, in line with that reported on the effect of SNX-111 in experimental stroke. Under optimal conditions, SNX-111 significantly improved the mitochondrial respiratory chain-linked functions, such as the electron transfer activities with both succinate and NAD-linked substrates, ar the accompanied energy coupling capacities measured as respiratory control indices (RCI) and ATP synthesis (P/O ratio), and the energy linked Ca2+ transport. In order to assess the applicability of these data to the clinical setti we have initiated studies with brain tissue which has to be resected during surgical treatment. Five patients suffered from brain trauma, one from intracranial hypertension due to stroke (noninfarcted tissue was taken), and o from epilepsy. Our data revealed that brain mitochondria derived from the patient with intracranial hypertension and the patient with epilepsy were tigh coupled with good respiratory rates with glutamate and malate as substrates, and high P/O ratios. The rates of respiration and ATP synthesis were severel impaired in the brain mitochondria isolated from traumatized patients. These results indicate that investigation of brain mitochondrial functions can be use as a measure for trauma-induced impairment of brain energy metabolism. Th time window for the effect of SNX-111 in mitochondrial function and the (preliminary) similarity between mitochondrial dysfunction in experimental animals and humans make the drug appear to be well suited for clinical trials

severe head injury.

PMID: 9192388 [PubMed - indexed for MEDLINE]
